REDESIGN OF TUBULAR INLET GEOMETRY TO REDUCE FIBER ACCUMULATION IN UF MODULES.

Edgard Chehab

A THESIS

SUBMITTED TO THE SCHOOL OF GRADUATE STUDIES IN PARTIAL FULFILLMENT OF THE REQUIREMENTS FOR THE DEGREE OF MASTER OF APPLIED SCIENCE IN THE DEPARTMENT OF CHEMICAL ENGINEERING UNIVERSITY OF OTTAWA.

May 2nd 95

ISBN 0-612-11544-5

UNIVERSITÉ D'OTTAWA
UNIVERSITY OF OTTAWA

ABSTRACT

Many ultrafiltration applications are utilized by industry in such sectors as the food, pharmaceuticals, biotechnology, water purification, chemical and paper industries.

One of the processes used in the pulp and paper industry is the ultrafiltration (UF) of fiber suspensions using tubular membrane modules to control effluent composition and recover chemical products. Effluent treatment by UF includes bleach effluent treatment, deresining of the pulp wash water, whitewater processing for fiber recovery, and de-inking of effluent. However the behavior of the suspension in the entrance region of a tubular membrane is typically problematic. Modules having tubes with an inside diameter less than one inch are subject to blockage of the inlet tubes due to the accumulation of dewatered fiber within the module header.

This study deals with the influence of the inlet geometry on the concentration build-up within a model tubular module. Hence a module was designed to achieve this purpose. The module cell consisted of a header and five impermeable tubes (of equal diameter less than one inch). The inlet geometry of the tubes was varied by changing the inlet angle of a disk lying on top of the tubes. In addition to the influence of the inlet geometry on the concentration build-up in the distribution header, the influence of the inlet flowrate and pumping time was studied.

In addition to the transient flow experiments described above, several additional qualitative and quantitative factors were measured. These included the effect of suspension density on its viscosity, the effect of fatigue due to pumping on the length distribution of the fibers, the hydrodynamic behavior of the suspension inside the tubes in both laminar and turbulent conditions, the effect of pumping on the stiffness of the resulting sheet, and the pressure distribution within the flow cell.

It was found that an increase from 0° to 60° in the inlet angle for the 1/4" tube inner diameter reduced the accumulation of fibers in the header region by 25%. Likewise,

fiber build-up was reduced by 10% with decreased inlet flowrate from 1 to 0.75 l/s. Further, pumping was found to break down the fibers.

A Reynolds number was defined in terms of the inner diameter of the tube, the inlet flowrate, and the inlet angle where the density and viscosity data were measured earlier. Finally, a correlation between this modified version of the Reynolds number and the concentration build-up within the cell was generated.

ACKNOWLEDGMENTS

The author is extremely grateful to Dr. A. Tremblay and Dr. D. Taylor for their indispensable guidance, direction and encouragement throughout the course of his work. The author is also indebted to Dr. W. Kozicki for his invaluable input. In addition, he wishes to thank Mr. L. Tremblay and Mr. F. Ziroldo for their help with the set-up of the experiment. He would also like to thank St. Laurent Paperboard Inc. and Tembec Inc. for their donations of samples and analyses.

Special thanks are owed to his spouse, Rima, for her support and encouragement during this period. Last but not least, he would like to thank his parents and family for their love and care.

NOMENCLATURE

A	cross sectional area of a tube, ($\pi R^2/4$) [m^2]
A'	axis ratio of the fiber [1/m]
B	function relating shear to dynamic viscosity from equation 9 [m/s]
C	pulp concentration [weight %]
C_f	final fiber concentration in the header chamber [weight %]
C_i	initial fiber concentration in the feed tank [weight %]
C_o	critical concentration of pulp suspension [weight %]
CI	confidence interval [unit of corespondent parameter]
D	diameter of the hole at the inlet surface of the header plate [m]
D_z	average diameter of the cone opening in the header plate [m]
D_{sp}	diameter of the sphere used during the falling ball method experiment [m]
f	friction factor, (dimensionless)
G	velocity gradient, (dv/dy) [1/s]
g	acceleration due to gravity [m/s^2]
h	elevation from the ground [m]
ID	inner diameter of the tubes in the cell [m]
k	dynamic viscosity [$kg(m^{-1})^n sec^{-1}$]
K, K'	fluid consistency indices [$kg(m^{-1})^n sec^{-1}$, $kg(m^{-1})^{n'} sec^{-1}$]
l	length of the cylindrical shell used during the falling ball method experiment [m]
l'	fiber length [m]
m	mass of dry Kraft liner used to prepare the suspension [kg]
m_{sp}	mass of the sphere used during the falling ball method experiment [kg]
n, n'	flow-behavior indices (dimensionless)
OD	outer diameter of the tubes in the cell [m]

P potential pressure of the flowing suspension in the tubes, $(p - gh)$ [Pa]

p pressure of the flowing suspension in the tubes [Pa]

Q volumetric flowrate of the suspension [m^3/s]

r radius of a coaxial fluid element [m]

R radius of the tubes [m]

Re Reynolds number for Newtonian fluids from equation 17, (dimensionless)

Re' Reynolds number for non-Newtonian fluids from equation 20, (dimensionless)

T characteristic period of rotation (s/m)

t time [s]

t' fiber thickness [m]

u, v, U flow velocity of the flowing suspension in the tubes [m/s]

U_m mean flow velocity [m/s]

V volume of the suspension collected from the distributor header chamber [m^3]

v_t terminal velocity of the sphere used during the falling ball method experiment [m/s]

w fiber width [m]

x film thickness parameter [mm]

z ratio $\frac{r}{R}$ (dimensionless)

Greek Letters

α	inlet angle [degrees]
α'	fiber specific volume [m^3/g]
β	shape factor coefficient, (dimensionless)
Δa	a_2-a_1 differential indices [unit of the differentiated parameter a]
Φ	volume fraction of fibers (dimensionless)
ζ_d	friction factor in a smooth pipes (dimensionless)
δ	film thickness [mm]
δs	dry sheet thickness [in]
ρ	density of the suspension [kg/m^3]
ρ_{sp}	density of the sphere used during the falling ball method experiment [kg/m^3]
γ	velocity gradient of the flowing suspension in tubes [1/s]
η	apparent viscosity for non-Newtonian fluids [kg $m^{-1}sec^{-1}$]
μ	viscosity for Newtonian fluids [kg $m^{-1}sec^{-1}$]
τ	shear stress of the flowing suspension in the tube [N/m^2]
τ_R	shear stress of the flowing suspension at the wall of the tube [N/m^2]

CONTENTS

LIST OF TABLES

LIST OF FIGURES

CHAPTER 1: INTRODUCTION

One of the processes used in the pulp and paper industry is the ultrafiltration (UF) of fiber suspensions using tubular membrane modules to control effluent composition and to recover chemical products. However, the behavior of the suspension in the entrance region of a tubular membrane is typically problematic. Modules having tubes with an inside diameter less than one inch are subject to blockage of the inlet tubes due to the accumulation of dewatered fiber within the module header.

This study deals with the influence of the inlet geometry on the concentration build-up within a model tubular module. Given this, some background in the paper industry, ultrafiltration and fiber suspension behaviour are order.

1.1 Historical background of paper

The word "paper," comes from "papyrus" which is the name for both a reed-like plant found growing along the Nile River and an ancient writing material derived from the same. In ancient Egypt, papyrus writing sheets were made by removing the fibrous layers found in the plant and placing these side by side. A second set of layers was placed on top at right angles. The sheet was then dampened and pressed. When it dried, the layers were held together by the plant sap which acted as a glue (Britt, 1981).

Modern paper technology, however, has its origin in China. In the 1st Century AD, the Chinese used fibers from the inner bark of bamboo and mulberry to make paper. The fibers were first beaten in water to soften them and make them more flexible and then were pressed onto a screen to create a mat. The cellulose in the fibers caused them to bond together upon drying, creating a strong sheet.

Most innovations in the pulp and paper industry are the result of research carried out within the industry itself, i.e. the paper manufacturers and equipment and material suppliers. Governmental agencies and academic institutions have also contributed to

research in this field. In the last ten years, the industry has increasingly relied on scientific discoveries, laboratory findings and experimental models.

Modern paper consists of a matted or felted sheet of fibers formed from an aqueous fiber suspension and usually modified by additional materials. The fibrous raw materials or "pulp" is the most important raw material for the paper industry. It has been stated that paper of some sort can be made from the fibers of any vascular plant found in nature. This is probably true in a technical sense but from an economic standpoint, the number of plant materials suitable for paper making is much more limited (Britt, 1964).

In natural fibers, it is the cellulose that determines the character of the fiber and permits its use in paper making. Cellulose is a carbohydrate, being composed of carbon, hydrogen and oxygen with the latter two elements in the same proportion as in water. Of all the products of photosynthesis in the plant kingdom, cellulose is the most abundant; enormous amounts are produced annually by natural plant growth.

1.1.1 Fiber properties

Cellulose has a number of properties which are essential to the function that it must perform in nature and which meet equally well the requirements of a fiber for paper making. Cellulose fiber has long been recognized for its high tensile strength. In making strength comparisons, it is important to give consideration to the method of reporting. There are two methods by which the tensile strength of materials may be expressed: first, the force required to rupture the material per unit of cross-sectional area of the specimen and second, the force required to rupture the material per unit of linear mass. The first method is really a measurement of the strength per unit volume and is used extensively where the material is essentially homogeneous and non-porous. The second is a measurement of strength per unit weight and is suitable for materials that are not

homogeneous, that may be porous and which have cross-sections that are difficult to measure accurately.

Paper-making fibers generally exist in a great variety of sizes and shapes. Not only is there a wide range in fiber dimensions among such different plant sources as coniferous wood, cotton, flax, hemp and straw, but there is also considerable variation in fiber size and shape from one geographic region to another. In addition, the beating and refining of paper stock results in a cutting and bruising of the fiber and in the creation of short fragments or "fines". With rare exceptions, therefore, paper made from fibrous particles will consist of fibers of wide-ranging dimensions (Paavilaine, 1990). It is generally accepted that many paper products benefit from being composed of both long fibers and short fibers or fragments. The short, fine fibers tend to fill the spaces among the longer, coarser fibers. The resulting sheet shows a favorable combination of strength, contributed by the longer fibers, and a smooth, uniform surface, brought about by the short and fine fibers (Wahren, 1980). It is recognized that fiber flexibility is critical in that it allows fibers to make intimate contact with neighboring fibers during sheet formation. Fiber flexibility is also a determining factor in the area and strength of interfiber bonding. A fiber that is soft and flexible in the wet, swollen condition will promote interfiber bonding while one that is stiff will resist such bonding.

1.1.2 Testing and evaluation of pulp

The test methods available for the evaluation of the pulp are essentially empirical in nature. These methods depend upon exposure of pulp samples to carefully defined chemical or physical procedures leading to measurable chemical or physical results (Britt, 1979).

Chemical testing of pulp

Pulps may vary in their cellulose content or purity, i.e. in their content of lignin or other non-cellulosic material. Furthermore, the cellulose content itself may vary in its proportion of highly resistant cellulose to the less resistant or more easily dissolved cellulose. Non-cellulosic ingredients react rapidly with acidified $KMnO_4$ whereas cellulose reacts slowly and with difficulty. This fact permits a rapid, empirical test method capable of classifying a wide range of pulps for relative purity with respect to cellulose.

Physical properties

From a physical point of view, it was decided to evaluate pulps by a combination of procedures as follows:

i) the ratio of long fibers to fines where fiber length is measured or indicated by two general methods: (a) by microscopic examination and direct measurement of a representative number of fibers and (b) by classification of a sample of pulp into fractions by screens of different fineness;

ii) the drainage time in accordance with TAPPI Standard T221-m;

iii) the percentage of shrinkage of the sheet during drying; and

iv) the stiffness of the sheet after drying (burst factor sheets TAPPI Standard T220-m).

1.1.3 Water

Britt (1964) confirms that water, as a raw material used in the manufacture of pulp and paper, is second in importance only to the fiber itself. Thus it is natural that the pulp and paper industry should gravitate to regions where water supplies are abundant and of high quality.

In those cases of poor water quality, a treatment should be made of the supplied water before it is used in suspensions. The extent of treatment given to the water supply of a pulp and paper mill will depend upon the condition of the water as received and upon the

quality requirement of the product. The treatment may vary from simple screening to complete sterilization and demineralization. The modern trend is towards increased purification of the water supply in the interests of better machine operation, higher quality products and cleaner piping. The purification process consists of filtration, where water is passed through filter beds to remove suspended solids and coagulation, a series of colloidal chemical reactions used to flocculate the residual from the water before filtration in order to obtain more rapid filtration and improved clarification of water.

For many years, the paper industry has striven for more economical use of water. To date, remarkable progress has been made in this area. Most paper mills today operate their white water systems in such a way that each gallon of water is re-used several times before it is finally discarded from the mill. In a typical, well-closed white water system, 87% of the water is re-used. It is difficult to run a white water system completely closed because fresh water must be used for make-up purposes and for certain types of cleaning equipment where water containing any significant amount of suspended solids would be unsuitable. Such re-use of water permits the paper manufacturer to recover huge quantities of fiber, additives, pigments, and other paper-making chemicals which might otherwise add to the pollution of water sources (Winston, 1992).

One of the most important installations for the re-use of water and the recovery of fiber and pigment is the saveall system. Savealls are of three general types; each kind may have an advantage over the other systems, depending on the particular requirements. The sedimentation type of saveall consists of a large concrete or tile tank to which all waste waters are pumped. Suspended solids settle to the bottom from where they are removed for further processing. The vacuum filter saveall is a rotary vacuum drum which filters flocculated solids from the processing waters. Finally, the flotation saveall operates by continuously dispersing and dissolving air in the white water under pressure (Britt, 1964).

Following the widespread application of membrane modules in separation processes, a tubular membrane module has now been introduced to perform such separations. However, due to the blockage problem defined earlier the current use of such modules is limited.

1.1.4 Beating of the fiber

The fundamentals of the beating process have been well explained by Emmerton (1957), who found that when cellulose fibers are beaten in water and made into paper, the sheet characteristics change considerably as the degree of beating is increased. It has been observed that bursting and tensile strength, tearing resistance, and folding endurance rise to their maxima and then decrease with further fiber processing. However, the maximum for each occurs at strikingly different parts of the beating cycle. Tearing strength rises very quickly to a maximum with processing and then decreases sharply to a much lower level for the duration of the beating cycle. Bursting and tensile strengths, however, rise for a greater part of the mechanical processing and decrease much more slowly.

The following properties are known to be important in the beating processes for many types of papers and boards (Brett, 1964):

(1) the chemical and physical composition of the fiber;

(2) the fiber dimensions;

(3) the fiber strength;

(4) the filtration resistance of the fiber suspension in water, depending on

  (a) the hydrodynamic surface area of fibers; and

  (b) the swollen specific volume of fiber;

(5) the fiber flocculation;

(6) the bonded surface area between fibers in paper;

(7) the unbonded surface area of fibers in paper;

(8) the bonding strength per unit bonded area in paper;

(9) the distribution of fiber bonds in paper;

(10) the stress distribution in paper;

(11) the fiber flexibility or conformability in the wet condition.

It is apparent that many of these properties are interrelated and that the majority of them govern either fiber-to-fiber bonding or individual fiber strength.

1.1.5 Adhesion and fiber to fiber bonding

In the study of adhesion, it has been well established that secondary intermolecular forces determine the strength of the bond between contiguous cellulose fibers. Much scientific evidence supports the theory that the strength of the paper and the board depends primarily upon hydrogen bonding and other intermolecular bonds between fibers, and not upon mechanical entanglement and frictional effects between fibers (Brett, 1981, and Paaviaine, 1990). On the other hand, it was reported by Skowronski (1987) that bond strength increases with beating due to an increase in the total fibre-to-fibre bonded area.

1.1.6 Characterization of Paper Pulp Flocs

The quality of paper, as reported by Jagannadh (1991), depends on how well fibers are distributed in the final sheet. Non uniformity in a paper sheet is associated with both thin regions and flocs, i.e. regions of low and high fiber concentrations. It is not possible to define exactly what a floc is other than that it is a higher mass concentration of fibers at any point in the sheet. Jagannadh reported that flocs are expected to result from the dynamic interactions between paper fibers and the carrier fluid, primarily water, during the processing of the pulp at the wet end of paper manufacturing. These interactions are induced by the existing turbulent flow, which creates rotations and stagnation regions within the flow. Similar work has been done by Hourani (1988) on how to quantify the

primary effects (effect of flow on fibers) and the interaction effects (fiber to fiber and fiber to medium interaction effects) of selected factors on floc size distribution and on the uniformity of the fiber dispersion.

The modelling of fiber flocculation in turbulent flow was carried out by Steen (1991) who found that the flocculation intensity can be calculated using a transport equation holding source terms for both the rate of floc rupture and aggregation. The rate of floc rupture is proportional to the turbulent strain rate. The floc aggregation rate is proportional to consistency within the floc itself and the consistency in the surrounding regions. Bonano (1984) has undertaken similar modelling in order to study the dynamics of fiber floc breakup and formation in relatively concentrated fiber suspensions.

1.1.7 Flow characteristics and circular pipe flow of pulp-suspensions

Although the flow mechanism and rheological properties of pulp-suspensions greatly influence paper-making processes, they have not yet been understood sufficiently. Researchers have spent considerable time in examining the behavior of suspensions in circular pipe flow (Norman, 1977; Daily and Bugliarello, 1961; Meyer, 1964; Karter, 1966; Duffy, 1978; Mih and Parker, 1967; Durst and Jenness, 1959; Kurronen and Wahlstrom, 1974), Circular pipe flow of pulp-suspension has been classified into three flow steps: plug flow, mixed flow and turbulent flow. However, the hydrodynamics of the suspension at the inlet region of these circular tubes has only received cursory examination.

1.2 Ultrafiltration process using tubular membrane module

1.2.1 General overview of ultrafiltration

Ultrafiltration (UF) in general is primarily a size-exclusion-based pressure-driven membrane separation process. UF membranes typically have pore sizes in the range from

10 to 1000 Å and are capable of retaining species in the molecular weight range of 300 to 500,000 daltons. Typical rejected species include sugars, biomolecules, polymers, and colloidal particles. Most UF membranes are described by their nominal molecular weight cutoff (MWCO), which is usually defined as the smallest molecular weight species for which the membrane has more than 90% rejection (Winston, 1992).

Generally, the driving force for transport across the membrane in both UF and reverse osmosis (RO) processes is a trans-membrane pressure difference. Because UF membranes do not typically reject salts, osmotic pressure differentials are typically small compared to those found in reverse osmosis processes. UF processes operate at 2 to 10 bars, although in some cases up to 25 to 30 bars have been used (Winston, 1992).

Feed (liquid) phase mass transfer resistance and resistance due to gel layer formation on the membrane surface are extremely important effects in many UF processes. Consequently, system design and operating protocol are as important as membrane selection. Membrane selection is aimed at decreasing the fouling tendencies of the membrane surface. The base polymer surface chemistry can be modified in order to increase hydrophilicity, which increases the transmembrane flux and reduces fouling in most aqueous applications. In commercial modules, concentration polarization is decreased by increasing the fluid shear at the membrane surface or by inducing turbulence by the use of channel spacers (Winston, 1992 and Belfort, 1989).

1.2.2 Tubular membranes modules

Membranes with cylindrical geometry can be further differentiated by their bore diameters:

i) narrow-bore tubes (3 to 8 mm); and

ii) wide-bore tubes (10 to 25 mm).

Tubular membranes are usually cast in place within supporting tubes or can also be inserted into individual tubes. Examples of various tubular membranes can be seen in Figure 1. Feed normally flows through the bore of the tube, except in those instances where the membrane is coated on the porous tube exterior and feed flows though the annulus between the membrane and the external holder. The bore size required is determined by the size of the largest particulate in the feed. The tube's inside diameter should be at least ten times that of the particle diameter (Belfort, 1989).

Tubular modules have several disadvantages: low surface area/volume ratio, high flow rates requiring large energy consumption, and high holder volume. However, the ease of clean-up and their ability to withstand plugging can outweigh these drawbacks.

Cutaway view of various tubular systems.
Tube diameters are 0.5 to 1 in.
Membranes are cast into support tubes within PVC housings.

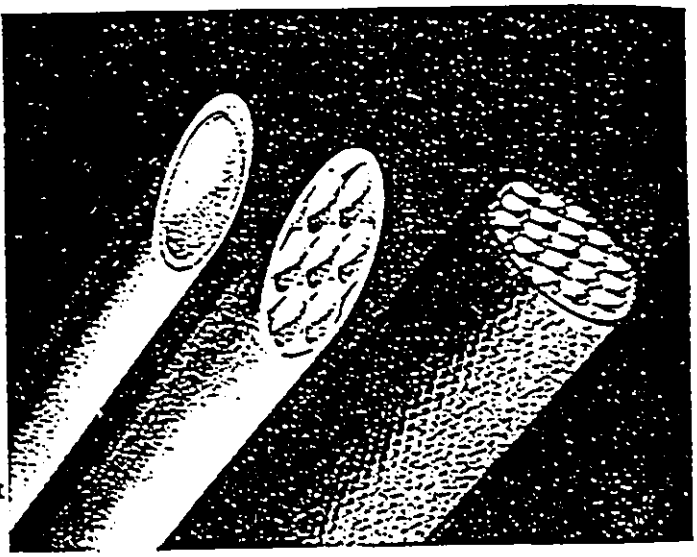

Ceraflo ceramic filter element containing nineteen 3-mm ID tubes
Feed flows through the bore while permeate travels through the microporous walls of the element into the surrounding shell for withdrawal.

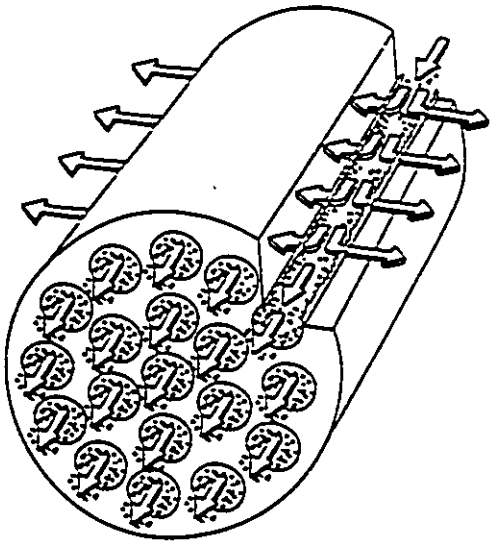

Figure 1: Various tubular membrane modules (Winston 1992).

1.2.3 Tubular module design

Figure 2 gives details of design of a module using three tubular integrally supported UF membranes, as reported by Sourirajan (1985). The module is suitable for industrial use involving low operating pressures (690 kPag or less); furthur, the number of tubular membranes within the module can be increased depending on the application needs. The module consists essentially of a cylindrical shell for housing the supported membranes through appropriate end plate connections. All parts of the module are preferably made of stainless steel material when high operation pressures are required.

Referring to the numbers indicated in Figure 2 (as reported by Sourirajan, 1985), the shell has a flange (2) at each end, which is bolted to the end plate through O-ring contacts; the shell has also suitably spaced openings for the removal of the membrane permeated product water. The end plate consists of two parts: an inner ring (3) which is bolted through O-ring contacts to the outer plate (1). The ends of the membrane tubes (6) are inserted into identical openings in the inner ring (3) and the outer plate (1). An end sleeve (4) is inserted inside each membrane tube to withstand the pressure of the O-ring. By bolting the two parts of the end plate with O-rings around each of the three membrane tubes, the latter are held firmly to the end plate. With the membrane tubes firmly in place, the end plate is inserted into the shell. The end plate and the flange in the can are then bolted together with O-ring contacts in-between. In order to keep the membrane tube rigid within the shell, a spacer (5) holding the membrane tubes in place is placed in the can at suitable space intervals. The end plate connections at each end of the shell are identical. By attaching a suitable header to the end plate, the module will be ready for operation with parallel feed flow through the membrane tubes. If series feed flow through the three membrane tubes in the shell is desired, it is only necessary to attach an additional header plate (7) to the outer plate (1) in the end plate. Thus the module is suitable for parallel or

series feed flow through the membrane tubes. Any number of such module units can be connected in series for large scale industrial operation.

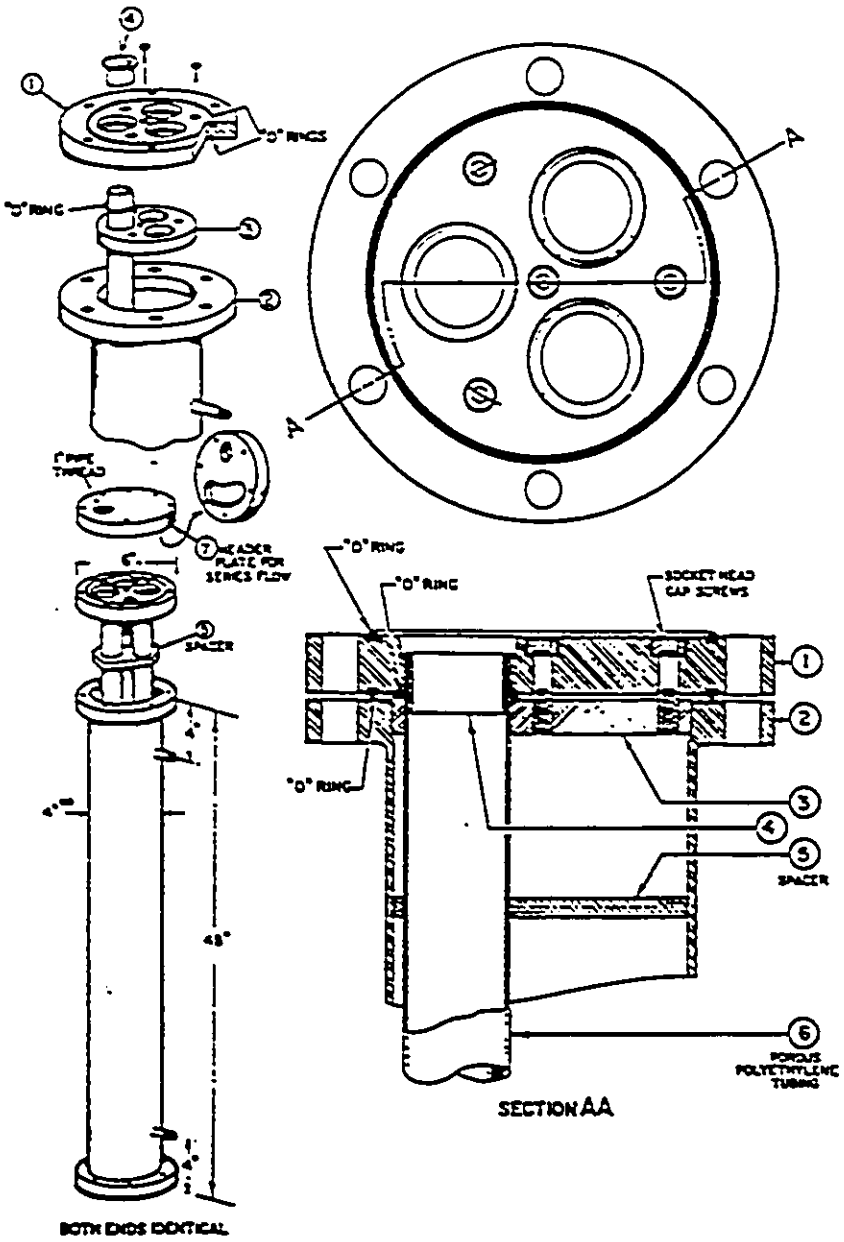

Figure 2: Details of design of a 3-tube UF module (Sourirajan 1985).

1.2.4 Applications of ultrafiltration membranes in pulp and paper industries

Many ultrafiltration applications are already being utilized by industry and others are being studied. Several important UF processes using tubular modules are tabulated in Table 1 (Winston, 1992; Belfort, 1989). One of the most widespread applications is in effluent treatment, where various waste streams are being successfully recycled.

The pulp and paper industry uses UF processes in several effluent control and product recovery applications. Lingnosulfonate separation from spent sulfite liquor and lignin and color removal from Kraft black liquor are applications still being developed that demonstrate some limited commercial use. Other effluent treatment by UF could include bleach effluent treatment, deresining of pulp wash water, whitewater processing for fiber recovery and de-inking effluent.

Table 1: List of some of applications where tubular UF modules are used (Winston 1992).

Process	Separation
Electrophoretic paint	Process rinse water, recycle paint to dip tank. allow reuse of rinse water
Cheese way	Concentrate/fractionate proteins from Lactose and inorganics
Juice clarification	Remove haze components from apple juice
Wine clarification	Remove haze components from red and white wines
Kaolin concentration	Partial dewatering of clay slurry before centrifugation
Water treatment	Concentration before Slurry dewatering
Reverse osmosis pretreatment	Retain colloidal silica, bacteria
Effluent treatment	Control effluent and product recovery reuse of rinse water

1.3 Thesis objectives

Since much research has been conducted on the hydrodynamic behavior of fiber suspensions inside a circular tube, and since the ultrafiltration of similar suspensions has always been problematic when a less then one inch module was used, this thesis was undertaken to examine the accumulation of fibers due to dephasing effects and the hydrodynamic behavior of similar suspensions in the inlet region of a tubular membrane module.

The early concern in this study was to design a prototype module. This module was to hold 5 tubes each of diameter less than one inch, where the inlet geometry of each was to vary from a smooth cylindrical entry to more conical shape entry.

The evaluation of some characteristic property of the prepared suspension was found to be an important factor in this study. In addition to the density, viscosity, and the fiber length distribution, the behavior of the fiber suspension in the turbulent regime was also evaluated. The influence of fiber length distribution on the stiffness of the dried sheet was also examined.

Finally, a mathematical relationship was developed which correlated fiber accumulation with all of the varied parameters.

CHAPTER 2: THEORETICAL BACKGROUND

2.1 General Flow Characteristics of Fiber Suspensions

The flow of fiber suspensions is a complex, mostly non-Newtonian phenomenon that varies greatly with the following factors (references containing further discussion of these effects are given where available):

- temperature (Stenuf and Calo, 1975);
- properties of the matrix, especially its viscosity and density (Kerekes, 1972);
- volumetric concentration of the fibers and other suspended materials;
- fiber dimensions, length, width and thickness (often expressed as length plus axis ratio);
- fiber density and settling;
- fiber flexibility and non-uniformity along the length of the fiber (Jeffrey, 1922 and Mason, 1950);
- size distribution of fibers (Paavilaine, 1990);
- fiber uniformity (Paavilaine, 1990);
- fiber entanglement and inter-fiber friction;
- inter-fiber attraction or repulsion, surface action, and bonding (Skowronski, 1978);
- flocculation resulting from the above interactions (Hourani, 1988);
- shear forces (Duffy, 1975);
- turbulence;
- wall friction; and
- the presence of flocculation agents, deflocculants, and electrolytes (Chang, 1967).

There are great similarities between the rheological behavior of fiber suspensions and that of long chain polymer solutions. While the dimensions of these two systems differ by several orders of magnitude, their rheological and geometrical similarities are both so

great that it is reasonable to consider fiber suspensions as macroscopic analogs of polymer suspensions.

The hydrodynamic behavior of fibers of various flexibility was first reported by Mason and coworkers (1950; 1954; and 1956). In a shear field, single stiff fibers were found to behave according to Jeffrey's theory (1922), rotating about the axis with a characteristic period of rotation T in an x-y plane:

$$T = \frac{2\pi A'}{\beta G}, \tag{1}$$

where x is the direction of flow, y is the normal to the planes of shear, A' is the axis ratio of the fiber, G is the velocity gradient dv/dy along y, and β is a shape factor (1 for prolate ellipsoids, 1.4 for rigid cylinders, and 1.4 to 2 for $20 < A' < 120$ respectively).
In this case the axis ratio A' is defined as

$$A' = \frac{\pi l'}{2wt'}, \tag{2}$$

where l', w and t' are the fiber length, width, and thickness respectively. The rotations of fibers of various flexibility suspended in a shear field are shown in Figure 3.

The rotation of a rigid fiber of class 1 is at a minimum when parallel to the direction of flow and at a maximum when perpendicular to it. In Quadrant 1 the entire fiber is at first parallel to the direction of flow and moving at one velocity. As the fiber rotates into Quadrant 2 it experiences a velocity gradient. The shear field rotates the fiber while exerting an axial compressive force on it. In Quadrant 3 the compressive force is removed while the ends of the fiber are subjected to the greatest velocity difference, so that a maximum rotation rate results. In Quadrant 4 the rotation decreases while the fiber

is subjected to axial tension. Quadrant 5 is the same as Quadrant 1, with the fiber turned 180° while shear forces that tend to rotate the fiber reach a minimum. Thus each fiber is aligned in the flow direction causing general flow alignment of fibers in the shear field.

Fibers of classes 2, 3 and 4 are progressively more flexible and are deformed by the shear field. The change of shape of each fiber is a function of flexibility and uniformity. In natural fibers, weak points due to pores, pits, or mechanical damage caused by beating produce hinges or knees. Synthetic fibers usually lack such non-uniformities. Natural fibers also differ from synthetic fibers in that they have a hollow centre called a "lumen." The lumen causes thin-walled fibers such as softwood springwood to collapse upon drying. The original shape is rarely restored on rewetting.

Mason and coworkers (1956) produced and studied motion pictures of fibers in a shear field between concentric cylinders that rotated in opposite directions. Mason's work laid the foundation for our current understanding of the hydrodynamics of fiber suspensions. While rigid fibers in a shear field rotate in the same orbit indefinitely or until they collide with another particle, flexible fibers undergo a complex pattern of continually modified paths.

An investigation of the stiffness of wood fiber showed that the removal of lignin from wood pulp changes the distribution of the orbital class as defined in Figure 3. High yield pulp (wood fiber with lignin) consists almost entirely of class 1 "rigid" fibers. Class 2 "springy" fibers peak at about 70% yield, while class 3 "snake turn" and "loop turn" and class 4 "complex" fibers become predominant as more lignin is removed.

The flexibility and the type of rotation of fibers are obviously a function of length as well as axis ratio. This was observed when rayon fibers of uniform diameter and various lengths were suspended in various shear fields. Short fibers of axis ratio $A' < 120$ rotated stiffly according to class 1 behavior. Longer fibers ($120 < A' < 240$) exhibited mainly class 2 behavior. Axis ratios greater than 240 result in flexible class 3 and 4 behaviors. The

period of rotation decreased abruptly with an increase in the fiber axis ratio to around 250. This sudden change in the period of rotation clearly separates the stiff fibers from the longer, flexible fibers.

Mechanical work, or "beating", of wood fibers increases flexibility not only by creating hinge points but also by relaxing internal stresses in the fiber wall and allowing water to move into interstices opened between concentric lamellae of the fiber wall. In this state, fibers swell radially with water. The increased diameter leads to increased stiffness. However, in the swollen fiber, individual lamellae are free to move axially over each other and, being thin, buckle under compressive stress on the concave side of the fiber. The fiber thus becomes more flexible in spite of its larger diameter. The fact that stiff fibers rotate at the lowest rate when parallel to the axis of flow is extremely important in the paper industry where fiber suspensions are ejected through a slice onto a moving wire screen. Suspensions of cellulose fibers are the most common fiber suspensions encountered in present-day technology. Not surprisingly, most of the available literature on this subject is from the pulp and paper industry.

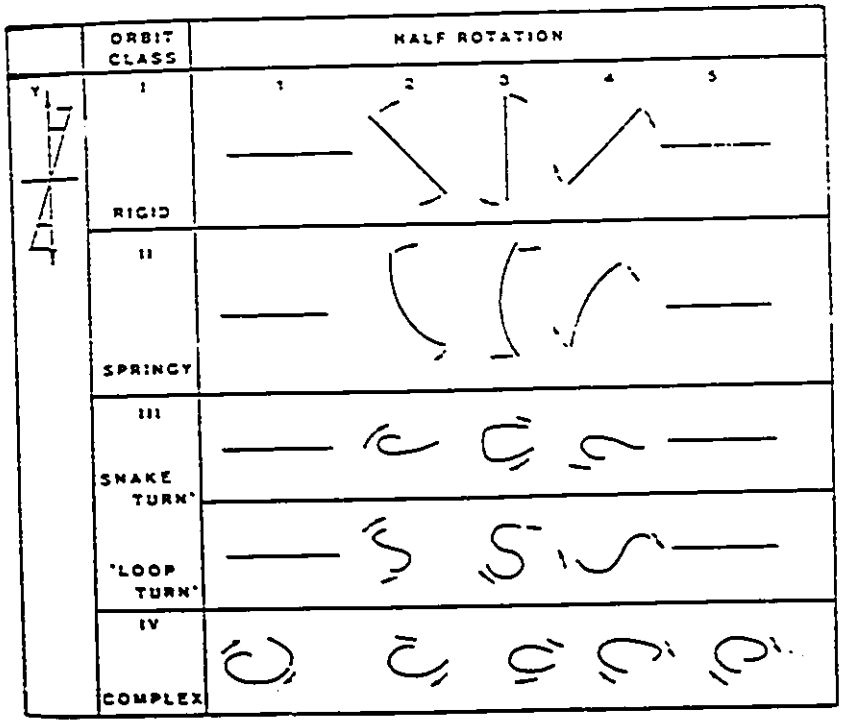

Figure 3: The rotations of fibers of various flexibility suspended in a shear field (Cheremisinoff, 1986).

2.2 Factors Affecting the Flow of Fiber Suspensions

2.2.1 Fiber properties

The relevant fiber properties affecting flow include length, axis ratio, branching uniformity, flexibility, fiber to fiber friction, hydrodynamic specific volume and specific surface area, flocculation and density. Paavilainen (1990) found that when using fiber length to characterize softwood Kraft fibers (common to the pulp & paper industry), it should be recognized that, with regard to paper-making potential, the fiber length distribution is from two different sources: fibers and fines. As the cell wall thickness and process conditions affect both fiber shortening and fines formation, special attention must be paid to the methods used to characterize fiber length and fines. It was found that fines play an important role in fiber-to-fiber bonding through Campbell's forces (the attraction force between fibers) and may also distribute local stress concentrations over the whole bond surface. Fines also improve the tensile strength of summerwood pulp to the extent that the removal of fines reduces tensile strength as much as does a reduction of the fiber length to that of its original value.

2.2.2 Presence and interaction with other suspended matter

Air bubbles, dirt, pigments and other additives can affect the flow of fiber suspensions. Since 1965 polyelectrolytes have been introduced into the paper industry as coagulants and flocculants to improve the retention of fines. Coagulants as reported by Kerekes (1983) reduce the repulsive force between the negatively charged surfaces of cellulosic fibers by adsorbing on them oppositely charged ions from an electrolyte ($MgCl_2$, NaCl, $Al_2(SO_4)_3$, etc.). This is called "charge neutralization." If the surfaces can consequently approach each other closely enough they can be held together by van der Waals forces and produce a floc. Certain polymers can also serve as deflocculants or

"formation aids" in papermaking. Nonionic materials increase the viscosity of the matrix and inhibit entanglement of fibers.

2.2.3 Forces acting on the system

These forces include pressure, gravity, shear and turbulence. Shear and turbulence are distinguished here because the flow properties depend greatly on the history of the suspension, so that measurable differences exist between steady flow in a pipe and flow downstream of a pump and downstream of fittings (Francis 1992).

Due to gravitational forces fiber suspensions have high ability to sediment. If various fibers are dropped into water they sink to the bottom, occupying a volume similar to that of the same aggregate in air. On stirring, these fibers are dispersed. Stiff glass fibers disperse poorly and, after agitation ceases, settle to the bottom occupying almost the same volume as before. Nylon fibers and wood fibers, in contrast, disperse readily, fill the vessel with a uniform dispersion for an appreciable time after stirring stops, and slowly settle to a sedimentation volume that is considerably larger than its volume before dispersion. Longer fibers settle to a larger sedimentation volume than short ones. In each case shear forces tend to disperse the fibers. The glass fibers do not interact significantly, while nylon and wood fibers form continuous networks that withstand sedimentation (Cheremisinoff, 1986).

2.2.4 Interaction of fibers in flowing liquids

Fibers orbiting in shear flow sweep out a much larger volume than their own. When these orbitals intersect fiber interactions result. Mason introduced the concept of "effective volume" which he considered to be the statically averaged shape of the described orbit. The concentration at which the sum of the swept volumes equals the whole volume is called "the critical volume concentration." The critical concentration C_o

of a suspension of cylinders in spherical orbit, where the sum of the effective volumes is equal to the total volume, is given by

$$C_o = \frac{3}{2A^2 \alpha'} \qquad (3)$$

where α' is fiber specific volume. The spherical orbit just assumed is the extreme case that applies only in turbulent flow. It gives a lower limit for the critical concentration of 0.00125 to 0.00014 g/cc for cellulosic fibers of axis ratios from 20 to 60 respectively, assuming the specific volume of the fibers to be 3.0 cc/g, a typical value for paper pulp. In a one-dimensional shear field, the volume generated by the rotating particles is smaller and can be represented by a double cone. The calculated value of C_o is then about 1/4 of that described above.

Cylindrical particles rotating freely in a shear field transfer momentum from regions of high velocity to regions of low velocity. This momentum transfer manifests itself as additional viscous drag proportional to the shear rate. The viscosity of the suspension thus increases with concentration and axis ratio until the critical concentration is reached. Above this concentration fibers interlock and form rotating aggregates called "flocs" which in turn rotate freely.

2.2.5 Surface roughness of the pipe

The pipe friction curves for fiber suspensions have several distinctive features that are characteristic for each concentration of a specific composition. Extremely low concentration fibers exhibit rotations and statistical alignment during laminar flow as already described and fairly random dispersion in turbulent flow. At the "moderate" concentrations (0.3-4 wt. %) normally used in the paper industry, a "plug" (fiber network) forms and a finite pressure (yield value) must be applied before flow begins. When the

mean velocity is increased, the pressure loss per unit length of pipe increases to a maximum value, then frequently decreases to a minimum value, and drops below the friction curve for the suspending medium in the turbulent flow range. Thus the pressure loss for the suspension is greater than it would be for the Newtonian matrix at low velocities, while at high velocities drag reduction leads to a pressure loss that is lower than that for the matrix. At very high concentrations, the fibers absorb all or most of the suspending medium so that the fibers actually become the "matrix" and their movement resembles the conveying of solids.

Finite difference solutions have been obtained for the equation of flow for dilute suspensions of high aspect-ratio fibers in Newtonian fluids through an axisymmetric circular concentration by using the continuum theory, which includes a statistical average velocity with respect to the orientation distribution function of fibers. The presence of fibers drastically changes the tubular entry flow field; the corner vortex grows as the volume fraction and/or aspect ratio of fibers increases, as reported by Chiba and Nakamura (1990). These investigators also found that the vortex length decreases with an increase in the Reynolds number due to fluid inertia. It has been confirmed that the growth of the corner vortex with increasing $\phi\mu/\eta$ (where η is the viscosity of suspending Newtonian fluid, ϕ is the volume fraction of fibers, and $\mu$is a material constant) suppresses the increase in the first normal stress difference along the centerline, i.e. the enhancement of the vortex results in the so-called stress relief phenomenon in axisymmetric converging flows of rigid fiber suspensions.

It was also reported that, as $\phi\mu/\eta$ increases, the vortex boundary changes from a straight interface to a convex with its center of rotation and the main flow becoming nearly conical. These flow patterns for rigid fiber suspensions present a striking contrast with the wine-glass shape pattern observed for flexible molecule systems. Furthermore, as reported by Boger et al. (1990) while flexible molecule systems show significant vortex

enhancement with flow rate, the vortex length of rigid fiber suspensions is almost independent of flow rate, provided that the Reynolds number is not greater than unity and that inertia is not an important variable in flow. Thus, not only is the particle aspect ratio and concentration important in understanding the kinetics of entry flows but also, it would seem, is the flexibility of the fiber itself.

2.3 Suspension viscosity and fiber characteristics

The viscosity of fiber suspensions is directly related to the nature of the fibers and its blending procedure. Suspension viscosity also depends on the solvent and other additives to the solution. Branderberg (1993) reported that variations in agitation and pH levels result in measurable changes in the dispersion of particles within white water systems. Fiber dispersion quality (the degree of fiber dispersion) deteriorates with water containing calcium ions such as those found in hard water. Care must be exercised when adding fresh water containing calcium to a white water system. Dispersion is much less affected by soft water or water containing principally sodium ions.

Live microorganisms also impact on the viscosity of a white water system but do not affect the dispersion quality. Dead microorganisms increase the viscosity to a greater extent and interface was occuring with the dispersion of glass fibers.

Chase (1989) showed that the viscosity of hardwood pulp suspensions increased linearly with consistency and decreased with freeness (when water is drained through a forming mat or sheet of fibers, the resistance of the fibers to the flow of water is the freeness). The viscosity of softwood pulp suspension similarly increases linearly with consistency. At high consistencies, the viscosity initially increased and then decreased with a decrease in freeness.

Zhao (1993) reports that the uniformity of fibers suspended in a liquid of increasing shear viscosity has been shown to improve dramatically, reaching levels of near

perfect uniformity at a concentration in which water alone would yield gross flocculation. A possible mechanism has been presented, based on decreased relative motion among fibers resulting from decreased turbulent motion of the fluid and higher shear forces on fibers. The decreased turbulent motion resulted from decreased initial turbulence and faster decay of higher viscosity fluids.

2.4 Modeling the flow of pulp suspensions in pipes

During the modern development of membrane separation processes, early workers recognized the intimate relationship between mass transfer and convective fluid flow. Since mass transport to a membrane surface is dependent on the fluid flow above the surface, clearly, a detailed understanding of the fluid mechanics in various ducts (slits, tubes and annuli) is prerequisite to studying mass transport problems such as concentration polarization and fouling.

2.4.1 Flow regimes

A study done by Myreen (1989) developed the typical pressure drop versus mean flow velocity curves for water and a chemical pulp suspension in a 100 mm pipe. In the case of water, the pressure drop is proportional to the mean flow velocity in the laminar regime and, after passing a transitional regime into the fully developed turbulent regime, proportional to the mean velocity squared. However, the pressure drop for a typical pulp suspension shows quite a different behavior, characterized by the four flow regimes outlined below.

At low mean flow velocities, the pattern is similar to laminar water flow but the curve has a lower slope. In this regime, the fibers are in contact with the pipe wall.

At a certain critical velocity, the flow enters a transitional regime in which the pressure drop decreases with increasing flow velocity. The decrease is typically observed

for unbeaten chemical pulps but not for mechanical pulps. In this regime an annulus consisting of water essentially free of fibers is formed along the pipe wall and the suspension flows as a plug inside this annulus.

At a still increasing flow velocity, the pulp pressure drop curve approaches and may cross the turbulent water curve, particularly for suspensions at a low consistency. In this regime, the suspension pressure drop increases parallel the turbulent water pressure drop. The suspension flow pattern is typically plug flow with an annulus of suspension with an essentially lower consistency than in the plug.

When the flow velocity is further increased, the plug is suddenly disrupted. At this point the consistency gradient disappears and the suspension behaves as a turbulent homogeneous liquid. The flow velocity at which this phenomenon occurs is usually much higher than the turbulent transition normally experienced by water in pipelines.

Hydrodynamic theory in regime 1

According to general hydrodynamic theory, the pressure drop per unit length of pipe is given by

$$\Delta p = \left(\frac{2}{R}\right)\tau(R), \tag{4}$$

where R is the pipe radius and $\tau(R)$ is the shear stress at the wall. The same formula applies for a coaxial fluid element of radius r,

$$\Delta p = \left(\frac{2}{r}\right)\tau(r). \tag{5}$$

A combination of these two equations gives the radial distribution of shear stress in the fluid:

$$\tau(r) = \left(\frac{r}{R}\right)\tau(R). \qquad (6)$$

So far no assumptions have been made regarding the rheology of the fluid. If the fluid is pseudoplastic then,

$$\tau(r) = k\left(\frac{-dU}{dr}\right)^n, \qquad (7)$$

where U is the flow velocity with the flow direction perpendicular to the r direction at this point, k is a dimensional constant and n is a dimensional constant typical for the fluid. (If the fluid is Newtonian one, n=1 and k= dynamic viscosity)

In this case

$$\frac{r}{R}\left[\tau(R)\right] = k\left(-\frac{dU}{dr}\right)^n. \qquad (8)$$

By setting

$$B = \left(\frac{\tau(R)}{k}\right)^{\frac{1}{n}} R, \qquad (9)$$

and

$$z = \frac{r}{R}, \qquad (10)$$

we can write

$$dU = -Bz^{\frac{1}{n}}dz \tag{11}$$

to yield

$$U(z) = \frac{n}{(n+1)}B\left(1 - z^{\frac{(n+1)}{n}}\right). \tag{12}$$

By relating B to the mean flow velocity U_m as $\left(\frac{Q}{\pi R^2}\right)$, where Q is the volumetric flowrate, and after substitution, one can write that the velocity profile is

$$U(z) = \frac{3n+1}{n+1}U_m\left(1 - z^{\frac{(n+1)}{n}}\right). \tag{13}$$

The pressure drop per unit length is then

$$\Delta p = 2\left(\frac{3n+1}{n}\right)^n kU_m^n R^{(1-n)}. \tag{14}$$

Hence a relationship between the pressure drop and velocity of a dilute suspension when the characteristics of the fluid (behavior indice n, and consistency indice k) are known.

Hydrodynamic theory regime 2 and 3

In these instances, the local concentration of the pulp fiber increases as the radial position approaches the pipe axis and is referred to as the Magnus effect (a domination of higher concentration at an optimum location far from the walls) on the pulp fibers. The values of the concentration can be recognized to be the cross-average values of the local concentration (i.e., the average concentration in a cross-sectional area). The viscosity of the pulp suspension at a given radial position is different from that at another position according to the local concentration of the pulp fiber. However at every radial position the suspension behaves as a Newtonian liquid with respective local viscosity.

The plug flow of the pulp suspension is investigated by measuring the pressure loss, the velocity at the wall and the local velocity. Though the pulp suspensions are considered to be Newtonian liquids, from the experimental measurements of the pressure loss and the flow rate and of the shear stress and the velocity gradient at the wall, the experimental relation between the velocity gradient at the pipe wall and the flow rate is not the same as for Newtonian liquid. In fact

$$\Delta P = \zeta_d \frac{1}{2} \rho_f U_m^2, \tag{15}$$

where

$$\zeta_d = 0.0089 \frac{\delta^2}{x} \tag{15a}$$

This equation is recognized as the standard formula for calculating the pressure drop per unit pipe length for homogeneous flow. However, the formula in this case was derived by assuming plug flow surrounded by a laminar film of Newtonian liquid. For a Reynolds number of approximately 10^6, which is typical (i.e., turbulent flow), the friction factor has a value of 0.011 in smooth pipes.

At low consistencies the film thickness tends to increase quite rapidly with increasing flow rate. This leads to reduced shear stress in the film at the wall and

consequently to the reduced pressure drop per unit pipe length, typical for some pulps in flow regime 2. When the film thickness has reached its maximum the flow enters the flow regime 3 and the pressure drop increases with increased flow velocity.

Hydrodynamic theory in Regime 4

Introducing solid particles in a turbulent flow field will modify the turbulent structure (length scales, intensities) based on the particle size and density. The form of fiber suspension in this regime is continuously modified through the break-up and reflocculation process . Free fluid eddies can only exist in the strong shear (high vorticity) small scale regions between flocs. Depending on the degree of crowding factor, free fibers can rotate and create extra energy at scales of the order of the fibers' size. While the first mechanism is likely to happen in the core, the latter is more pronounced in the wall region (Steen, 1989).

The eddies are entrained by the flow and, at a certain distance from the particle, they disappear while being replaced by new eddies. Due to eddy formation and their breaking away from the particle, a low-pressure zone forms at the front of the particle. Hence, as described earlier, a pressure gradient is formed between the front and rear of the particle. This gradient is responsible primarily for the resistance to particle motion in the medium. The amount of this resistance depends on the energy expended toward eddy formation; the more intensive this formation, the greater the energy consumption, and hence, the greater the resistance force. The inertial forces generated by eddies play an important role. They are characterized by the mass and velocity of the fluid relative to the particle.

2.4.2 Reynolds number-friction factor relationship and the evaluation of suspension viscosity

Under the assumption that flow characteristics of the pulp suspension are uniform in a circular pipe, Ogawa (1990) found that suspensions with a concentration below 1% in weight behave as Newtonian liquids in the laminar regime and that it is possible to determine the viscosity based on Hagen-Poiseuille law:

$$\mu = \frac{\left(\frac{\Delta P}{L}\right)\pi R^4}{8Q}. \tag{16}$$

where the Reynolds number is defined as,

$$\mathrm{Re} = \frac{2\rho u R}{\mu}. \tag{17}$$

In this case u is the cross-average velocity and R is the pipe inner radius. The friction factor then is calculated as the ratio of 16 over the Reynolds number. In the turbulent regime, the friction factor-Reynolds number relation is more complicated, particularly if the fluid behaves as a non-Newtonian liquid, as discussed below.

The fanning friction factor is defined by

$$f = \frac{2\tau_R}{u^2\rho}. \tag{18}$$

When neglecting the wall effect (u_R=0) τ_R is then given by

$$\tau_R = K'\left(\frac{4u}{R}\right)^{n'}, \tag{19}$$

n' and K' are fluid parameters which depend on the sheer at the wall of the pipe. After substitution, the Reynolds number in the turbulent regime for non Newtonian fluids derived by Dodge and Metzner (1959) is given by,

$$\mathrm{Re}' = \frac{D^{n'} u^{2-n'} \rho}{8^{n'-1} K'}. \tag{20}$$

Dodge and Metzner also derived an extension of that formula and postulated a general relationship between the Reynolds number and the friction factor that is applicable in the turbulent regime for non-Newtonian liquids in two complimentary equations as

$$\frac{1}{f^{1/2}} = \frac{4}{n'^{0.75}} \log[\mathrm{Re}'(f)^{1-n'/2}] - \frac{0.4}{n'^{1.2}}, \tag{21}$$

and,

$$\mathrm{Re}' f^{(1-n'/2)} = \frac{D^{n'} \rho^{n'/2} \tau_R^{1-n'/2}}{2^{(3.5n'-4)} K'}. \tag{22}$$

These equations can be used to evaluate the behavior of a liquid in the turbulent regime, by evaluating n' (n'=1 Newtonian fluid).

2.5 Application of the ultrafiltration process

During the development of modern membrane separation processes, workers recognized early on the intimate relationship between mass transfer and convective fluid flow. With the appearance of a comprehensive essay dealing with momentum, energy and

mass transport, models of varying complexity were developed that linked convective fluid flow and mass transport for pressure-driven membrane processes. Although membranes have been packaged in pressure modules of various designs, in the majority of modules the feed solution moves across the membrane in tangential flow (also called cross-flow), allowing fluid to be removed laterally by suction through the duct or channel walls. It has been known for some time that the performance of a pressure-driven membrane process is related to the tangential fluid mechanics across the membrane surface and that the build-up of dissolved solutes, or concentration polarization, can be predicted and controlled at the membrane-solution interface through an understanding of the fluid mechanics and mass transfer. However, until recently, very little theoretical analysis had been undertaken on the effect of even dilute suspensions on membrane performance.

The pulp and paper industry is one of the major industries where UF has been applied to treat effluent consisting of suspensions. Effluent treatment by UF could include bleach effluent treatment, deresining of the pulp wash water, recovery and reuse of the chemicals spent during the Kraft process of pulping where the chemicals are separated from the pulp at the washing stage along with wood residue, and white water processing for fiber recovery. During these processes, the behavior of the suspension in the entrance region of a tubular membrane has been typically problematic. Any module having tubes with an inside diameter less than 1 inch was unusable because of the blockage of the inlet tubes due to an accumulation of dewatered fiber. This fouling is caused by the formation of vortices on the dead spot between the entrance holes, resulting in a drop in the inlet velocity to the membrane and an increase in the pressure drop at the entrance zone (Belfort, 1989).

One of the most interesting applications was carried out by Marrov (1992) who found that the flux of a dextran solution may be improved by introducing different inserts into tubular ultrafiltration modules. The introduction of inserts with variable cross-sectional

areas results in a non-uniform field of tangential stress and thus interrupts the formation of a gel layer. Inserts with cone-shaped repeating units performed even better than smooth cylindrical ones.

Another interesting application was undertaken by Spiazzi (1993) who introduced a new generator of pulsatile flow that consisted of a rotating distributor disc judiciously perforated and placed in front of the entrance plane of a tubular membrane bundle. The disc reduced the cross flow velocity by 50% while keeping the same power consumption per unit permeate flux as required for steady cross-flow filtration.

Arising from the high legislative demands and consumer pressure for green ecolabelling, paper-making processes today must utilize various pollution control techniques, ultrafiltration being one of them. Therefore the importance of solving the current problems that delay the use of such applications in the pulp and paper industries is growing, providing the thrust for this project.

CHAPTER 3: EXPERIMENTAL DESIGN

For this project, it was necessary to design two cells: the module header cell and the burst tester cell. The module header cell was a prototype of the tubular membrane module in which the permeable tubes were replaced by regular non-permeable tubes. This cell was required to study the hydrodynamic behavior of fiber suspensions at the inlet zone of the tubes. The burst tester cell was essential for the determination of the pressure required to burst a sheet of Kraft board. In this chapter, design constraints will be considered for both cells.

3.1 Main test cell

3.1.1 Design considerations

In this research, the hydrodynamic behavior of the pulp suspension at the inlet zone of a series of tubular membranes was studied. Hence, one of the main objectives of the research was the design and construction of a prototype of an existing module. The ideal prototype would hold tubes of a diameter of less than one inch (the minimum criterion of an existing application). From a design perspective, it was particularly worthwhile to focus on possible complicating factors typical in tubular membrane modules, such as a header design which could reduce dewatering of the pulp. Since the research focus was on the behavior of pulp suspensions at the inlet region of the tubular membrane series and not on the performance of the membrane itself, the tubular membranes could be replaced in the prototype by normal tubes to simplify the apparatus.

3.1.2 Design constraints

The first sketch of the main cell is shown in Figure 4, illustrating the division of the main cell into three distinct parts: the top part called the distributor header chamber, consisting of an inlet tube of 1" diameter which expands to a 3"-long tube with a 6" inner

diameter and providing a total volume of 1.2 liters; the end part, which holds the tubes together; and the middle part called the distributor header plate, which is an exchangeable disk with a diameter equal to that of the expanded tube that lies on top of the end part to provide smooth entry. All three parts are connected to each other by four long screws that are attached to the top part and to the end part following installation of the disk on top of the tubes.

The first design criterion to be addressed was the selection of cell dimensions, namely the total number and inlet diameter sizes of the tubes, their location on the disk, and the thickness of the disk. The determination of which dimensions should be kept constant during the construction of the various headers was the most critical aspect of this design. Since the main objective of this research was to study the influence of the inlet geometry of the tubular membrane module, the space between the center of the tubes was selected to be equidistant for all different shape entries. In addition, the space located between the center of the disk and that for the tubes was to be fixed and equal. The geometry of the inlet of the tube was changed by varying a deviation construction angle, also called the inlet angle α . The angle α resulted from the deviation with the vertical orientation of the tube which is normally equal to zero. The entry then follows a smooth normal cylindrical geometry; hence, any deviation will lead to a more conical shaped entry.

As discussed earlier, all industrial applications have used membranes with an inside diameter of 1"; any application employing membranes with a smaller inner diameter have tended to be problematic. Examining the worst case scenario, tube inlet diameters of 1/2, 1/4, and 1/8" respectively were chosen for each of the three inlet angles selected: zero referring to an existing form, 30° and 45° designating the two other conical shapes. Consequently, nine Plexiglas disks in total needed to be constructed. Plexiglas material was the ideal choice since it allowed for clear observation and effectively prevented corrosion. The single remaining unknown to be considered was the number of tubes

required. In order to determine this, a standard hydraulic theory, which yields a proportional relationship between the surface area of the inlet tube and the surface area of the total outlet tubes, was applied. The average number of tubes with an inlet diameter of 1" was 5, all sealed to the end part of the cell. For an industrial application, this number was not significant, but for bench-scale purposes, it was considered sufficient.

Each of the nine disks was of 3" thickness and 6" diameter. They were placed on top of the tubes and pierced with a series of five holes, each of which was at the same distance from the center and was equidistant from the others, as discussed earlier. The diameter of each hole was equal to that of the tubes. Three disks were made for each of the inner tube diameters discussed above. One disc was left as is, to be defined with zero angle of deviation while the other two required some changes to produce a conical shape with different inlet angles. For that reason, the other two discs were modified as follows: to create a conic shaped entry hole, the hole was shaped using 0.5" from the top as the departure point for deviation angle α (30, 45 degrees respectively). An extra disk was made for the 1/4" application with an angle α of 55 degrees. Figures 5 and 6 represent the top and cross-sectional views of the designed disks.

The other design criterion addressed was the allocation of the pressure ports along the cell. To determine this, it was necessary to pre-determine the needs for similar pressure tracking locations on the cell. Since the objective of this study was to investigate what would occur in the entry region of the tubes, two pressure ports were installed on the surface of the disk, one at the centre and the other in the mid-space between the wall of one of the tubes and that of the cell. These ports can be clearly seen in Figure 7 as ports 2 and 3 respectively. Port 2, located at the centre of the disk, is needed to indicate the pressure at which the flow splashes and fills the void volume of the cell. Port 3 is used for vortex pressure tracking purposes because, from a design perspective, the main vortex is predicted to occur in that dead surface. Port 1 was located on the centre of the wall of the

first part while ports 4, 5, and 6 were installed from top to bottom along one of the tubes to track the pressure inside the tube. The reference pressure port was located at the inlet tube of the cell.

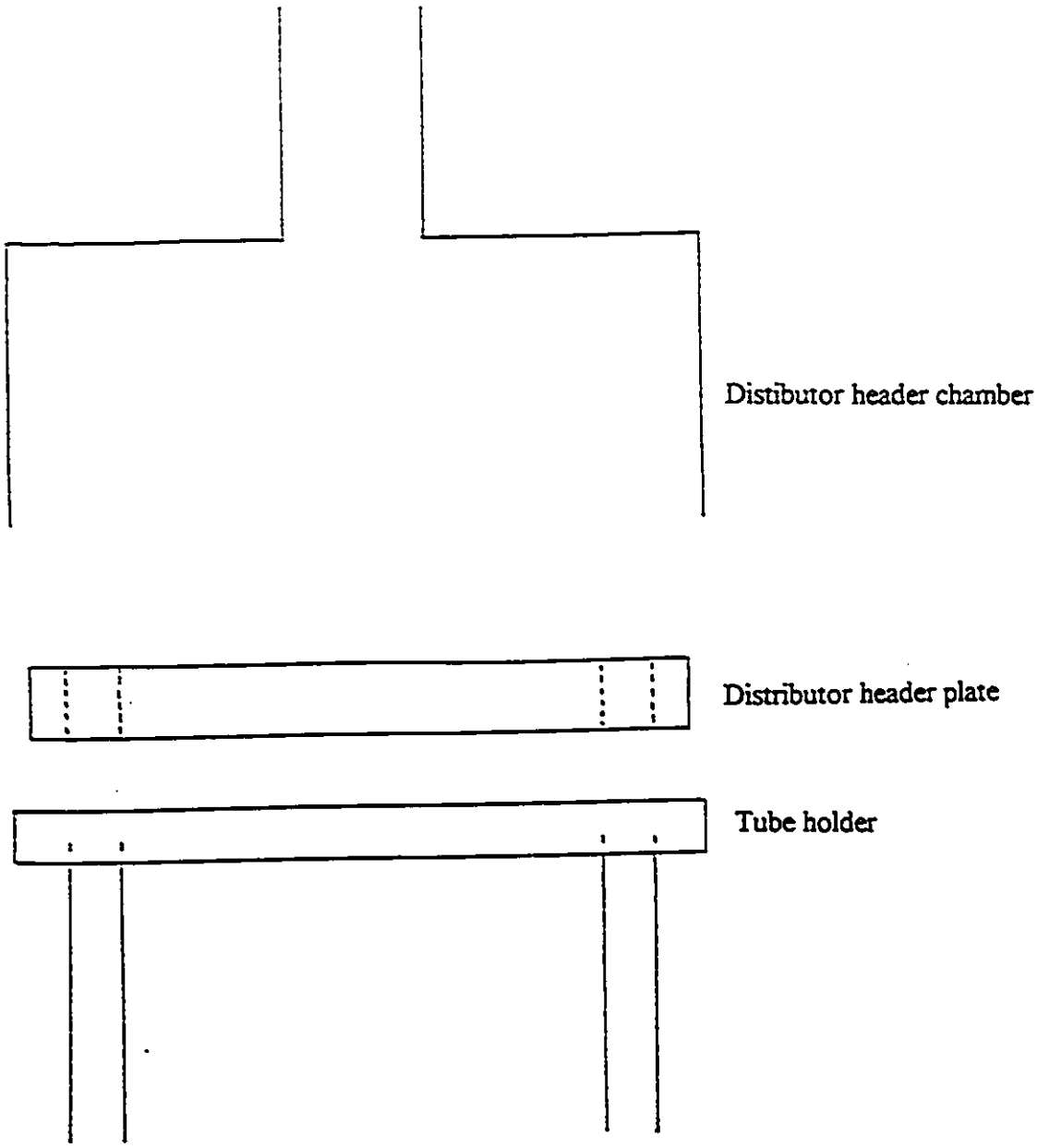

Figure 4: Schematic diagram of the main cell: early sketch in 2 dimensions.

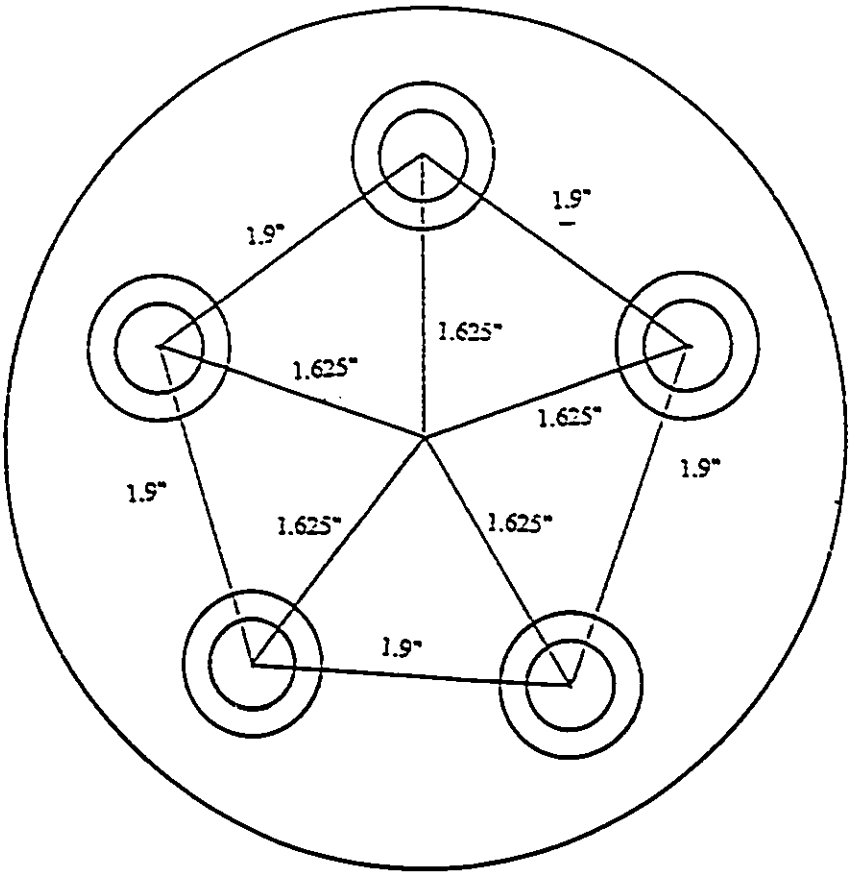

Figure 5: Schematic diagram of the top view of the header plate.

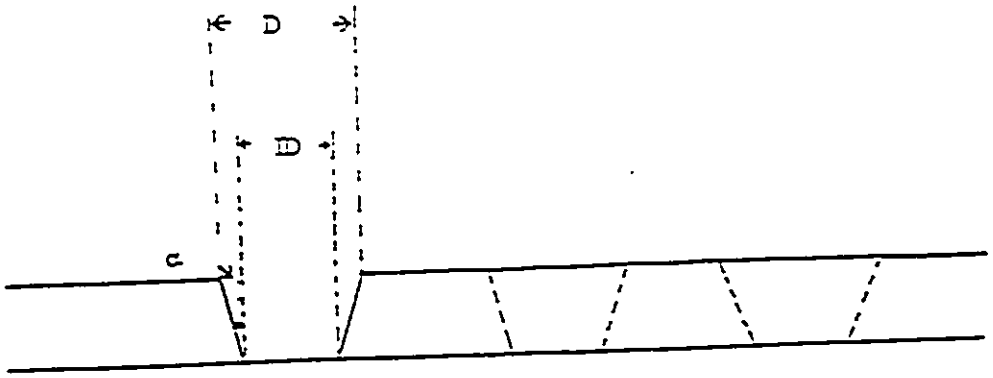

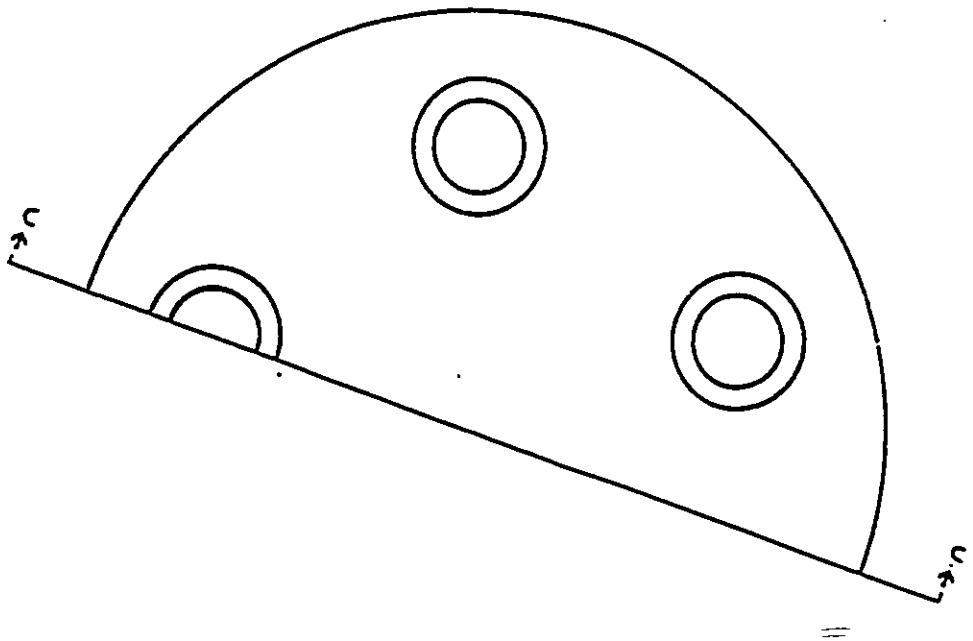

Figure 6: Shematic diagram of the cross-sectional view of the header plate.

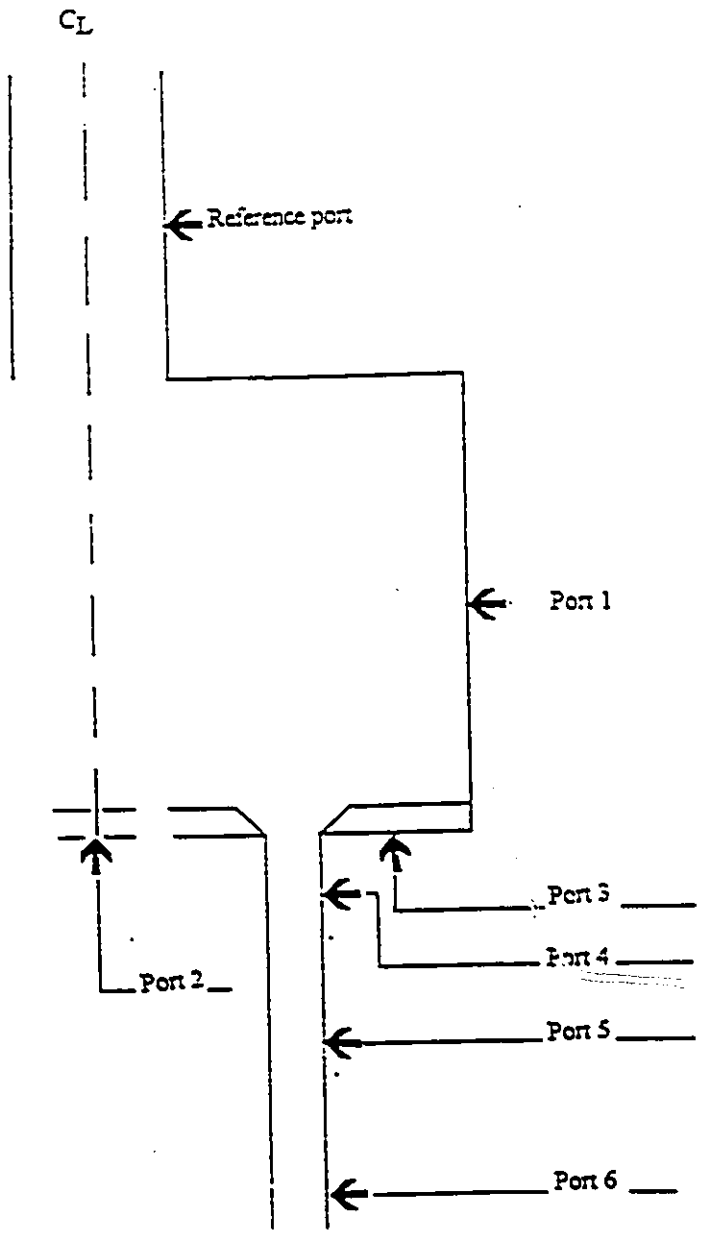

Figure 7: Schematic diagram of the pressure port location along the prototype module.

3.2 Burst test cell

3.2.1 Design considerations

The stiffness and rigidity of the dried sheet is a function of the fiber length distribution of the suspension, i.e., the fines to fibers ratio that, when increased, results in a stiffer sheet. Hence, this information could shed light on the transient nature of the fiber size distribution which, in turn, will affect the process of accumulation in the header. For that purpose, a burst test was recommended to examine the pressure needed to burst a fixed area of resulting sheet and the manner in which this pressure will vary with pumping time of the suspension. The construction of a burst test cell for a laboratory-scale application was necessary in order to serve as a prototype of an existing industrial tester. Based on a survey of the literature, the oldest and most widely used of the strength tests for paper and paper board is the Muller test (Britt, 1964). The TAPPI method, T403 3m53, defines bursting strength as the hydrostatic pressure in pounds per square inch (psi) required to produce rupture of the material when the pressure is applied at a controlled increasing rate though a rubber diaphragm to a circular area, 1.2" in diameter, of the material under test (the test area being initially flat and held rigidly at the circumference but free to bulge under increasing pressure of the test). The burst test cell was designed to be similar to, but less advanced than, the existing tester.

3.2.2 Design constraints

Design constraints for this cell were not as complex because of the information provided by the industrial tester. The cell was chosen to be an aluminum cylindrical cell of two parts. The first part allowed a controlled measurable compressed air flow to enter in a 1/8" national pipe thread tapped hole and to be expended in a burst chamber of 1.25" inner diameter, where the paper to be tested would lie at the circumference of a cell of 2.5" diameter, rigidly held by two o-rings fixed on the bottom part at the circumference of

the burst void surface. The end part held a similar outlet hose to exit the compressed air once the paper was burst. The only construction criterion required was the smooth rounded entry of the void chamber of the cell necessary to eliminate any edge blast of the tested paper. Figure 8 shows the top and the cross-sectional views of this cell.

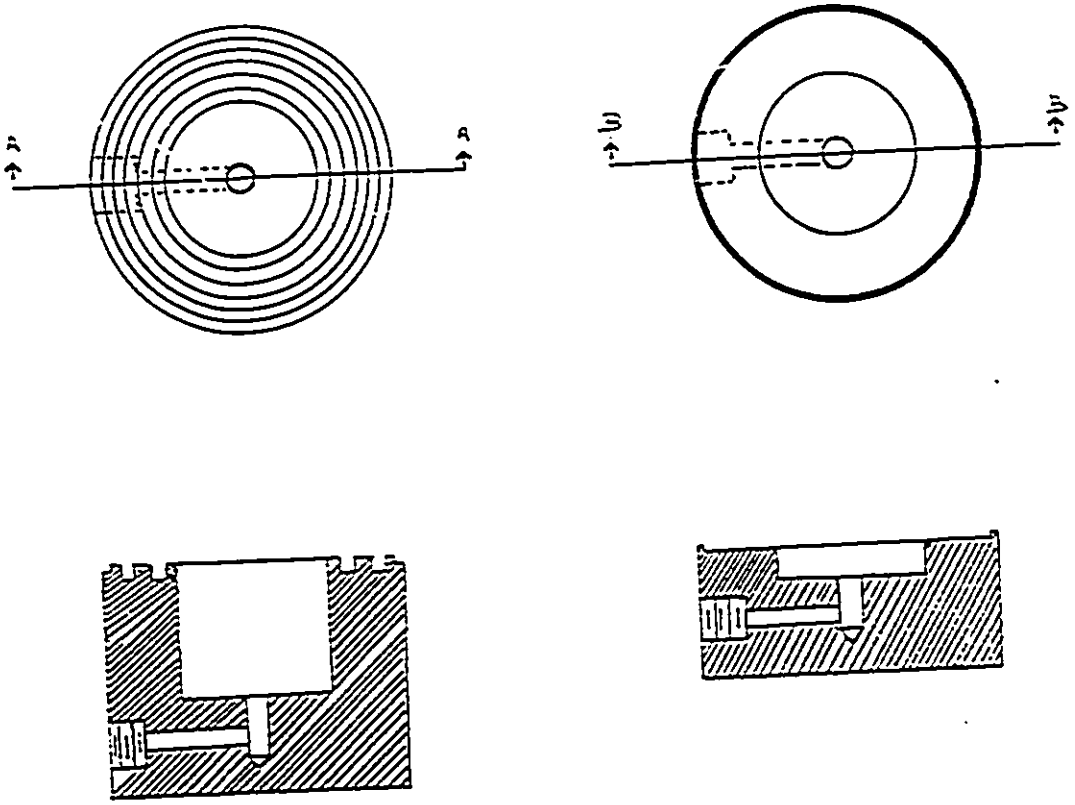

Figure 8: Shematic diagram of the top and cross-sectional view of the burst tester cell.

CHAPTER 4: METHODOLOGY

4.1 Characterization of pulp suspensions

Once the prototype module was constructed attention was focused on the proper preparation of the suspension and the evaluating of its characteristic properties, i.e., its density, viscosity, and fiber length distribution. Kraft board was blended with water at a mass percentage of 0.5% in a automatic two speed blender. The water was previously treated in a reverse osmosis system. Care was taken to ensure no entraeneous materials or contaminated equipment was used.

4.1.1 The density of the suspensions

For determining the solution density, a simple mass over constant volume relationship was used. One liter of well mixed suspension was weighed and the density computed thrice for each concentration to obtain reliable results. Six 50% dilutions were prepared from an initial concentration of 0.5 wt. % by replacing half the volume of the well mixed suspension with water. The density of each diluted suspension was again computed thrice by the procedure above.

4.1.2 The viscosity of the suspensions

After calculating the density of the solutions, a determination of their viscosity was made. For this, two methods were used.

The falling ball method

This method is usually used only with homogeneous solutions, but given the low concentration of the suspension, it was thought to be feasible for this application as well. The goal was to determine the terminal velocity of a sphere freely falling through the suspension for each of the six diluted concentrations. A two meter long cylinder with a diameter of 5 cm, with graduations every 10 cm was used in conjunction with a Plexiglas

sphere of 0.25" diameter. The time needed by the ball to cross these graduations was measured; once the time remained constant, after several equidistances, the terminal velocity (v_t) was calculated as

$$v_t = \frac{d}{t} \tag{23}$$

where d is the distance travelled at constant velocity and t the time taken. Once the terminal velocity was known, the friction factor was calculated using the following equation:

$$f = \frac{4gD(\rho_s - \rho)}{3v_t^2\rho}, \tag{24}$$

where all the variables were directly measurable. The Reynolds number was determined using Figure 9 relating Re with the friction factor (f). Once the Reynolds number was determined, the viscosity was calculated as follows:

$$\mu = \frac{Dv_t\rho}{\mathrm{Re}}. \tag{25}$$

In order to obtain a more accurate result, a small computer program was written in Maple to relate the Reynolds number with the friction factor, circumventing a visual graphical procedure. It is useful to note that the falling ball method was not feasible with a concentration of 0.5 wt. %, since the terminal velocity was difficult to determine because of the increased contact between the fibers and the sphere; but for diluted suspensions the terminal velocity was easily reached. The viscosity was directly calculated using this method for suspensions with 0.25, 0.125, 0.0625, and 0.03125% weight of fibers. For a suspension with a fiber concentration of 0.5 wt. % the viscosity was indirectly determined by extrapolating the previous results after applying a third order polynomial fit.

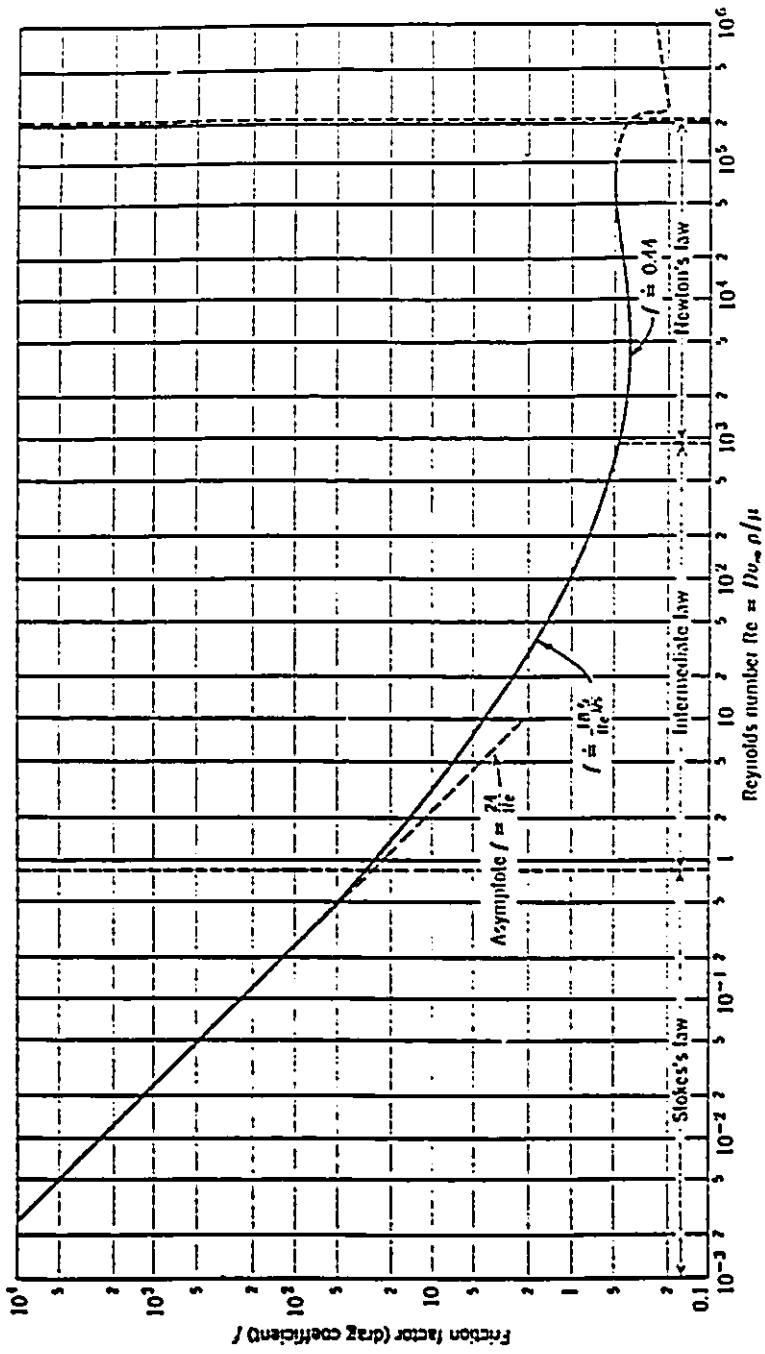

Figure 9: Friction factor for spheres moving relative to a fluid with a velocity v (Bird, Steward, Lightfoot, 1960).

The Poiseuille equation for viscosities

The major assumption in using the falling ball method to evaluate the viscosity of a fiber suspension is the feasability of adopting this method to a suspension. Hence a more reliable method was also used to check the validity of the results obtained earlier.

It was reported by Ogawa (1990), that fiber suspensions with a concentration below 1% behave as Newtonian fluids in the laminar regime. Accordingly, a tube of 1.5m length with pressure ports located at each end was used to calculate the viscosity in the laminar regime. After setting a low flowrate and tracking the pressure difference along the tube, the viscosity was calculated from

$$\mu = \frac{\pi R^4 \Delta P}{8LQ}. \tag{26}$$

4.1.3 The behavior of the suspension in the turbulent regime

The standard experimental method of evaluating the flow behavior of a liquid is to examine the relationship between the velocity gradient at the wall and the flowrate. If they relate linearly, the liquid is referred to as Newtonian.

To experimentally calculate the value of the velocity gradient, the addition of a special probe to the set-up discussed above would have been necessary. As an alternative, an analytical method was used to determine the fluid behavior based on the pressure difference along the horizontal tube. Knowing ΔP at different flowrates in the turbulent regime, the shear stress at the wall was calculated as follows:

$$\tau_w = \frac{R\Delta P}{2L}. \tag{27}$$

The characteristic viscosity, K' was determined from the relationship

$$K' = \frac{\tau_w D^{n'}}{(8u)^{n'}}, \tag{28}$$

where

$$u = \frac{Q}{A}, \tag{28a}$$

and n' is the power law constant (Metzer and Dodge, 1959).

Metzer and Dodge also relate the Reynolds number to the friction factor in the turbulent regime for unknown behavior through two equations already defined as equations 21 and 22.

By substituting all the parameters determined above into equation 21 and by re-substituting them into equation 22, a single equation defining n' was obtained. A value of 1 for n' indicates that the suspension behaves as Newtonian fluid.

4.1.4 Evaluating the fiber build-up in the flow cell

This effect was evaluated as follows. After installing one of the nine heads, the pump was started at a fixed flowrate and the pressure was registered at six different locations along the cell (see Fig 7). The pump was then shut off and all the suspension in the cell was collected in a tray. A constant weight of suspension was then introduced into an oven and the liquid evaporated. By calculating the mass fraction of the fibers after drying and comparing it to that of the initial feed, the concentration build-up was computed as

$$\text{Conc. build-up} = \left(\frac{(C_f - C_i)}{C_i} \right) * 100 \tag{29}$$

where C_f is the final concentration in the chamber after a time t and C_i is the initial concentration in the feed tank at time t=0.

4.1.5 The disintegration of the fiber with pumping time

After the end of each pumping cycle, the suspension was examined under a microscope to observe the increase of fines population relative to the fiber population and the increase in the population of deformed fibers. This method is obviously dependent on scale of examination and the representativeness of the pulp sample. This method then provided only a rough estimate of the increase in fines in the suspension.

4.1.6 The stiffness of resulting sheets

This was determined by the bursting strength of the dried fiber sheets in a special cell designed for that purpose (see Chapter 3).

When undertaking the burst test, compressed air was provided from an air supply connected to a regulator valve (see Figure 10). The outlet of the valve was divided into two streams by a simple T-joint; one end was connected to a pressure gauge of 60 psi capacity with a least count of 0.2 psi, and the other end was connected to the burst cell. The paper to be tested was coated with a piece of paraffin coated paper to make it impermeable to air. Having determined that the paraffin paper alone had a bursting pressure of 11 psi, the sample was then tested. If the sample required a bursting pressure of less than that of the paraffin paper (< 11 psi) the rising pressure indicated on the gauge would fall briefly before continuing to rise again up to 11 psi when rupture of the parafin coated paper occurred. The 'pause' as observed on the pressure gauge is the bursting pressure of the sample. If the required bursting pressure of the sample was higher than that for the paraffin paper (> 11 psi), then the pressure rose until reaching that level, at which time both the sample and the paraffin burst simultaneously.

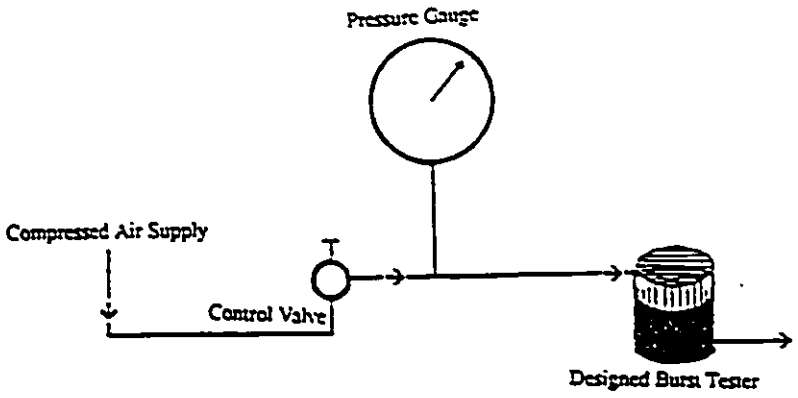

Figure 10: Schematic diagram of the burst tester set-up.

4.2 Design of the experimental set-up

The schematic diagram of the experimental set-up is shown in Figure 11. After connecting the holding tank to the pump, the outlet stream was divided in two using a by-pass ball valve. One stream returned to the tank in order to provide agitation to ensure maximum homogeneity in the tank. The second stream was connected to a rotameter in order to measure and vary the flowrate. The outlet stream from the rotameter was again divided in two by a T-joint. One stream was used to connect the system to the prototype cell mounted vertically above the feed tank to provide a closed system. This stream was controlled by a ball valve which could be shut off at any time. The other stream was connected to the system through a 1.5 m long 1/2" ID horizontal tube after reduction from 1" to 1/2" by a reducer. The tube outlet discharged into the feed tank to provide a closed system.

Two stirrers were provided in the tank for agitation when the pump was stopped to eliminate any growth of bacteria. A cooling coil was also introduced in the tank to maintain a constant temperature of 22 °C.

1/4" teflon tubing was used to interconnect the pressure ports on the cell to the 6 port valve, the pressure transducer, and the two pressure ports on the horizontal tube. A three port valve were installed at each end of the pressure transducer in such a way as to provide a total isolation between the cell pressure ports and the ports on the horizontal tube. The output signal from the pressure transducer was connected to an RS232 board which received the signal as a voltage and input it into a program in QBasic, installed on an microcomputer. The program then converted these signals to equivalent pressure values (psi).

When the valve connecting the system to the horizontal tube was closed and the valve connected to the cell was opened, and the pump timer was activated. Nine time intervals (t= 15, 30, 45, 60, 120, 240, 480, 960, and 1440 minutes), three different chamfer angles

for three different diameters and two flowrates were used to give 162 different cycles. At the end of each cycle, the suspension inside the cell was collected and weighed. The water was then evaporated to calculate the mass fraction of the remaining suspension after the desired time interval. During each cycle, the pressure transducer aquisition system was used to compute the pressure difference between the inlet hose and six different locations along the prototype cell (see Figure7). As mentioned previously, the fibers were examined after each cycle to observe the disintegration due to pumping.

A clean in-place process was used after each long cycle experiment (one full time sequence from 15min to 24hours). The entire suspension was emptied and the tank, the pump, the rotameter and interconnecting tubes were then cleaned with water before re-loading a fresh suspension charge. In addition, the pressure ports and tubes had to be cleaned of any residual fibers that could affect the pressure results. This was done by emptying the tubes, cleaning them with compressed air and then cleaning them again with water. Once this process was completed, they were filled with water and then reconnected to the system.

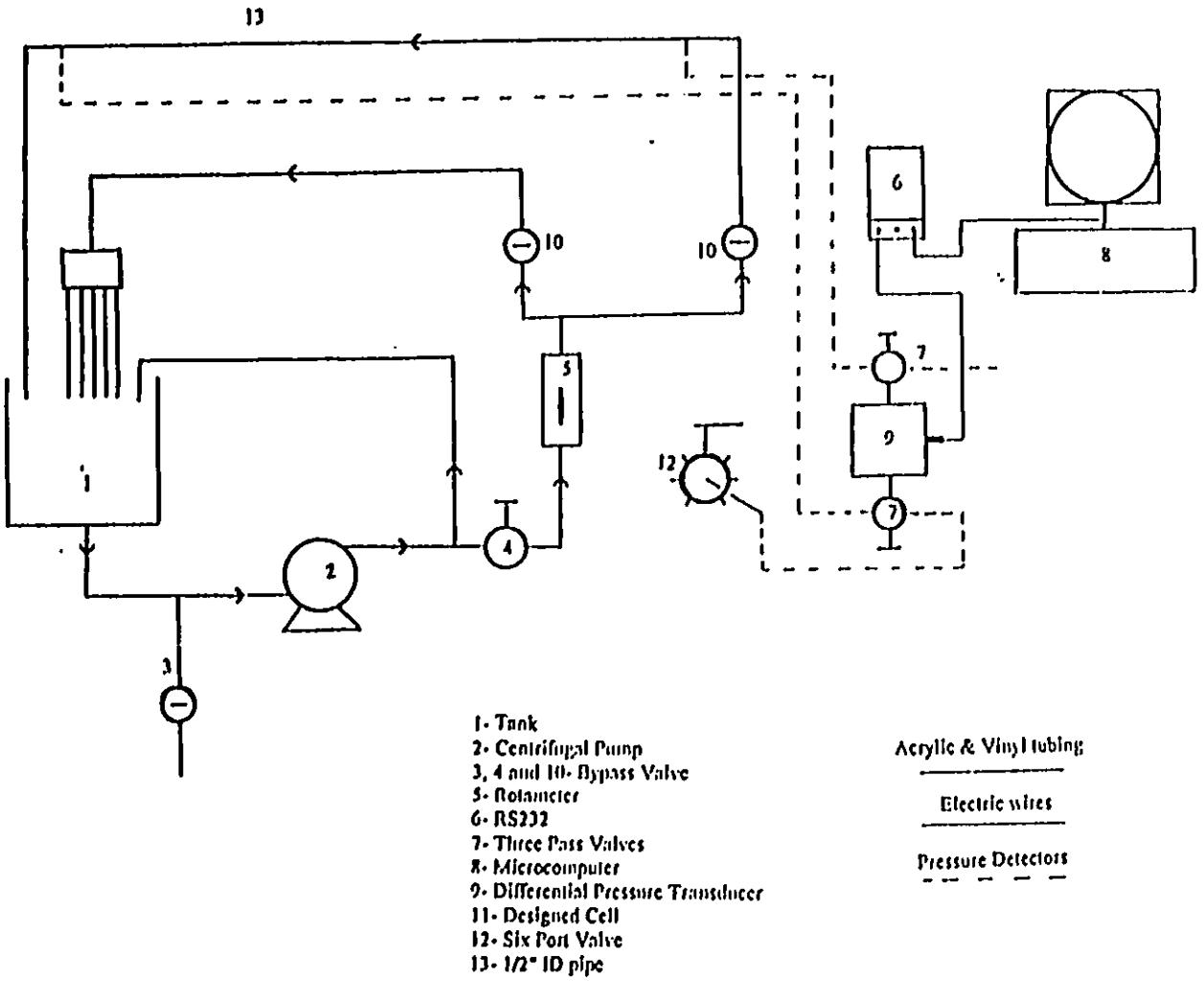

Figure 11: Flowchart of the experimental set-up.

4.3 Computational method

As stated above, the pressure transducer was connected to an RS232 that received the pressure signal as a voltage and transmitted it to a PC having a receiver compatible with the RS232 board output. In turn, the computer contained a program written in QBasic which received the voltage signal and then calculated in 20 seconds the average of 20 input data received at each port. Once one port was scanned, it signalled the manipulator to switch to the next port until the procedure was completed. The software was programmed in a way to compile and store the data in a file that could be exported to any spreadsheet for further processing.

In addition to this program, other programming work was undertaken to process the data. These programs are provided in Appendix D.

CHAPTER 5: PROPERTIES OF MATERIALS & EQUIPMENT SPECIFICATIONS

5.1 Material properties

The pulp used in this research was prepared by blending Kraft board liner and water in such a way as to obtain a 0.5 wt. % pulp suspension. No additives were used. Note that it is standard practice in industry to employ chemicals to eliminate microbial growth.

The fibers used were a 90-10% mixture of unbleached liner Kraft board and bleached liner Kraft board respectively. The unbleached liner Kraft was obtained from St. Laurent Paperboard Inc. (1250 Rene-Levesque Blvd West, Montréal, Québec H3B 4Y3), while the bleached liner was received from Tembec Inc (Temiscamingue, Québec J0Z 3R0). Table 2 lists the analytical and physical information regarding these two products, as provided by the manufacturers.

Table 2: Manufacturers' analytical and physical information.

	Unbleached	Bleached	Test Code[1]
Brightness, %	95	15	WI-351-A013
Ash, %	0.243	0.323	WI-351-A005
Basis weight, g/m^2	690	160~390	WI-351-A019
Pulp pH	7.3	7.1	WI-351-A008
density, g/cc	0.63	0.77	WI-351-A018

1 Internal test code, WI: work Instruction of Tembec inc..

The water used to prepare the pulp was taken from a reverse osmosis membrane module in order to minimize the level of calcium which, as stated above, will effect the fiber, and to ensure a neutral pH of 7.

5.2 Auxiliary equipment specifications.

5.21 Equipment used during preparation of the fiber suspension

The suspension was prepared in a two speed blender capable of processing up to 1 litre of sample at 15,500 - 18,300 rpm. The container was of stainless steel. Two mechanical mixers were also used during the preparation of the suspension.

5.22 Auxiliary equipment used in the module flow tests

The fiber suspension was held in a polyethylene cylindrical tank. The tank's translucent walls permitted visual inspection of the contents at all times. The tank volume was 120 litres.

A magnetically decoupled centrifugal pump with a plastic impeller, made by Marathon was used to circulate the suspension. The pump was driven by an electric motor (model HQM56C34F2900A, volt-115/205-230, RPM 3450). This pump provided a maximum flow of 2 L/s and a head pressure of 28 psi.

A differential pressure transducer with symmetrical pressure cavities of stainless steel, made by Validyne Engineering Corp., was employed during pressure measurements. A variable reluctance pressure transducer with a carrier demodulator provided a 5 Vdc output when operated from an unregulated 10.8 to 32 Vdc input power source. Fluid pressures acted directly on a central diaphragm in a balanced variable reluctance design which eliminated the need for internal isolation of fluids.

A programmable RS232 signal conditioning module (+/-5 volt input/RS232 output) was used during data acquisition (the RS232 provided a complete sensor to computer signal conditioner as a single channel data acquisition system). It received analog sensor inputs, provided signal conditioning and isolation, and converted the signal into digital voltage in order for the data to be transmitted to the computer. A microcomputer with an RS232-compatible receiver was used for data acquisition.

A six port distribution valve with ports of 1/4-28 UNF female thread, made by Alltech Associates, Inc., was used to connect the six pressure ports located on the main cell with the pressure transducer.

A heavy-duty rotameter, made by Schutte and Koerting Co., with a large-size pin (rotor of 60 J) was used to measure the flowrate of the circulated suspension up to maximum flow of 1.8 L/s. Pipes, ball-valves and fittings (90 degree elbows) of PVC material, made by Canus Plastic Inc., were employed in the flow system.

Finally, cooling coils were used to maintain a stable suspension temperature and to prevent suspension heating due to friction.

CHAPTER 6: RESULTS & DISCUSSION

The problem of dewatering of fibers at the inlet zone of tubular UF modules is particularly pronounced with modules having tubular membranes with an inner diameter less than one inch. The objective of this research project was to investigate the influence of the inlet geometry on the concentration build-up within a module header. A large portion of the research was devoted to the design and construction of the flow cell. The fabrication of the cell was followed by the development of an appropriate experimental protocol for the acquisition and analysis of pulp samples taken from the distribution header of the cell.

6.1 Characterization of the prepared suspension

Once the suspension was prepared and before running the main procedure, it was necessary to evaluate several factors which were considered critical to be known before any further work was undertaken. These factors include the density and viscosity of the suspension at different fiber concentrations, and the length distribution of the fibers within the suspension.

6.1.1 Density

As discussed in the methodology, the density of the suspension was calculated using the standard method of dividing a measurable mass by its volume. The results of the density of suspension at 0.5 wt. % fiber and the other six 50 wt. % diluted suspensions are shown in Table 3 and Figure 12. It is clear from these results that, as we add fiber to the suspension, its density decreases. This is expected since the density of both bleach and unbleached fiber is less than that of water as shown in the material properties section.

The density of the suspension at 0.5 wt. % fibers was found to be 970.2 Kg/m^3. The density of pure water at 25°C is 998.5 Kg/m^3, which is in good agreement with the experimental results listed in Table 3.

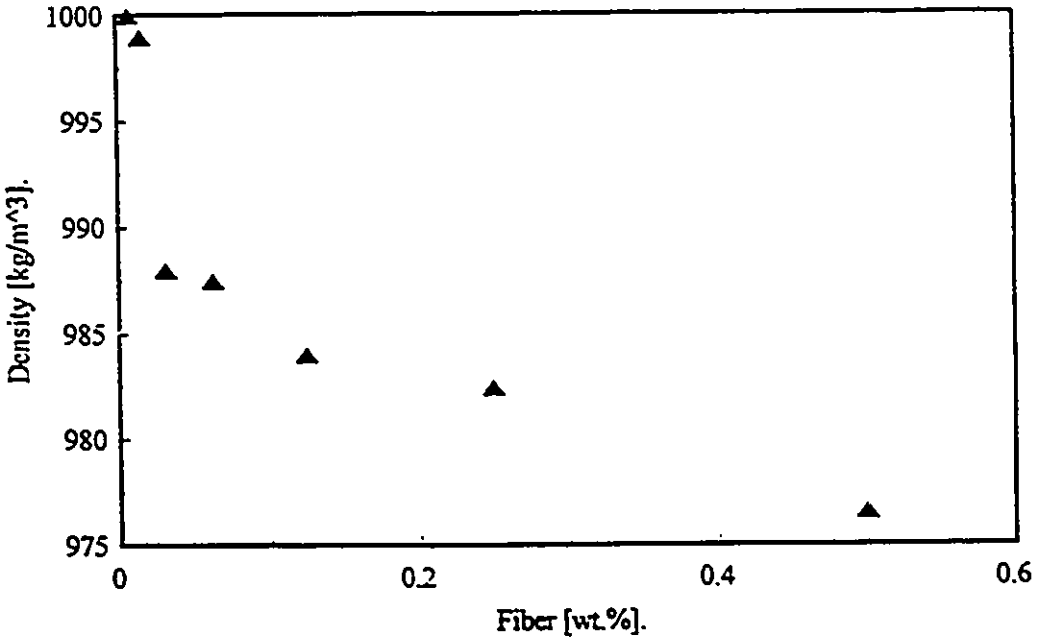

Figure 12: Density of pulp suspension at different fiber concentrations.

Table 3: Experimental density for each diluted suspension.

Fiber wt. %	Calculated density [kg/m^3]
0.500	970.2
0.250	976.6
0.125	982.4
0.0625	984.0
0.0312	987.5
0.0156	988.0
0.00781	999.0
0.0 (pure water)	1000

6.1.2 Viscosity

As discussed in the methodology, two methods were used to determine the viscosity of the suspension: one based on the falling ball method, and the other using the Poiseuille formula in the laminar regime. The results of these methods are as follows. Falling ball method; This method was made at the end of each dilution (6 in total). The terminal velocity was not reached for the original suspension at 0.5 wt. % fibers, because of the interaction between the sphere and the fibers in the suspension. Once the terminal velocity was known, the friction factor was calculated using equation 24, and the Reynolds number was evaluated using Figure 9. The viscosity was then calculated using equation 25 for each case.

To test the validity of this method it was necessary to evaluate the viscosity of pure water. It was found to be 1.17cp at 21°C. Knowing from the literature that at this temperature the viscosity is 1.002cp, there resultant error is 16.77 %. This last test result proves the validity of this method for homogenous solutions. The significant experimental error can be attributed to non focusing of the sphere at the center of the cylinder, even

after using a funnel to drop the sphere. Assuming that the falling ball method was valid for very dilute suspensions, the calculated viscosity for the six dilutions are shown in Figure 13 and Table 4. Figure 14 is the residual plot of the experimental viscosity obtained by the falling ball method compared to the viscosity calculated using a cubic polynomial fit.

The viscosity of the suspension at 0.5 wt. % was then evaluated after assuming a linear trend between the fiber % and the viscosity calculated in diluted systems. After extrapolating the curve in Figure 13, the viscosity was estimated to be 11.8cp.

Table 4: Calculated viscosity using the falling ball method.

Fiber (wt %)	v_t [m/s]	f dimensionless	Re dimensionless	μ [cp.]
0.2500000	0.125	1.177	94	8.25
0.1250000	0.140	0.920	150	5.67
0.0625000	0.171	0.600	350	3.06
0.0315000	0.176	0.560	400	2.76
0.0156250	0.182	0.520	600	1.90
0.0078125	0.188	0.460	1000	1.18
Pure water	0.188	0.450	1050	1.17

It was useful to write a small program that relates the friction factor to the Reynolds number replacing the theoretical graph. The program was written in Maple and it is shown in Appendix D.

Because of the large error associated with this method and the assumption that the falling ball method is feasible to determine the viscosity of the diluted suspension, a new method was required to substantiate the earlier viscosity measurements.

After extending the set up of the experiment to hold a long cylindrical tube with two pressure ports at each end, the pump was run to circulate the suspension through that

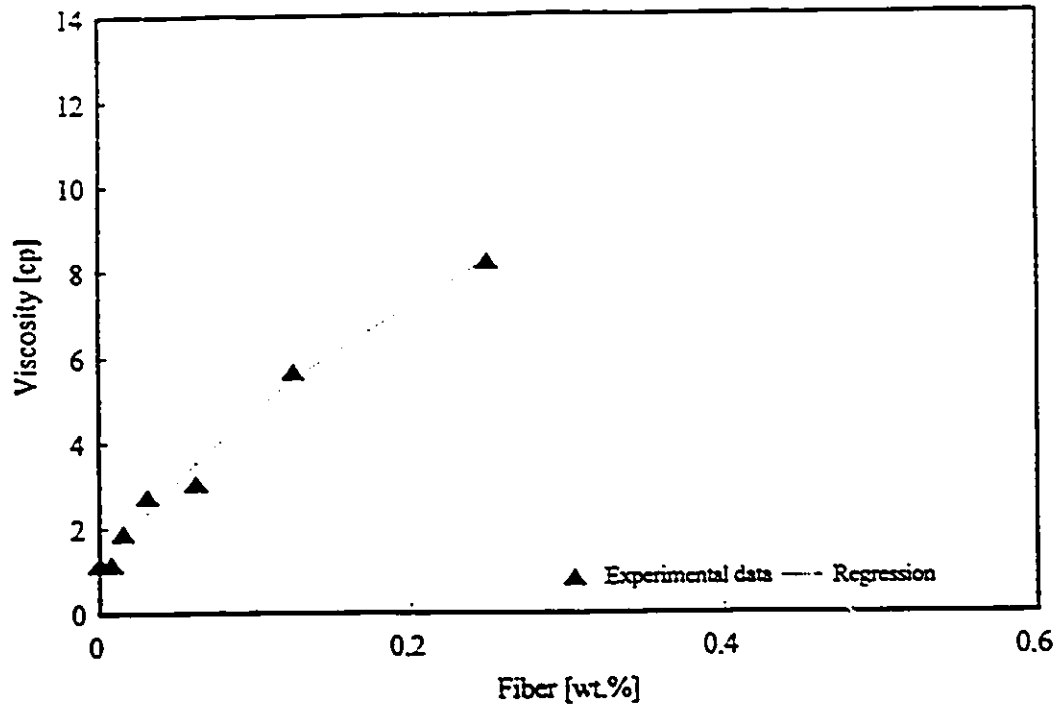

Figure 13: Calculated viscosity at different fiber concentrations using the falling ball method.

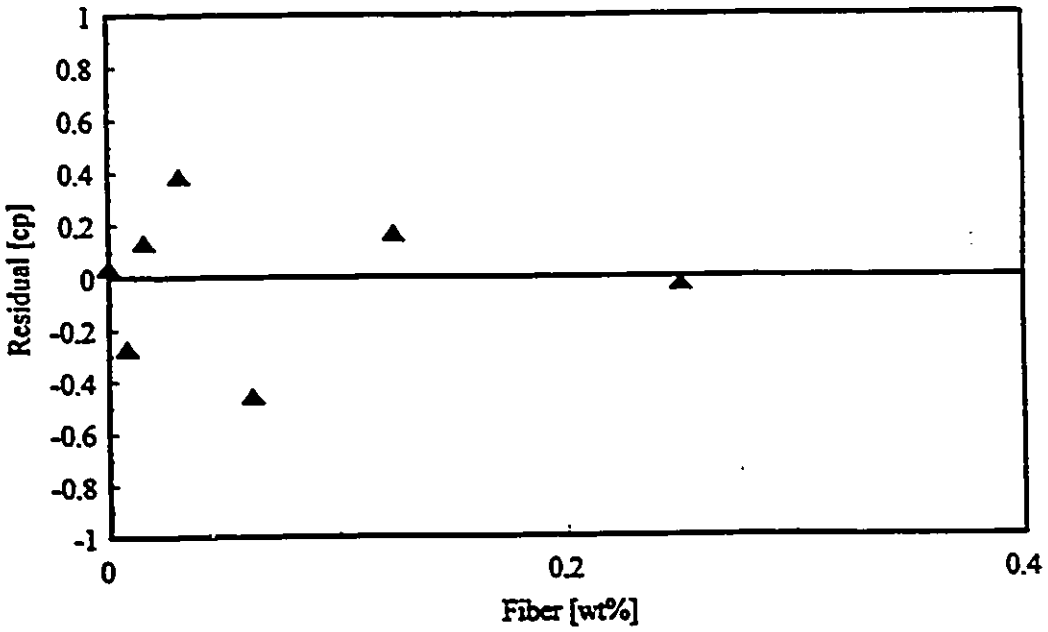

Figure 14: Residual plot of the viscosity calculated using the falling ball method.

tube after ensuring a very low flow (i.e., just enough to circulate the suspension). The pressure at each end of the tube was then measured. Once done, the flowrate was increased (always in the laminar regime) and the pressure was registered. This procedure was repeated 6 times for 6 different flowrates in the laminar regime. To calculate the viscosity, it was only necessary to calculate the slope of the line from the plot of $\frac{\Delta P}{L}$ vs Q, as seen in equation 26. Then the Reynolds number was calculated for each flowrate using equation 25 to assure that the flow was in the laminar regime (i.e., Re is less then 2100). The viscosity of the suspension at 0.5 wt. % fiber concentration using this method was 12.15cp. Figure 15 shows the relation between the pressure loss vs the flowrate of the suspension at 0.5 wt. % in the laminar regime. The results are tabulated in Table 5. Figure 16 presents the relation between the Reynolds number and the calculated friction factor.

Table 5: Poisseulle equation parameters.

ΔP [psi]	ΔP/L [Pa/m]	Q $[m^3/s] * 10^5$	Re dimensionless	f dimensionless
0	0	0	0	0
0.198	1820.07	9.4	754.12	0.0212
0.180	1652.27	8.4	676.44	0.0236
0.171	1573.02	7.8	628.14	0.0255
0.0755	694.20	3.5	284.09	0.0563
0.0264	242.74	1.1	91.96	0.174
0.106	975.036	5.7	460.70	0.0348
0.0962	884.70	4.3	347.84	0.0460

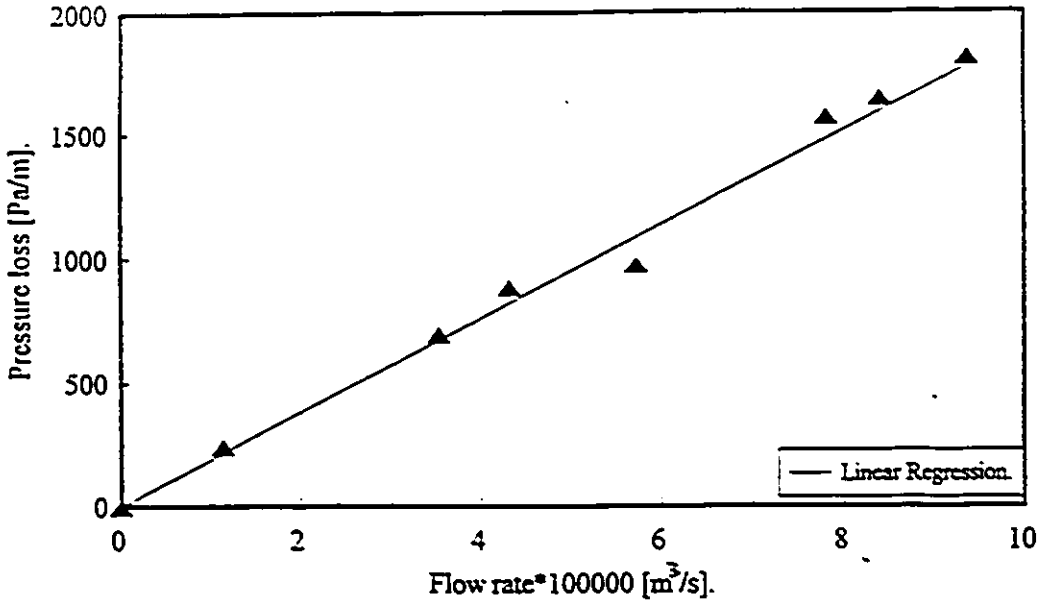

Figure 15: Pressure loss vs flowrate of fiber suspensions in laminar regime (evaluation of viscosity from Pouiseulle formula).

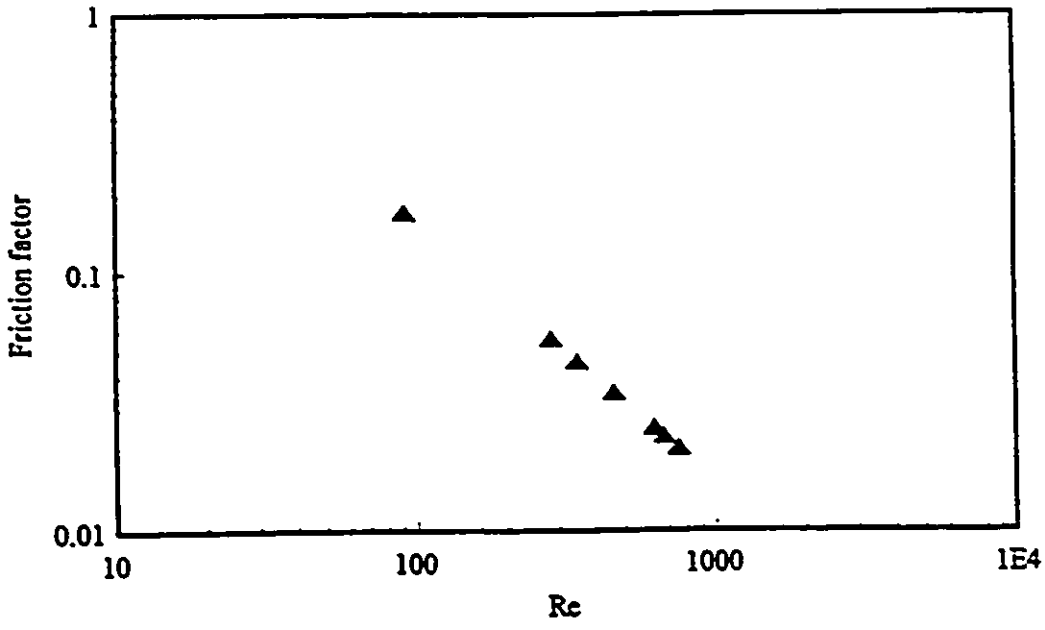

Figure 16: Reynolds number friction factor relationship in laminar regime.

The viscosity of the suspension at 0.5 wt. % fiber using both methods were within 2.9 % of each other, leading to the conclusion that the falling ball method can be used to estimate the viscosity of these dilute suspensions.

6.1.3 Fiber length distribution before and after pumping

Fiber length is recognized as one of the most important factors characterizing the paper making potential of pulp fibers. This property was measured by direct microscopic observation, which is one of several methods used for this purpose in similar applications such as indirect fractionation methods.

Once the sample was prepared, three samples were taken for microscopic examination. At this stage a high homogeneity in length distribution was observed. Two major distributions were noted: one with 90% abundance of long fibers with average length of 1.24 mm, and the other with an average length of 0.42 mm referred to as fines. The three samples showed to a certain degree a regularity in length distribution. Figure 5 shows a freehand drawing of the fiber sample as seen using the microscope. This microscopic examination was repeated regularly after each desired pumping time. The important observation was a change in the distribution of the lengths of fibers as the pumping time increased. In the early stage (first 10 hours), a deformation of fiber was clear (swollen fibers with middle peak were observed). As the pumping time increased, the fines population increased resulting in shortening of fibers. A 60% population resulted following 60 hours of pumping. The suspension became darker, the color changing from beige to dark brown.

This observation was in agreement with the theory if pumping can be considered a beating action. The fine formation resulted in a reduction of the numerical average fiber length. These results are clearly shown in Figure 17.

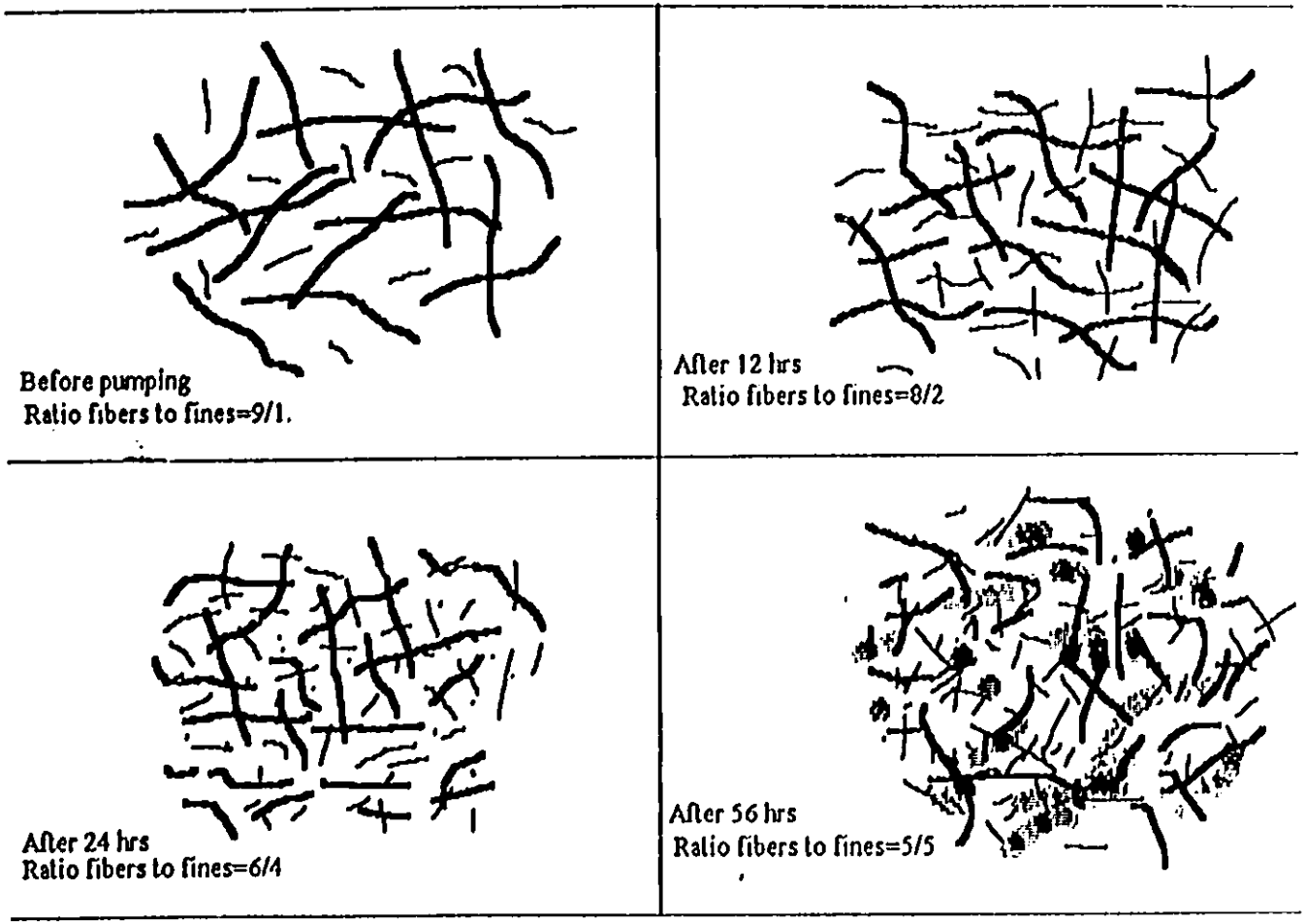

Figure 17: Effect of pumping time on fiber length distribution: sketch of a microscopic view.

6.2 Fiber suspension behavior in the turbulent regime

The standard experimental method to determine the flow behavior of a solution is to see the relation between the velocity gradient at the wall and the flowrate. If a linear relationship exists then we conclude that the solution is Newtonian in behaviour.

To experimentally calculate the value of the velocity gradient at the wall, special probes (platinum anode) would need to be introduced into the setup of the experiment. In order to simplify the characterization, a mathematical procedure was used instead to check the behavior of the suspension in the turbulent regime. Based on the shear stress at the wall at different flowrates, and knowing the differential pressure along the tube at high flowrates (within the turbulent regime), the shear stress at the wall was calculated using equation 27 and substituted in the Metzer and Dodge equations as defined in chapter 4. This was done to achieve one complex equation holding n' as an unknown. Solving for n' will indicate the behavior of the solution. At 0.5 wt. % fiber concentration the suspension behaved non-Newtonianlly ($n' = 0.24$). This is in agreement with that found by Myreen (1989) who calculated n' equal to 0.23 when using a new type of rotary viscometer suitable to calculate the viscosity of such a suspension. All resulting calculations are shown in table 6.

Table 6: Calculated shear stress at the wall in the turbulent regime.

Q [L/s]	ΔP [psi]	(8<v>D) [L/s]	τ [Pa]
0.60	0.8715	2983.60	25.43
0.77	1.09	3829.00	31.79
0.94	1.67	4674.00	51.22
1.05	2.15	5221.29	62.83
1.15	2.48	5718.56	72.37
1.20	2.64	5967.24	77.03

6.3 Effect of inlet angle, inlet flowrate, and inside diameter of tube on the concentration build-up in the header chamber

6.3.1 Preliminary tests

After mounting the first cell (ID=1/2", and α=0°), the early concern was to track any blockage due to dewatering of fibers within the cell when a 0.5 wt. % suspension was circulated through the system. A first run of 10 hours was performed but complete blockage was not observed. Hence the concern was deviated to study any quantitative changes occurring inside the distribution head after a given pumping time. It was decided to pump the suspension through the cell for 30 minutes at an inlet flowrate of 1 L/s, then collect the volume inside the cell and calculate the percentage of fibers in it to see if it changed from that of the feed. The result showed that for this period of pumping an increase of 13.7 % in concentration occurred. Repeating this test 3 times showed consistent results. At this early experimental stage many questions were asked: does the chamfer angle α, and/or the inlet flowrate have any effect on that concentration build-up, and what about the effect of the inlet diameter of the tubes? To answer these questions it was necessary to extend the experimental work as follows. The half hour pumping test was completed for all 3 cells in a way to cover the effect of flowrate, and chamfer angle α. Two different flowrates were selected: 1 L/s and 0.75 L/s, while three values for α (0,30, and 45°) were considered.

The concentration build-up inside the cell was a persistent phenomenon but it varied as the parameters discussed above were changed in such a way that it increased with decreasing α, with decreasing inside diameter of the tubes, and with increasing flowrate of the feed. These parameters as discussed in the procedure were studied separately. The results of the half hour pumping time test are listed in Table 7, and shown in Figures 18, 19, and 20.

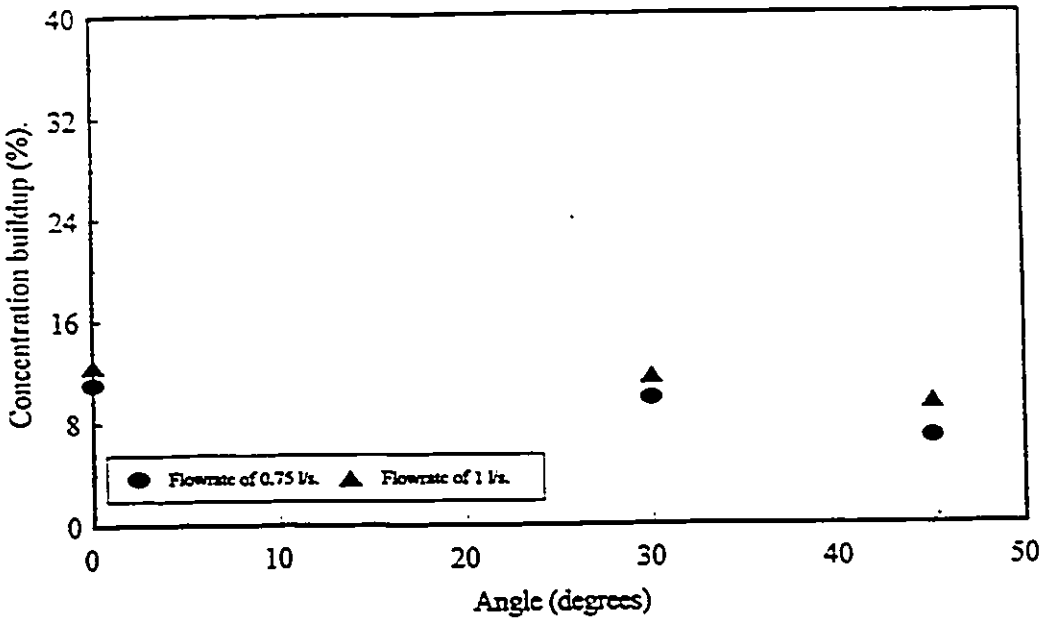

Figure 18: Fiber accumulation % (header conc. % build-up) vs inlet angle after half hour of pumping for ID = 1/2", at different Q and α.

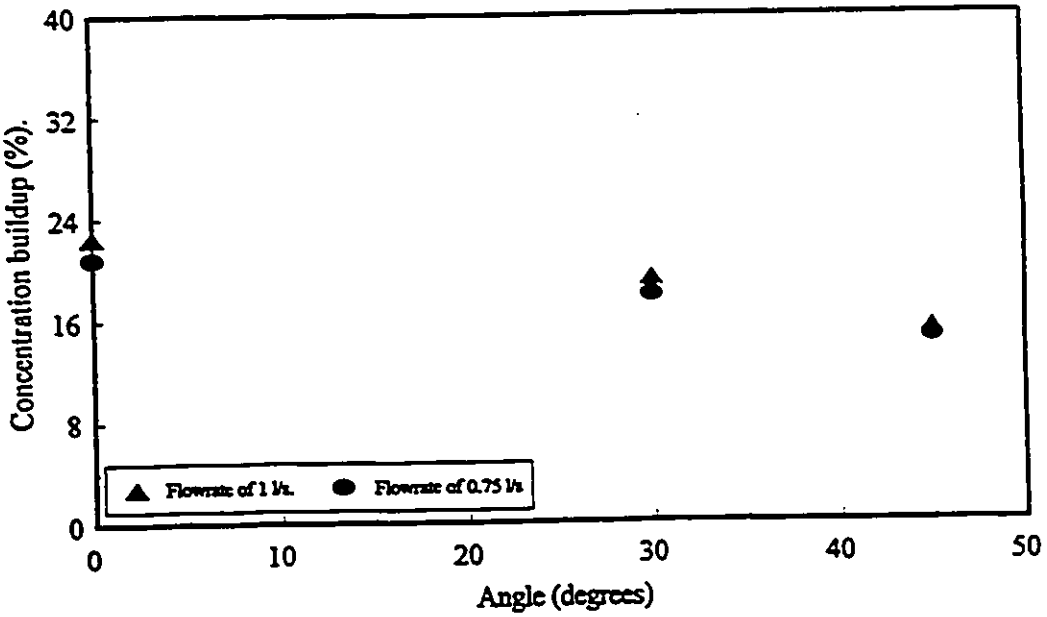

Figure 19: Fiber accumulation % (header conc. % build-up) vs inlet angle after half hour of pumping for ID = 1/4", at different Q and α.

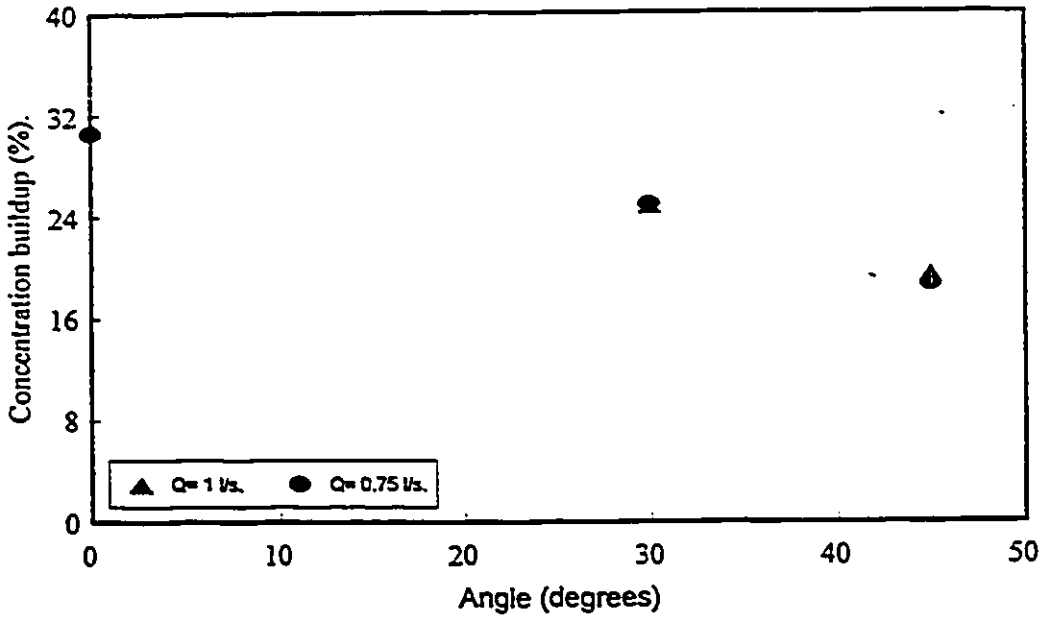

Figure 20: Fiber accumulation % (header conc. % build-up) vs inlet angle after half hour of pumping for ID = 1/8", at different Q and α.

The test done on the last cell having an inside diameter of 1/8" was always problematic: the suspension inside the cell after half hour of pumping was difficult to collect due to the blockage of the tubes.

Table 7: Concentration build-up results for a half hour pumping time.

Flowrate	0.75 L/s	0.75 L/s	0.75 L/s	1 L/s	1 L/s	1 L/s
ID=1/2"	Run 1	Run 2	Run 3	Run 1	Run 2	Run 3
0°	12.14	11.52	11.05	13.7	14.1	12.58
30°	10.2	9.52	9.84	12.446	12.77	12.634
45°	6.4	6.9	6.8	11.6	6.19	9.57
ID=1/4"	Run 1	Run 2	Run 3	Run 1	Run 2	Run 3
0°	21.14	22.17	19.325	23.35	22.3	22.05
30°	17.1	18.9	17.86	18.86	19.67	19.25
45°	14.09	14.57	14.963	15.12	15.24	15.401
ID=1/8"	Run 1	Run 2	Run 3	Run 1	Run 2	Run 3
0°	30.976	30.62	30.25	31.47	30.88	30.71
30°	25.254	25.02	24.6	25.83	24.23	24.7
45°	18.158	18.9	19.1	19.134	20.1	19.12

As the inlet angle α increases, the total dead surface on the disk decreases. This results in fewer dead areas on the distribution disk so that the contact between the fibers and the dead regions decreases. This could result in a freer fiber which could pass through the tubes resulting in less concentration build-up. It is also clear that as the inside diameter of the tubes increased the build-up in concentration decreased. This could be explained by noting that the cross sectional area of a tube increases as the diameter increases leading to a decrease in the differential resistance between fibers and water. Thus fibers and water

enter the inlet tube with almost the same difficulty. It was also observed that the higher the inlet flowrate, the higher the concentration build-up. That is achieved since more violent contact occurs between the fibers and the dead surface at higher flows, leading to these results. Up to this stage, any postulate regarding these result can be easily criticized since such limited experimentation is not enough to explain what is actually happening. Figures 18, 19, and 20 clearly show that, as we decrease the diameters of the tubes, the difference in concentration build-up associated with the two flowrates becomes lower. At an ID of 1/8" there is almost no difference between the concentration build-up when the flowrate was changed from 0.75 L/s to 1 L/s, regardless of the value of α. Differences in fiber accumulation were more pronounced as the tube diameter was increased to 1/4" and 1/2". Hence, size appears to control the accumulation process at its lowest value (i.e., 1/8"). However, as the diameter increases, its effect on the concentration build-up is no longer the controling one and the effect of feed flowrates become significant.

At this stage all measurements were taken at a single pumping time. To evaluate the effect of pumping time on the concentration build-up, a second series of tests were performed. Due to the difficulty in collecting samples with the 1/8" cell, it was decided to exclude it for this latter set of experiments. In addition, an extra distribution disk of α = 55° for the 1/4" cell was then introduced to get a clearer picture on the effect of the chamfer angle on the concentration build-up.

6.3.2 Long run tests

After installing the 1/4" ID cell, the objective was to evaluate the concentration build-up in the cell as a function of time. It was proved from preliminary testing that there is a concentration build-up after 30 minutes of pumping and that the effect varied with varying flowrate and the inlet angle. Nine run times were chosen: 15, 30, and 45 minutes and 1, 2, 4, 8, 16, and 24 hours. In each case inlet flowrate was varied from 0.75 to 1 L/s

and the inlet angle α was changed from 0, 30, 45 and 55 degrees. Triplicate runs for each set of conditions were performed to determine the reproducibility of these effects. Error bars in all plots indicate the 95 % intervals about the mean shown on the plot

Figure 21 shows the concentration build-up vs time for the 1/4" ID tubes at a fixed flowrate of 0.75 L/s and all 4 different inlet angle α. It is clear that, as the inlet angle increases, the concentration build-up decreases. From the same graph it is obvious that, after 4 hours of pumping, the concentration inside the cell had reached a steady state for 30, 45, and 55° angles; however, this effect is not as clear for the 0° runs.

Figure 22 shows the same phenomenon as discussed above but for a higher fixed flow of 1 L/s. The trends are similar to the previous case, though the concentration build-up is greater at the higher flowrate. This last observation is clear in Figures 23, 24, 25, and 26 where the concentration is plotted vs time at fixed α for both flowrates. Further, the calculated steady state concentration was always found to be higher at the greater flowrates. All results obtained with 1/4" ID are shown in Table 8.

Once the tests on 1/4" tubes were completed, the cell was changed to hold the 1/2" ID where a similar test was done for α =0°. The observed percentage concentration build-up was at its maximum for the higher value of flow. All results for 1/2" ID are shown in Table 9 and Figure 27.

The effect of ID is tabulated in Table 10 and, as clearly shown in Figures 28 and 29, lower inner diameters led to greater fibers accumulation; in addition, the steady state is reached sooner for the higher diameter tubes.

Figure 30 shows the same effects for a fixed period of 24 hours of pumping where for both cases the steady state is reached and the lower accumulation is achieved by the higher inner tube diameter module.

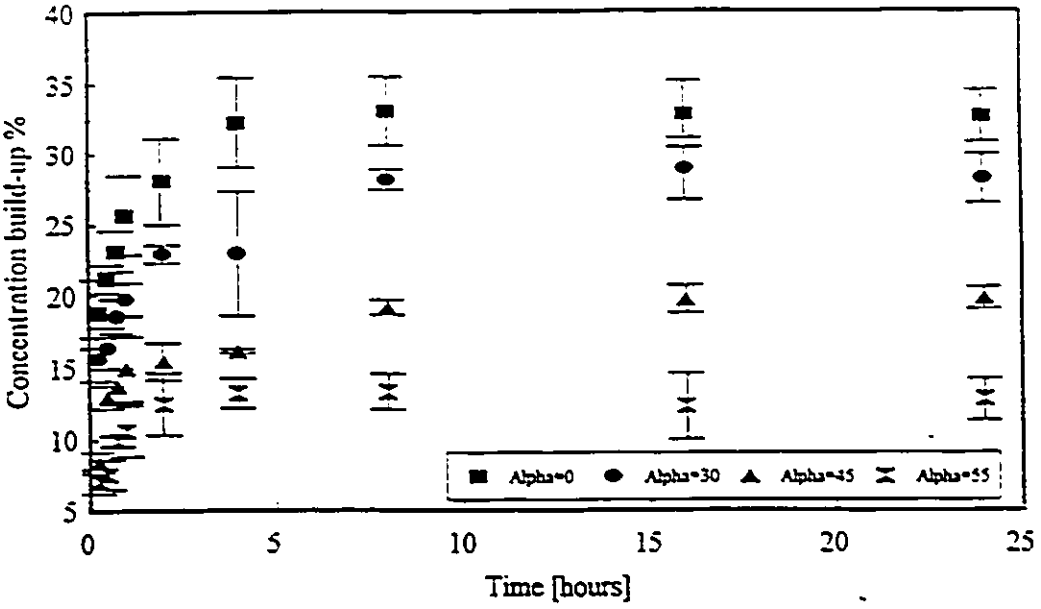

Figure 21: Fiber accumulation % (header conc. % build-up) vs time for ID = 1/4", Q = 0.75l/s and different α (CI = 95%).

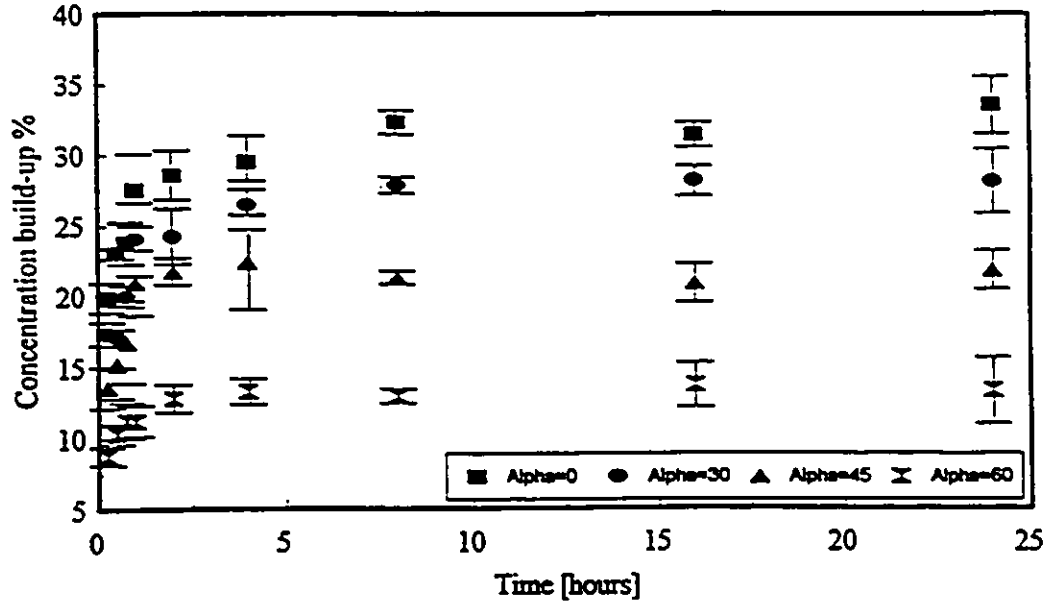

Figure 22: Fiber accumulation % (header conc. % build-up) vs time for ID = 1/4", Q = 1 l/s and different α (CI = 95%).

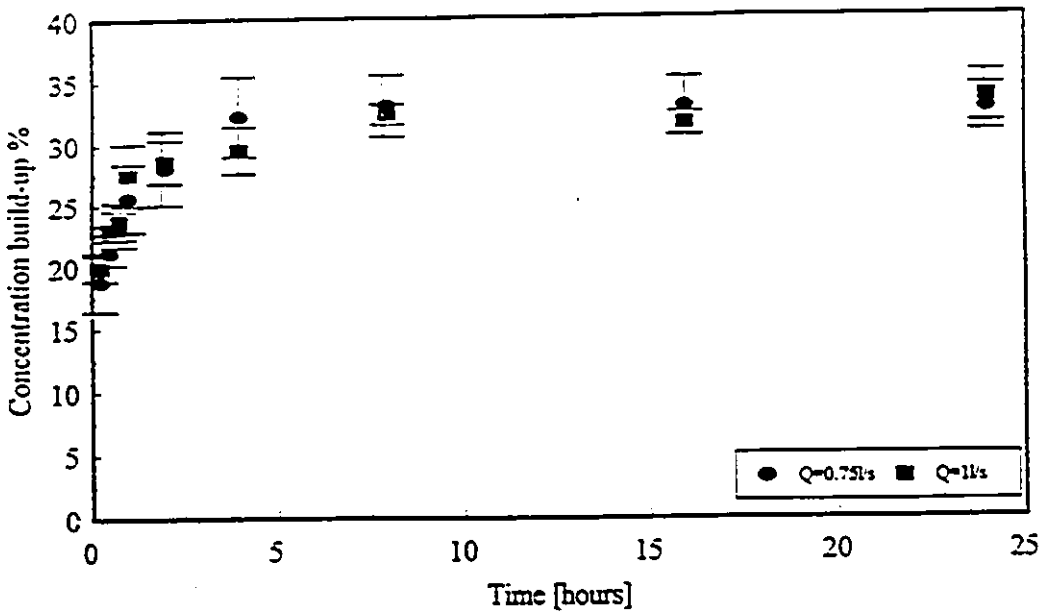

Figure 23: Fiber accumulation % (header conc. % build-up) vs time for ID = 1/4", α = 0°, and two different Q (CI = 95%).

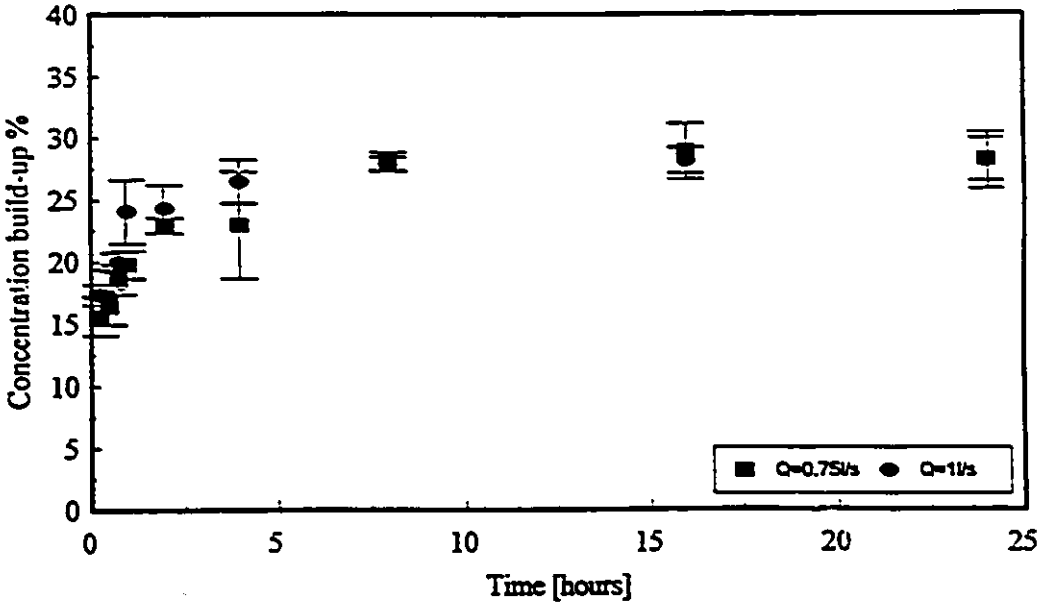

Figure 24: Fiber accumulation % (header conc. % build-up) vs time for ID = 1/4", α = 30°, and two different Q (CI = 95%).

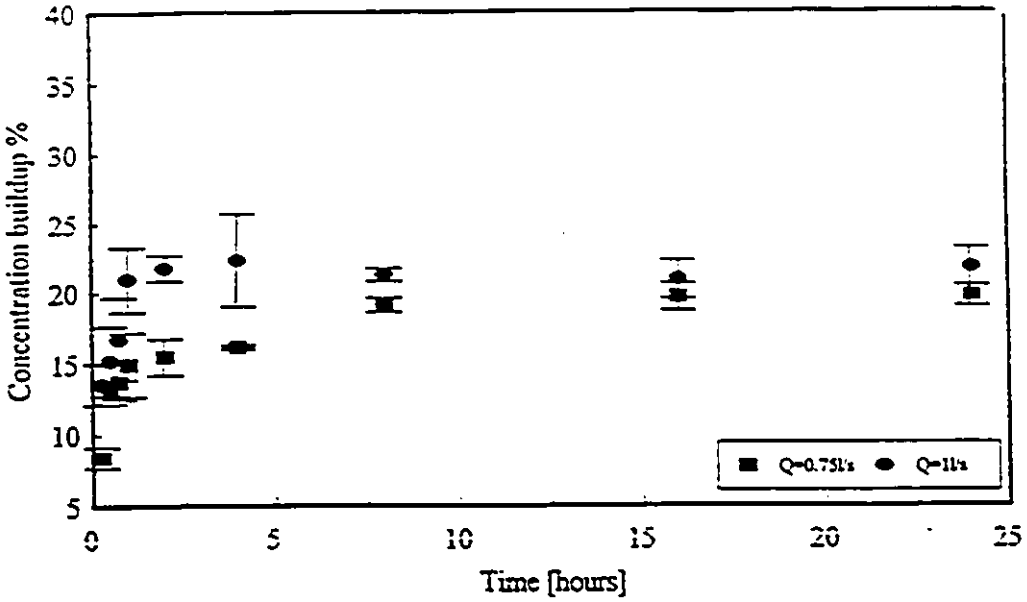

Figure 25: Fiber accumulation % (header conc. % build-up) vs time for ID = 1/4", α = 45°, and two different Q (CI = 95%).

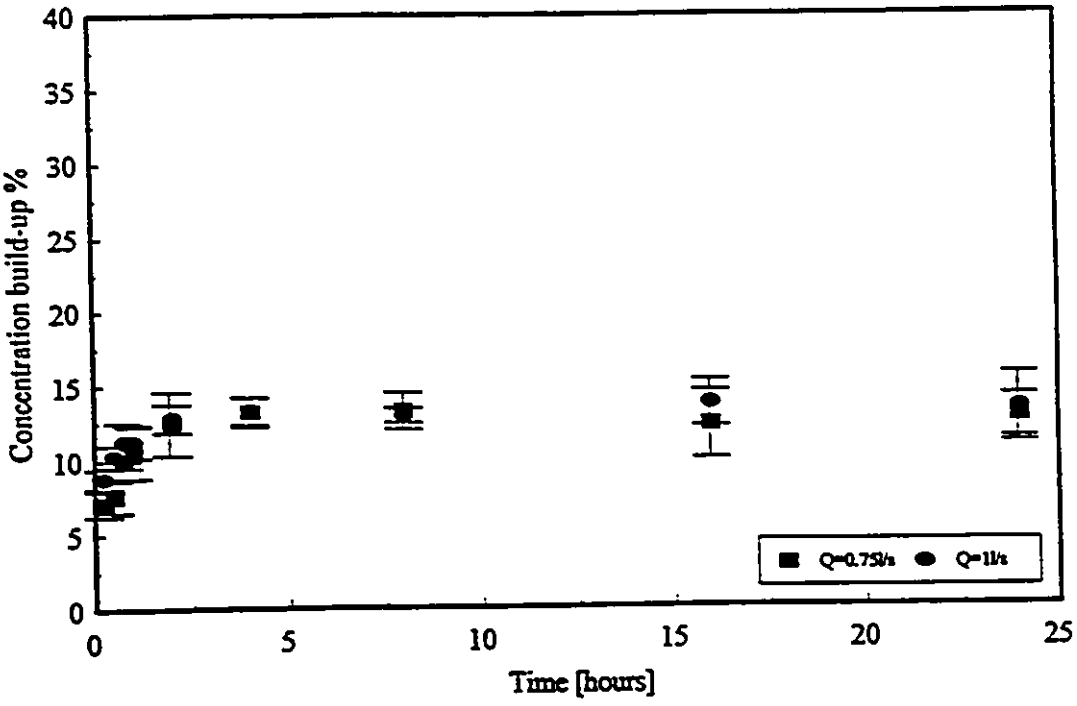

Figure 26: Fiber accumulation % (header conc. % build-up) vs time for ID = 1/4", α = 60°, and two different Q (CI = 95%).

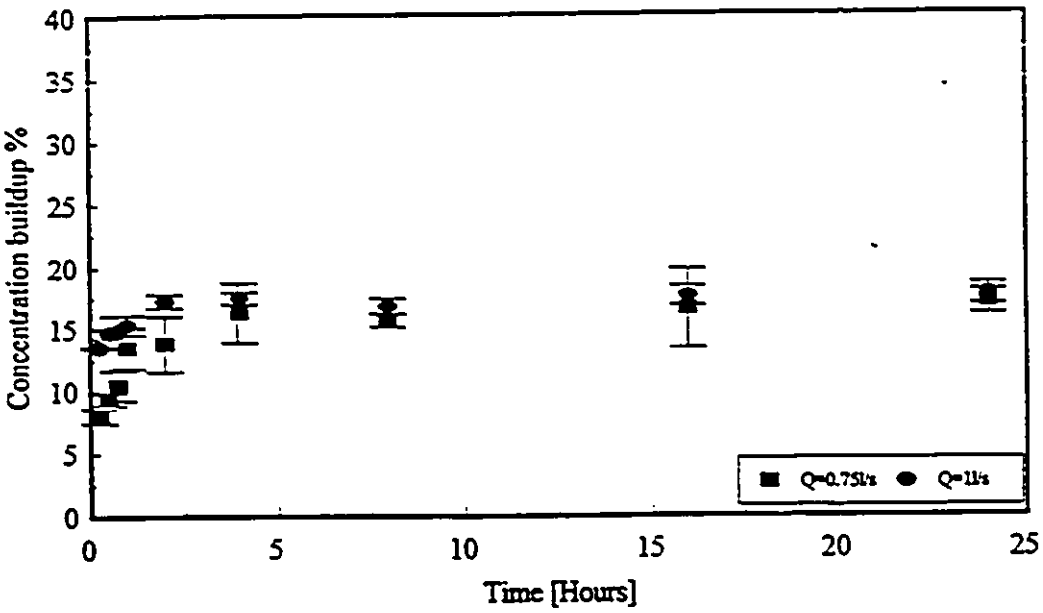

Figure 27: Fiber accumulation % (header conc. % build-up) vs time for ID = 1/2", α = 0°, and two different Q (CI = 95%).

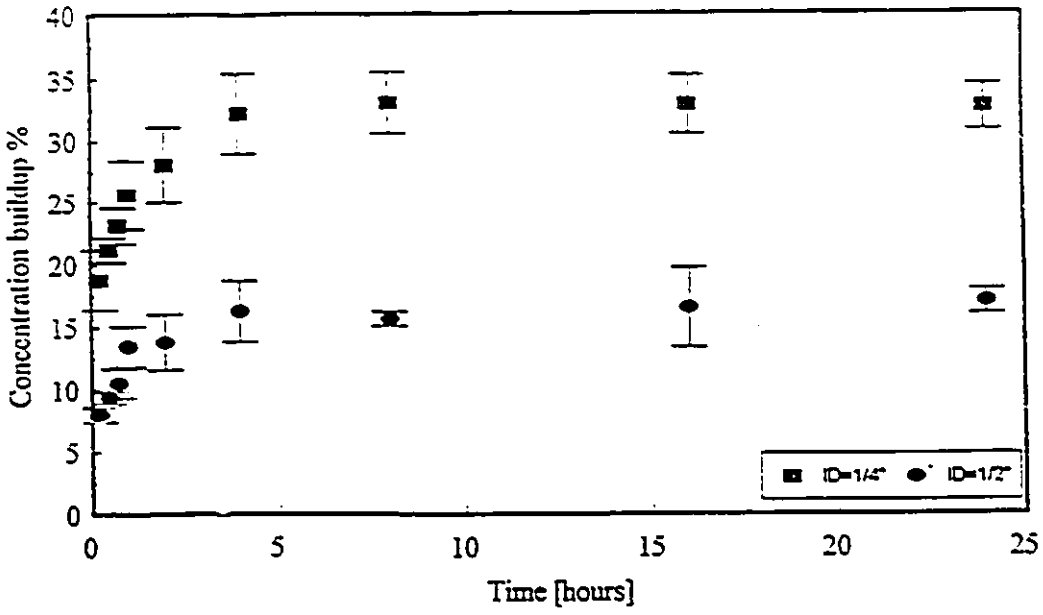

Figure 28: Fiber accumulation % (header conc. % build-up) vs time for $\alpha = 0°$, Q = 0.75 l/s, and different ID (CI = 95%).

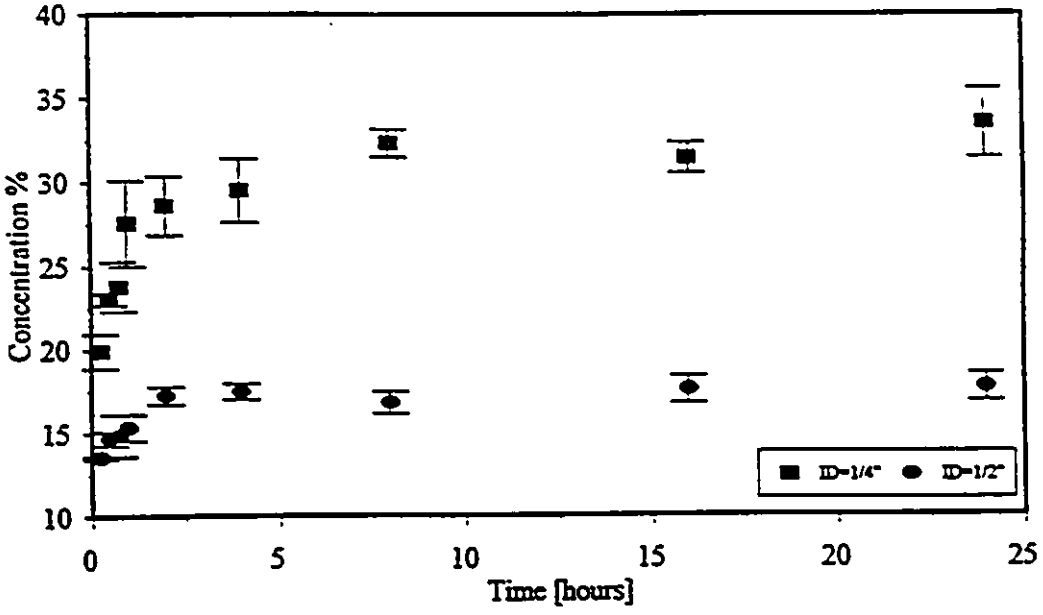

Figure 29: Fiber accumulation % (header conc. % build-up) vs time for $\alpha = 0°$, Q = 1 l/s, and different ID (CI = 95%).

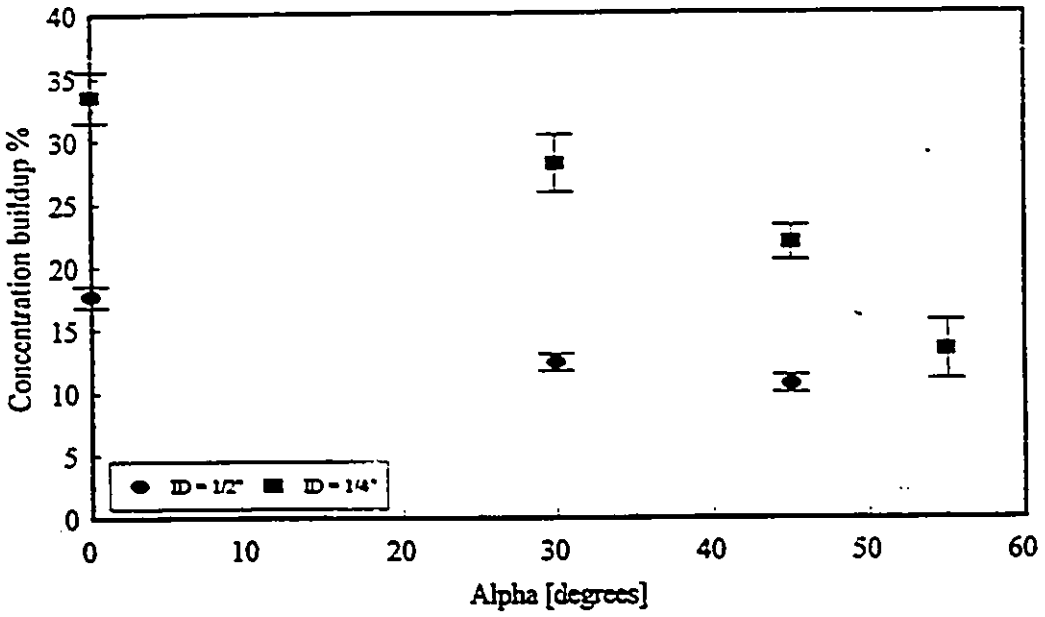

Figure 30: Fiber accumulation % (header conc. % build-up) vs inlet angle after 24 hrs of pumping, at Q = 1 l/s, and different ID.

Table 8: Concentration build-up % for ID = 1/4" at different Q and α.

Time in Hours	α =0° Q=0.75 %	α =0° Q=1 %	α =30° Q=0.75 %	α =30° Q=1 %	α =45° Q=0.75 %	α =45° Q=1 %	α =55° Q=0.75 %	α =55° Q=1 %
0.25	17.50	20.04	16.68	17.50	8.10	13.53	6.50	9.03
0.25	20.41	20.50	14.76	17.80	8.26	12.72	7.43	9.07
0.25	18.53	19.24	15.50	16.80	8.95	14.50	7.43	8.37
0.50	20.70	22.78	15.70	15.61	12.67	14.44	8.35	10.41
0.50	21.88	23.18	16.08	18.00	12.77	14.30	7.21	9.91
0.50	21.03	23.17	17.42	17.99	13.56	16.98	7.21	10.74
0.75	22.70	24.76	19.38	20.11	13.33	15.73	9.82	10.51
0.75	24.17	23.70	18.55	19.51	14.64	18.86	9.82	12.05
0.75	22.56	22.93	17.90	20.41	13.25	15.73	10.22	11.21
1.00	24.74	29.35	20.40	23.00	13.5	20.93	10.22	11.62
1.00	27.68	26.30	19.93	23.30	15.15	19.58	9.80	11.62
1.00	24.60	27.05	19.01	25.93	16.3	22.45	11.89	10.50
2.00	29.66	28.36	22.81	25.70	15.70	22.01	11.03	13.07
2.00	28.68	27.72	23.37	23.50	14.60	21.14	13.58	12.16
2.00	26.00	29.84	22.65	23.71	16.15	22.20	12.92	13.28
4.00	31.82	30.87	26.02	26.67	16.14	24.85	13.42	12.66
4.00	30.51	29.23	22.19	25.36	16.17	21.48	12.52	13.69
4.00	34.42	28.56	20.78	27.50	16.28	21.00	13.74	13.57
8.00	31.9	32.36	28.43	28.20	19.52	21.50	13.74	13.26
8.00	34.78	31.86	27.64	27.50	19.00	21.00	13.74	13.05
8.00	32.51	32.88	28.39	28.10	18.94	21.50	12.40	12.63

continued on next page

Table 8 (continued): Concentration build-up % for ID=1/4" at different Q. and α.

Time in Hours	α =0° Q=0.75 %	α =0° Q=1 %	α =30° Q=0.75 %	α =30° Q=1 %	α =45° Q=0.75 %	α =45° Q=1 %	α =55° Q=0.75 %	α =55° Q=1 %
16.00	34.54	32.11	28.64	27.50	19.147	21.43	12.20	12.90
16.00	32.18	30.99	27.77	28.75	17.70	20.00	10.96	13.56
16.00	31.85	31.4	30.48	28.44	20.33	21.50	13.78	14.82
24.00	32.24	33.33	29.38	27.11	19.40	21.50	12.40	14.70
24.00	33.98	32.40	27.25	29.75	19.76	22.84	13.78	11.81
24.00	31.84	34.90	28.10	27.61	20.30	21.25	12.11	13.56

Table 9: Concentration Build-up % for ID=1/2" and α =0° at different Q.

Time in Hours	Q = 0.75 L /s	Q = 1 L/s
0.25	8.19	13.50
0.25	8.33	13.55
0.25	7.64	13.60
0.50	9.02	14.40
0.50	9.53	14.92
0.50	9.53	14.73
0.75	10.50	14.00
0.75	9.77	15.07
0.75	11.27	15.50
1.00	12.45	14.83
1.00	13.57	15.81
1.00	14.49	15.35

continued on next page

Table 9 (continued): Conc. build-up % for ID=1/2" and $\alpha = 0^{o}$ at different Q.

Time in Hours	Q = 0.75 L/s	Q = 1 L/s
2.00	13.80	17.20
2.00	12.46	17.63
2.00	15.22	16.96
4.00	15.03	17.80
4.00	15.97	17.20
4.00	17.99	17.50
8.00	16.10	16.95
8.00	15.50	17.15
8.00	15.50	16.35
16.00	18.33	18.14
16.00	16.94	17.45
16.00	14.43	17.17
24.00	16.67	18.14
24.00	17.80	17.90
24.00	16.83	17.13

Table 10: Conc. build-up % at different α after 24 hrs of pumping at Q = 1 L/s.

α (degrees)	ID = 1/4"	ID = 1/2"
0.00	33.33	18.14
0.00	32.40	17.90
0.00	34.90	17.13
30.00	27.11	11.91
30.00	29.75	12.62
30.00	27.61	12.62
45.00	21.50	11.00
45.00	22.84	10.22
45.00	21.25	10.84

Figure 31 shows the pressure loss in port 3 (as shown in Figure 7) vs time for the 1/4" ID at different inlet angles and flowrates. It is clear that, as α increases for constant flow, ΔP becomes more negative yielding higher pressures drops. These higher pressure drops in a reduced dead surface area yield larger turbulent wall vortices and eddy formation. These results are in agreement with Chiba (1990), who found that the vortex length decreases with increasing Reynolds number due to fluid inertia. In our case, an increase in α reduces the dead surface area on the distributor plate and leads to a reduced Reynolds number within the distributor header chamber. This effect will yield lower accumulation, since an increase in vortex length will decrease the centrifugal forces acting on the fibers, since the centrifugal force experienced by a particle within this flow field is equal to the square of the velocity divided by the radius (Burton and Tcnhobanoglous, 1991). The pressure distribution on ports 1 and 2 are unaffected by the inlet flow and the inlet angle, as shown in Figure 32. The pressure distribution along the tube was also tracked and it is shown in Figure 33.

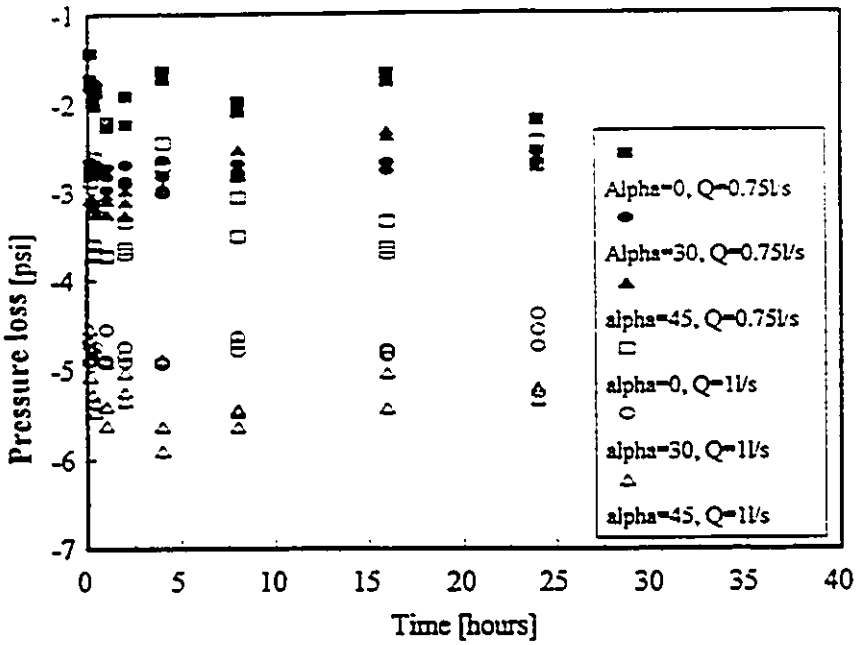

Figure 31: Pressure loss in port 3 vs time for ID = 1/4" and different flowrates and inlet angles.

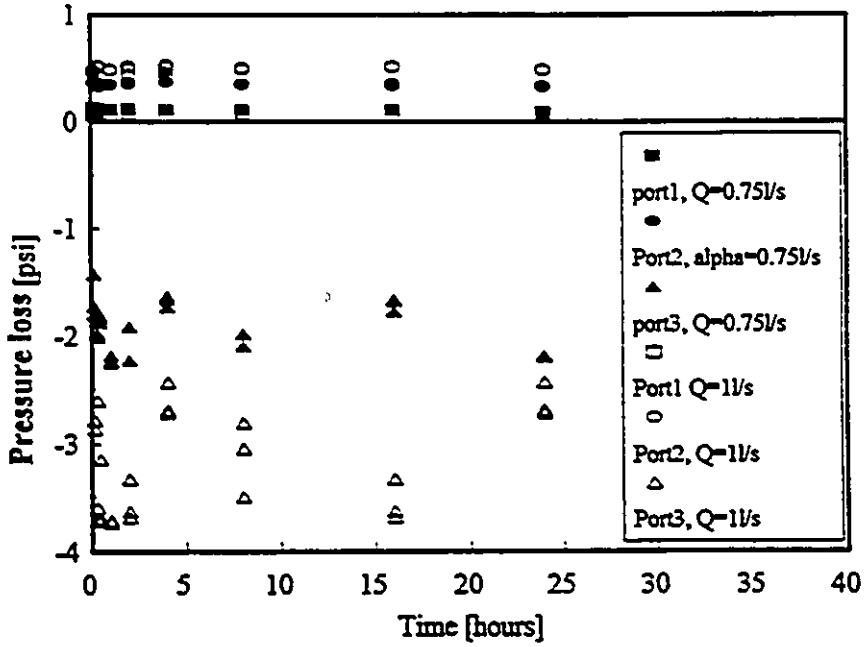

Figure 32: Pressure loss in the distribution header vs time for ID = 1/4", $\alpha = 0°$, and different flowrates.

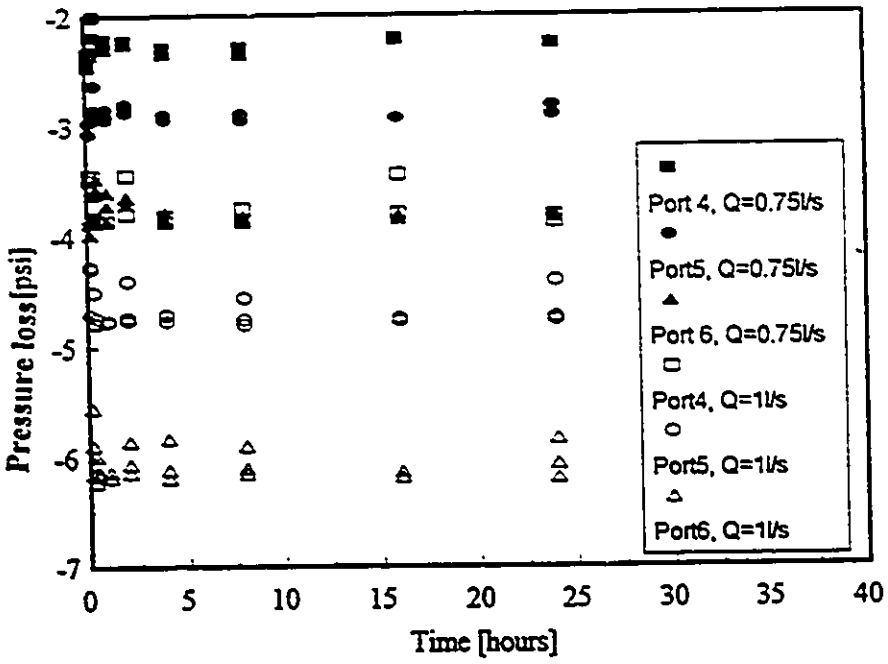

Figure 33: Pressure loss in the tube vs time for ID = 1/4"

$\alpha = 0°$ and different flowrates.

The fiber suspension used in this study has a high tendency to dephase. Leaving a certain volume of suspension for 3 minutes without mixing will lead to total settling due to dephasing caused by the gravitational forces acting on the fibers. While the accumulation of fibers in the distributor header chamber is due to dephasing, the detailed set of phenomena leading to this are uncertain at this time. However, several mechanisms could be postulated.

The dephasing occurring in the distribution chamber can be the result of the turbulence leading to eddy formation. It was clearly observed that once the pulp suspension fills the distribution header chamber the formation of eddies was observed. The centrifugal forces generated due to the eddy have the tendency to act on the fibers and enhance the dephasing, causing enrichment of large fibers in the header. The turbulence leading to eddy formation is proportional to the flowrate and to the inverse of the cross-sectional area of the flow at inlet of the tubes, as shown in Figure 34.

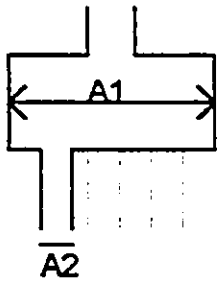

Figure 34: Decrease in crossectional area within the header.

The turbulence leading to eddy formation is proportional to $\frac{QA_1}{A_2}$. Hence an increase in the flowrate or decrease in A_2 (due to a decrease of the inner diameter and or the chamfer angle) will lead to an increase in the incidence of eddy formation yielding an increase in the centrifugal forces acting on the fibers which increase the dephasing in the system. Eddy

formation is also responsible for back mixing of the enriched suspension at the tube inlets produced due to the inertial effect discussed earlier.

The dephasing occurring in the distributor head could be also a result of the rebound of the suspension from the distributor plate. The rebound from the distributor plate is not limited to the dead areas alone but is also due to the back pressure developed in the tube as discussed earlier. Obviously, as the inlet angle on the distribution plate increases the total dead area for rebound decreases for a given flowrate, and tube ID, implying that the suspension has first to decelerate to zero velocity at impact, and then accelerate after rebound. This will clearly lead to dephasing, because the deceleration and acceleration will be different for the two phases and different for different sized fiber particles. Hence it would be expected that the steady-state concentration in the chamber will decrease with the increase in inlet angle. However, if the flowrate is increased for a constant inlet angle and ID of tube, the contribution to the rebound from the back pressure in the pipes increases. Hence it will be expected that the steady state concentration increases with increasing flowrate.

Decreasing the pipe diameter for a constant flowrate and inlet angle has the same effect, that is, it increases the contribution to rebound associated with back pressure. Hence it will be expected that the steady state concentration would increase with reducing ID for a constant chamfer angle and flowrate.

The tendency for the pipes to plug would depend on the felting nature of the suspension which again would be a function of the average fiber size distribution and concentration. As long as the steady state concentration in the distributor head remains below this critical plugging concentration no plugging would be observed. However, it can be expected that, if the ID of the pipe is sufficiently reduced and the flowrate increased, the steady state concentration may exceed this critical concentration and plugging would ensue. The critical steady state concentration, as explained earlier, is a function of the

basic characteristic of the suspension, with concentration, typical fiber size, fiber size distribution, and the general adhesive tendency of the fiber contributing.

It should be recognized that, under normal production conditions, fresh suspension would be continually introduced into the distribution head and the characteristics of the feed suspension would remain constant. However, recirculation of the same suspension leads to fiber break down because of the repeated exposure to the rebound effect and pumping action. This tendency would be even more pronounced at a high flowrate, low ID and low chamfer angle. This means that the characteristics of the inlet feed are continuously changing and correspondingly the critical properties will also continuously change, making the present system difficult to characterize.

The steady state concentration in the distribution head chamber is a function of the Reynolds number. As the flowrate increases and/or the diameter of the tube decreases, the Reynolds number increases yielding a higher steady state concentration. Increasing the inlet angle reduces the Reynolds number in the zone most affecting the mixing by increasing the average diameter of the tube inlet zone, as shown in Figure 35.

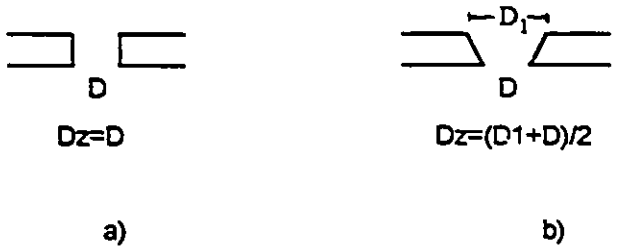

Figure 35: Inlet angle a) α=0°, b) α>0°.

Setting Dz as the average diameter of the tube inlet zone then from this brief schematic it is clear that, as α increases, Dz increases causing a decrease in the Reynolds number and

thus reduced fiber accumulation. Further, as the cross sectional area of the chamber zone increases, the back pressure is reduced resulting in a reduction in back mixing.

A correlation was introduced to relate the observed phenomenon of fiber accumulation to the parameters affecting it. For that, two correlations relating the steady-state (24 hrs) concentration build-up, expressed as a dimensionless ratio of C/Co, and the inlet angle and the inlet flowrate as variables of the Reynolds number at the inlet holes of the distribution head were developed for the two tube diameters (ID=1/4", 1/2"). From the calculation provided in Appendix C on dimensions of the header, it was found that the diameter of the each hole located at the inlet of the distribution head could be expressed as defined in equation 33 (in appendix C). Hence the total open cross sectional area for all tubes at the inlet of the header plate is given by

$$A = \frac{5\pi D^2}{4} = \frac{5\pi(tg\alpha + ID)^2}{4}. \qquad (30)$$

A modified Reynolds number can then be evaluated as

$$\mathrm{Re} = \frac{4\rho Q ID}{5\pi\mu(tg\alpha + ID)^2}. \qquad (31)$$

The correlation was then made for each tube diameter in the following form:

$$\frac{C}{C_o} = c(1 - \frac{a}{\mathrm{Re}^b}). \qquad (32)$$

As the flowrate increases and/or ID or α decreases, the Reynolds number increases leading to an increase in Re^b, so that $\frac{a}{\mathrm{Re}^b}$ decreases and $(1-\frac{a}{\mathrm{Re}^b})$ increases, resulting in an increase in final concentration which is in agreement with the experimental results. At

the limit as Re→∞, the final concentration tends to reach a maximum value which in this case is the steady state concentration .

The results are tabulated in Table 11 and Figures 36, 37, and 38. The statistical analysis is tubulated in Tables A18 and A19 (Appendix A). From these results it is clear that the correlation successfully fits the experimental data since in both cases it lies within the 95% confidence interval.

Table 11: correlation parameter results for both 1/4"and 1/2" Liner diameter case.

ID (inches)	a	b	c
1/4	12.04066	0.95258	1.37738
1/2	0.360290	0.21934	1.21627

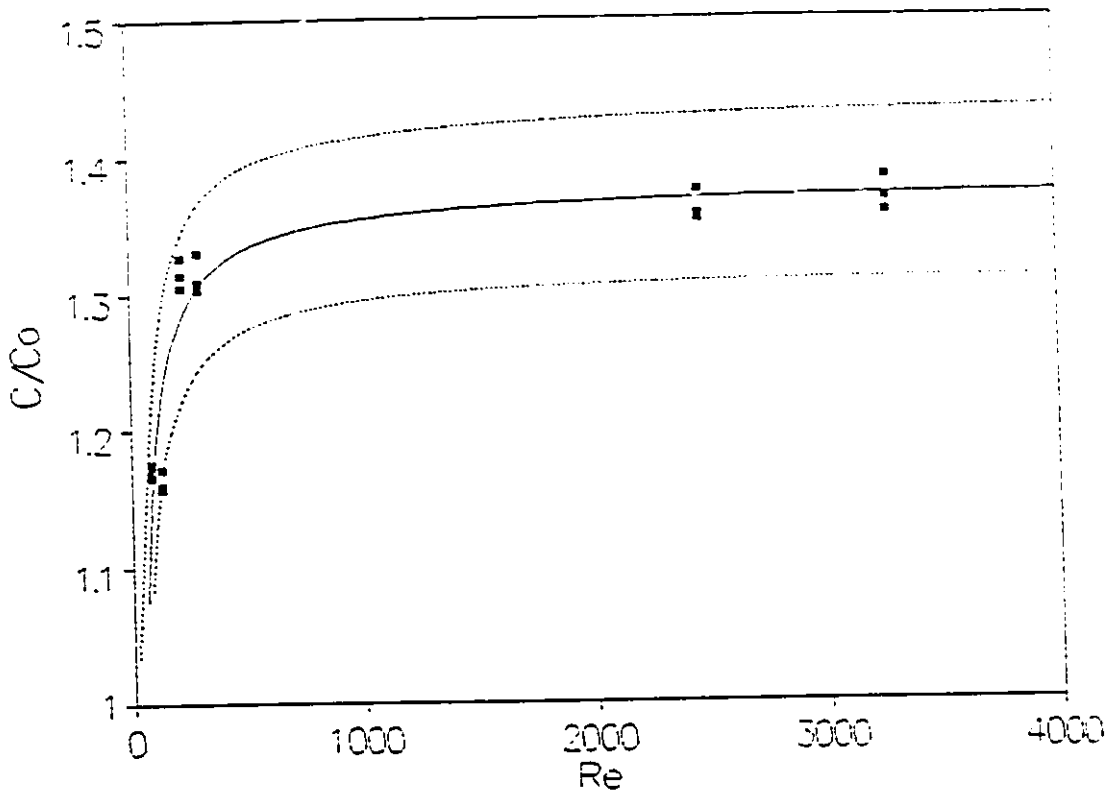

Figure 36: C/Co vs Re* fitted correlation ID = 1/4", with 95 % contour interval.

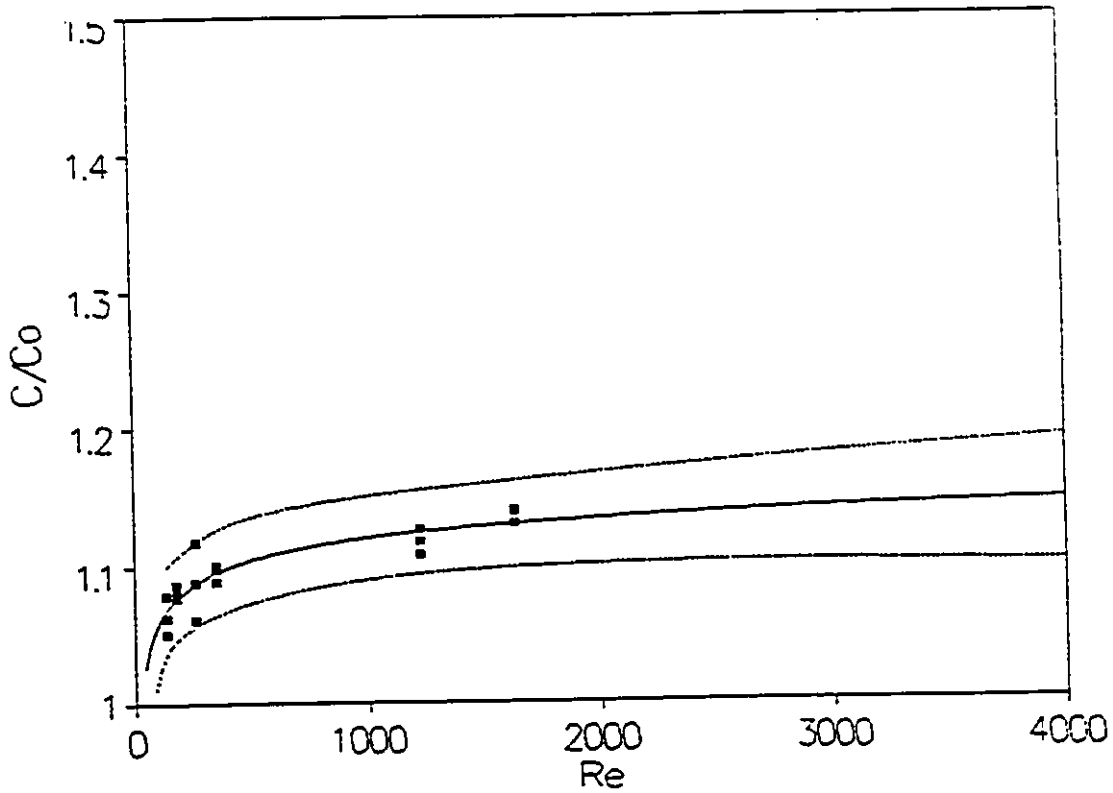

Figure 37: C/Co vs Re* fitted correlation ID = 1/2", with 95 % contour interval.

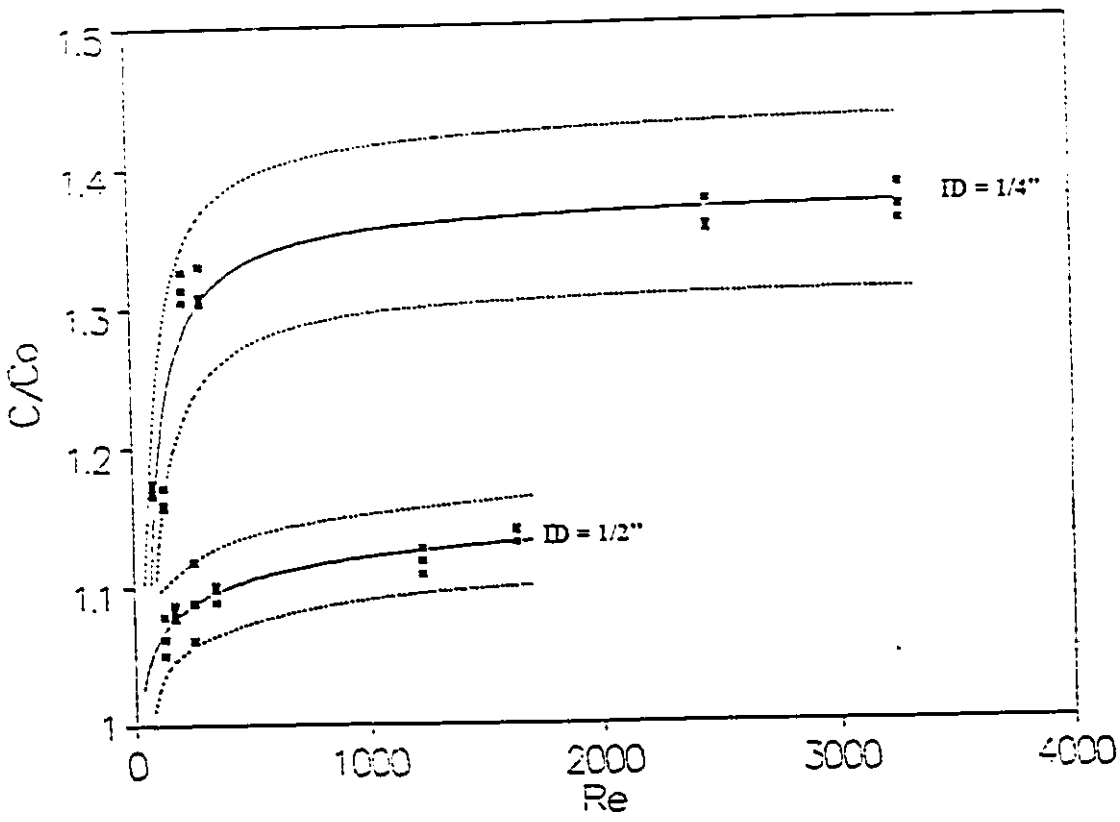

Figure 38: C/Co vs Re* fitted correlation comparison plot with 95 % contour interval.

6.4 Effect of Pumping on sheet stiffness and rigidity

The main objective of this research as outlined earlier is to study the hydrodynamic behavior of the suspension at the inlet region of tubular membrane module. As discussed earlier, the procedure was to pump the suspension for given time, collect all the suspension inside the header chamber, evaporate the water from it and, based on the mass of the resulting sheet, determine the concentration build-up within the header. It was observed that the sheet, after total evaporation, was getting darker throughout the procedure and more and more rigid. This change in stiffness was quantitatively evaluated using a burst test. A burst tester was used to evaluate the pressure needed to burst the sheet. All the results are tabulated in Table 12. Figure 39 shows the relationship between the required pressure to burst the sheet with the total pumping time. It is clear that, as we increase the pumping time, the sheet becomes more and more stiff. Obviously the amount of interfiber bonding and the individual fiber strength is of predominant importance in this effect.

From the literature, when cellulose fibers are beaten in water and made into paper it is found that sheet characteristics change considerably as the degree of beating is increased. Bursting and tensile strengths rise for a greater part of the mechanical processing and decrease much more slowly with further fiber processing (Britt, 1964). In the early experimental stages of this work it was observed microscopically that, as we increased the pumping time the fine population increased. From a theoretical point of view Paavilaine (1990) postulated that as the fines increase Campbell's forces increases and more fiber to fiber bonds are formed. Drying results in better activation of fiber segments by microcompression formation. If we consider centrifugal pumping as a mild beating process the results observed here are in agreement with the theory pronounced by Paavilaine.

Greater pumping times increase the amount of fines in the dry sheet. This results in a reduction of the local stress concentration within the sheet by distributing the stress over the whole surface of the bond when the network is strained, thus increasing paper strength. This is supported by the results shown in Figure 40 that indicate the effect of pumping time on the thickness of the sheets. It is clear that as the pumping time is increased, the dry sheet becomes thinner due to the increase in fines percentage, reducing the local stress concentration. However, centrifugal pumping cannot be considered a normal beating process because the decline of the stiffness after a certain time of beating did not occur as in the industrial beaten process (Britt, 1964). A plot of the ratio of the burst pressure over the sheet thickness and the total pumping time is shown in Figure 41. This further illustrates the beginning of a plateau after 24 hour pumping time; additional pumping may yield a decline in stiffness of the sheet similar to any normal beaten process. These data clearly indicate that the nature of the fiber suspension is changing with pumping time. Further study of the effect of fiber composition on plugging is warranted.

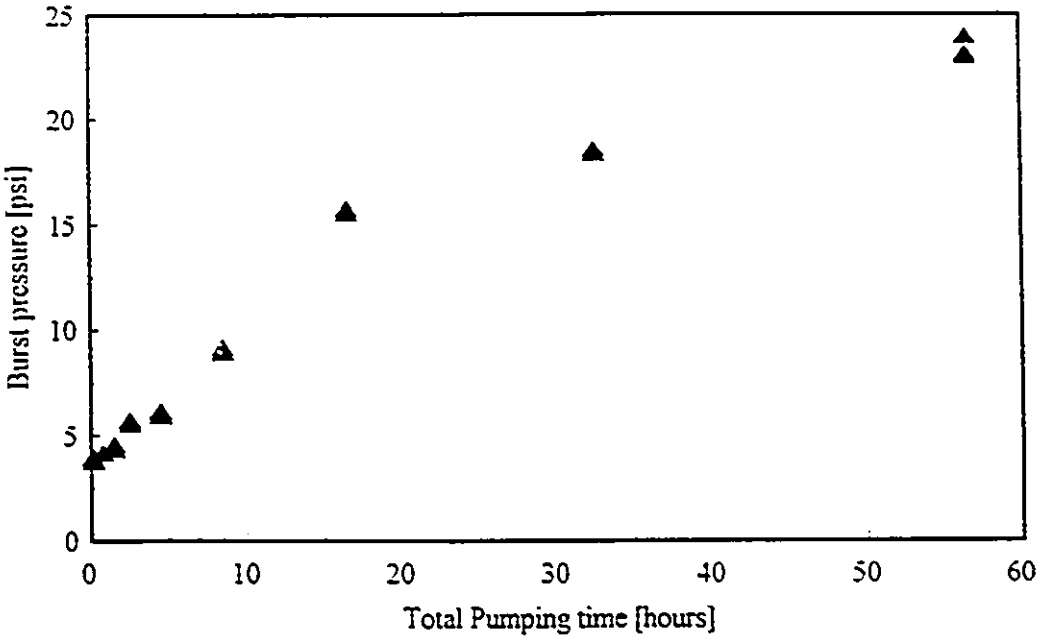

Figure 39: Effect of pumping time on the resulting liner sheet stiffness.

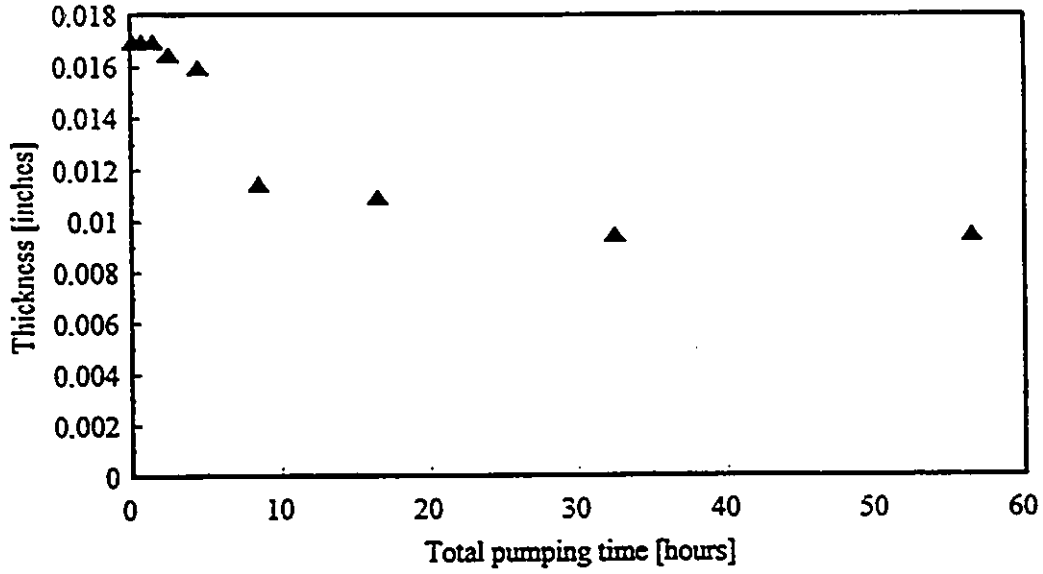

Figure 40: Effect of pumping time on the resulting liner sheet thickness.

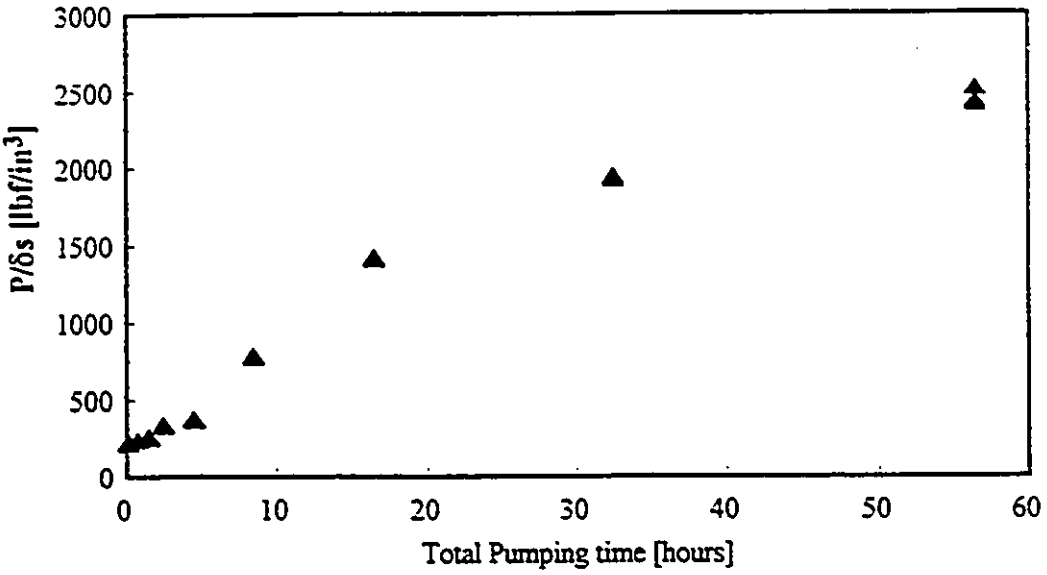

Figure 41: Effect of pumping time on the resulting liner sheet stiffness (pressure required/thickness vs time).

Table 12: Burst test results.

Total Pumping Time (hrs)	Burst Pressure (psi)	Paper Thickness (inchs)	P/δs (lbf/in)
0.15	4.0	0.0170	235.29
0.15	3.8	0.0170	223.53
0.15	3.8	0.0170	223.53
0.75	4.2	0.0170	247.06
0.75	4.2	0.0170	247.06
0.75	4.2	0.0170	247.06
1.50	4.6	0.0170	270.59
1.50	4.6	0.0170	270.59
1.50	4.4	0.0170	258.82
2.50	5.6	0.0165	339.39
2.50	5.6	0.0165	339.39
2.50	5.8	0.0165	351.52
4.50	6.0	0.0160	375.00
4.50	6.0	0.0160	375.00
4.50	6.2	0.0160	387.50
8.50	9.2	0.0115	800.00
8.50	9.0	0.0115	782.61
8.50	9.0	0.0115	782.61
16.5	15.8	0.0110	1436.36
16.5	15.8	0.0110	1436.36
16.5	15.6	0.0110	1418.18

continued on next page

Table 12 (continued): Burst test results.

Total Pumping Time (hrs)	Burst Pressure (psi)	Paper Thickness (inchs)	P/δs (lbf/in)
32.5	18.4	0.0095	1936.84
32.5	18.4	0.0095	1936.84
32.5	18.6	0.0095	1957.90
56.5	23.0	0.0095	2421.10
56.5	23.2	0.0095	2442.10
56.5	24.0	0.0095	2526.32

CHAPTER 7: CONCLUSIONS

1) The fiber suspension at 0.5 weight % was found to behave as a non Newtonian fluid in turbulent regime and its behavior indice n' was found to be equal to 0.24.

2) As the pumping time increased the percentage of fines in the suspension increased, and the color changed from beige to dark brown.

3) The quality of the dried sheet changed with increasing pumping time, it increased in stiffness and the required pressure to burst a fixed area on it increased.

4) The critical plugging concentration of the suspension in the distributor header chamber was not reached but the concentration was found to vary with following parameters;

- the chamfer angle on the distribution head,
- the inlet flowrate,
- the inner diameter of the tube,
- the total pumping time.

It was found that this concentration increased as the flowrate increased and/or the inlet angle or the inner diameter of the tubes decreased. It was also clear that this concentration was increasing with time for all cases until reaching a steady state concentration always smaller than the critical concentration for plugging.

5) The concentration build-up in the distributor header chamber was a result of suspension dephasing.

6) The tendency to dephase exists whenever an external force acts on the suspension with a consequent change in velocity. This tendency increases with the magnitude of the force. The magnitude of the force is proportional to volumetric flowrate and inversely proportional to the diameter of the tube.

7) A correlation relating the ratio of the concentration build-up with the inverse of a modified Reynolds number accounting for the flowrate, the tube inner diameter, and the inlet angle successfully predicted the experimental results.

CHAPTER 8: RECOMMENDATIONS

The novel nature of this research classified as a beginning step for more advanced studies. A number of recommendations are proposed to obtain a clearer picture of the state of affairs in a real industrial application.

1) Repeat the experiment with higher feed concentrations such as 1, 1.5, and 2% fibers.

2) Study the effect of the temperature of the suspension on the accumulation in the distribution head.

3) Perform these tests on an actual tubular module.

4) Model the system using computational fluid dynamic packages (FIDAP, PHEONIX, etc.)

5) Investigate other suspensions (e.g., sludges, etc.).

BIBLIOGRAPHY

Belfort G., "Fluid Mechanics in Membrane Filtration recent Developments," *J. Membr. Sci*, **40**, p123, (1989).

Bird, B., Stewart, W., Lightfoot, E., Transport Phenomena, John Wiley & Sons Publishing, New York, p192, (1960).

Bogger, D. and Binnigton, R., "Circular Entry flows of fluid M_1". *J. Non-Newtonian Fluid Mech.*," 35, p339, (1990).

Bonano, E. J., "A Study of Flocculation in Flowing Concentrated Fibre Suspension Using Coherence Functions," *J. Pulp Paper Sci.*, **10** (4), p102, (1984).

Brandenburg K., "Critical Process Variables in the White Water System that Affect Glass Fiber Dispersion," *TAPPI J.*, **76** (7), p145, (1993).

Britt, K., "Paper Sheet Formation: Observations Concerning Retention," *TAPPI J.*, **64** (5), p53, (1981).

Britt, K., "Physical and Chemical Relationships in Paper Sheet Formation," *TAPPI Eng. Conf.*, book 1, p177, (1979).

Britt K., Handbook of Pulp and Paper Technology, Reinhold Publishing corporation, New York, p29, (1964).

Burton, Franklin L., Tchobanoglous, George, Waste water Engineering, Metcalf & Eddy, inc., McGraw-Hill Publishing company, New York, p242, (1991).

Chang, M. and Robertson, A., "Flocculation Studies of Fiber Suspensions: Influence of Zeta Potential," *Pulp & Paper Mag. Can.*, 9, p68, (1967).

Chase, W., Donatelli, A., and Walkinshaw, J., "Effects of Freeness and Consistency on the Viscosity of Hardwood and Softwood Pulp Suspensions," *TAPPI J.*, 5, p199, (May 1989).

Cheremisinoff, N., Encyclopedia of Fluid Mechanics, Gulf Publishing Company, Houston, Texas. Volume 5, p291, (1986).

Chiba, K., and Nakamura, K., "A Numerical Solution for the Flow of Dilute Fiber Suspensions Through an Axisymmetric Contraction," *J. Non-Newtonian Fluid Mech.*, **35**, p1, (1990).

Daily, J., and Bugliarello, G., "Rheological Models and Laminar Shear Flow of Fiber Suspensions," *TAPPI J.*, **12**, p44, (1961).

Dodge, D., and Metzner, A., "Turbulent Flow of Non-Newtonian Systems," *AICh E. Journal* **5**, p189, (1959).

Duffy, G., Longdill, G., and Lee, P., "High-Consistency Flow of Pulp Suspensions in Pipes," *TAPPI J.*, **61**: (8), p85, (1978).

Duffy, G., and Tichener, A., "Disruptive Shear Stress of Pulp Networks," *TAPPI J.*, 78: (13), p74, (1975).

Durst, R., and Jenness, L., "Flow Properties of Paper Pulp Stock. Relationship of Shear Value to Pipe Friction for Pipes of Various Diameters," *TAPPI J.*, 42: (9) (1959).

Emmerton, H., "Fundamentals of the Beating Process," *Brit. Paper 7 Board Manufactures Assoc.* (1957).

Francis, W., and Kerekes, R., "Flow and Mixing Behavior of Low and Medium Consistency Fiber Suspensions Downstream of a Valve," *TAPPI J.*, p113, (Sept 1992).

Ho, W.S., and Sirkar, K., Membrane Handbook, Reinhold publication corporation, New York, p121, (1992).

Hourani, M., "Fiber Flocculation in Pulp Suspension Flow" *TAPPI J.*, p186, (June 1988).

Jagannadh, S., Jordan, H., and Brodkey, R., "Formation and Characterization of Paper Pulp Flocs," *Chem. Eng. Sci.*, **46** (12), p2997, (1991).

Jeffrey, G., "The Motion of Ellipsoidal Particles Immersed in a Viscous Fluid," *Proc. Roy. Soc.*, **A102**, p161, (1922).

Karter, E., and Durst, R. "Flow Characteristics of Deaerated Pulp Suspensions," *TAPPI J.*, **49** (6), p82, (1966).

Kerekes, R. J., and Douglas, W., "Viscosity Properties of Suspensions at the Limiting Conditions for Turbulent Drag Reduction," *Can. J. Chem. Eng.*, **50**, p228, (1972).

Kerekes, R. J., "Pulp Flocculation in Decaying Turbulence: A Literature Review," *Pulp & Paper Sci.* J., **9** (3), p86, (1983).

Kurronen, S., and Wahlstrom, P., "Flow of Pulp Suspensions," *Paper and Timber*, **11** p876, (1974).

Marrov, V., Nikolov, N. D., Islam, M. A., and Nikolova, J. D., "An Investigation on the Configuration of Inserts in Tubular Ultrafiltration Module to Control Concentration Polarization," *J. Membr. Sci.*, 75, p197, (1992).

Mason, S.G., "The Motion of Fibers in Flowing Liquids," *Pulp & Paper Mag. Can.*, **51** (5), p93, (1950).

Mason, S.G., "Fiber Motions and Flocculation," *TAPPI J.* **37** (11), p494, (1954).

Mason, SG., and Manley, R., "Particle Motions in Sheared Suspensions, Orientations, and Interactions of Rigid Rods," *Pro. Roy. Soc.*, **A238**, p117, (1956).

Meyer, H., "An Analitical Treatment of Laminar Flow of Annulus Forming in Fiber Suspensions in Vertical Pipes," *TAPPI J.*, **47** (2), p78, (1964).

Mih, W., and Parker, J., "Velocity Profile Measurement and a Phenomenological Description of Turbulent Fiber Suspension Pipe Flow," *TAPPI J.* **50** (5), p237, (1967).

Myreen, B., "Moduling the Flow of pulp of Pulp Suspensions in Pipes" *Paper and Timber* 5, p497, (1989). Part 2 Paper and Timber 7, p791, (1989).

Norman, B., et al ., "Hydrodynamics of Papermaking Fibers in Water Suspension," *Fiber-Water Interactions in Papermaking* (Oxford), p195, (Sept. 1977).

Ogawa, K., Yoshikawa, S., Suguro, A., Ikeda, J., and Ogawa H., "Flow Characteristics and Circular Pipe Flow of Pulp Suspension," *J. Chem. Eng.* of Japan 23 (1), p1 (1990).

Paavilaine, L., "Importance of Particle Size -fiber length and fines- for the characterization of softwood Kraft pulp," *Paper and Timber* 72 (5), p516, (1990).

Rosenberg, J., and Denn, M., "Simulation of Non-Recirculating Flows of Dilute Fiber Suspensions," *J. Non-Newtonian Fluid Mech.*, 37, p317, (1990).

Skowronski, J., and Bichard, W., "Fiber to Fiber Bonds in Paper. Measurement of Bond Strength and Specific Bond Strength," *J. pulp and paper Sci.*, 13 (5), p165, (Sept 1987).

Sourirajan, S., Matsuura, T., Reverse Osmosis, Ultrafiltration Process Principles, National Reasearch Concil Canada publication, Ottawa, p807, (1985).

Spiazzi, E., Lenoir, J., and Grangeon, A., "A New Generator of Unsteady-State Flow Regime in Tubular Membranes as an Anti-Fouling technique: A hydrodynamic approach" *J. Membr. Sci.*, 80, p49, (1993).

Steen, M., "Modeling Fiber Flocculation in Turbulent Flow: a Numerical Study," *TAPPI J.*, p175, (Sept. 1991).

Stenuf, T., and Calo, A., "Effect of Temperature on the Flow of Pulp Suspensions," *TAPPI Eng. Conf.* (Toronto), p143, (1975).

Wahren, D., "Fiber Network Structures in Papermaking Operations," *Paper Science Technol.* p112, (1980).

Zhao, R., and Kerekes, R., "The Effect of Suspending liquid Viscosity on Fiber flocculation" *TAPPI J.*, **76**, (2), p183, (1993).

APPENDIX A: Raw Data

Table A1: Average % build-up for ID = 1/4", Q = 0.75 L/s, and α = 0°.

Time	Average	Variance	Std.Error	CI=95%	Av+STf	Av-STf
0.25	18.81	1.45	1.20	2.37	21.19	16.44
0.50	21.20	0.24	0.50	0.98	22.18	20.22
0.75	23.14	0.53	0.73	1.43	24.58	21.71
1 00	25.67	2.01	1.42	2.79	28.46	22.88
2.00	28.12	2.40	1.55	3.05	31.16	25.06
4.00	32.25	2.63	1.62	3.20	35.45	29.05
8.00	33.06	1.54	1.24	2.44	35.51	30.62
16.00	32.85	1.43	1.20	2.36	35.21	30.50
24.00	32.69	0.86	0.93	1.83	34.52	30.86

Table A2: Average % build-up for ID = 1/4", Q = 1 L/s, and α = 0°.

Time	Average	Variance	Std.Error	CI=95%	Av+STf	Av-STf
0.25	19.92	0.27	0.52	1.03	20.95	18.90
0.50	23.04	0.04	0.19	0.37	23.41	22.67
0.75	23.80	0.56	0.75	1.48	25.27	22.32
1.00	27.57	1.68	1.30	2.56	30.13	25.01
2.00	28.64	0.80	0.89	1.75	30.40	26.89
4.00	29.56	0.94	0.97	1.91	31.46	27.64
8.00	32.36	0.17	0.42	0.82	33.19	31.54
16.00	31.50	0.21	0.46	0.91	32.41	30.59
24.00	33.54	1.06	1.03	2.03	35.58	31.51

Table A3: Average % build-up for ID = 1/4", Q = 0.75 L/s, and α = 30°.

Time	Average	Variance	Std.Error	CI=95%	Av+STf	Av-STf
0.25	15.64	0.62	0.79	1.55	17.20	14.09
0.50	16.40	0.54	0.74	1.45	17.85	14.94
0.75	18.61	0.36	0.60	1.18	19.80	17.42
1.00	19.78	0.33	0.58	1.13	20.92	18.68
2.00	22.94	0.10	0.31	0.62	23.56	22.33
4.00	23.00	4.91	2.22	4.37	27.36	18.63
8.00	28.15	0.13	0.36	0.72	28.89	27.44
16.00	28.96	1.27	1.13	2.22	31.19	26.74
24.00	28.24	0.77	0.878	1.73	29.97	26.51

Table A4: Average % build-up for ID = 1/4", Q = 1 L/s, and α = 30°.

Time	Average	Variance	Std.Error	CI=95%	Av+STf	Av-STf
0.25	17.37	0.18	0.42	0.82	18.19	16.54
0.50	17.20	1.26	1.12	2.21	19.41	14.98
0.75	20.01	0.14	0.37	0.74	20.75	19.27
1.00	24.08	1.73	1.32	2.59	26.67	21.49
2.00	24.30	0.98	0.99	1.95	26.26	22.35
4.00	26.51	0.77	0.88	1.73	28.24	24.78
8.00	27.92	0.09	0.30	0.59	28.51	27.33
16.00	28.23	0.28	0.53	1.05	29.27	27.18
24.00	28.15	1.31	1.15	2.26	30.41	25.90

Table A5: Average % build-up for ID = 1/4", Q = 0.75 L/s, and α = 45°.

Time	Average	Variance	Std.Error	CI=95%	Av+STf	Av-STf
0.25	8.44	0.14	0.37	0.73	9.16	7.71
0.50	13.00	0.16	0.40	0.78	13.78	12.22
0.75	13.74	0.40	0.64	1.25	15.00	12.48
1.00	14.98	1.30	1.14	2.25	17.23	12.73
2.00	15.48	0.42	0.65	1.27	16.75	14.20
4.00	16.20	0.004	0.06	0.12	16.32	16.08
8.00	19.15	0.068	0.26	0.51	19.67	18.64
16.00	19.73	0.233	0.48	0.95	20.68	18.77
24.00	19.81	0.15	0.38	0.76	20.57	19.05

Table A6: Average % build-up for ID = 1/4", Q = 1 L/s, and α = 45°.

Time	Average	Variance	Std.Error	CI=95%	Av+STf	Av-STf
0.25	13.58	0.53	0.73	1.44	15.02	12.15
0.50	15.24	1.52	1.23	2.43	17.67	12.81
0.75	16.77	2.18	1.47	2.91	19.68	13.87
1.00	20.99	1.37	1.17	2.31	23.30	18.68
2.00	21.80	0.22	0.47	0.93	22.74	20.87
4.00	22.44	2.94	1.71	3.38	25.82	19.07
8.00	21.33	0.06	0.24	0.46	21.80	20.87
16.00	20.98	0.48	0.69	1.36	22.34	19.62
24.00	21.86	0.49	0.70	1.38	23.24	20.49

Table A7: Average % build-up for ID = 1/4", Q = 0.75 L/s, and α =55°.

Time	Average	Variance	Std.Error	CI=95%	Av+STf	Av-STf
0.25	7.12	0.19	0.44	0.86	7.98	6.26
0.50	7.59	0.29	0.54	1.06	8.65	6.53
0.75	9.95	0.04	0.19	0.37	10.32	9.59
1.00	10.64	0.82	0.90	1.78	12.42	8.86
2.00	12.51	1.17	1.08	2.13	14.64	10.38
4.00	13.23	0.27	0.52	1.02	14.24	12.21
8.00	13.29	0.40	0.63	1.24	14.54	12.04
16.00	12.31	1.33	1.15	2.27	14.59	10.04
24.00	12.76	0.53	0.73	1.44	14.20	11.33

Table A8: Average % build-up for ID = 1/4", Q = 1 L/s, and α =55°.

Time	Average	Variance	Std.Error	CI=95%	Av+STf	Av-STf
0.25	8.82	0.10	0.32	0.63	9.46	8.19
0.50	10.35	0.12	0.34	0.67	11.03	9.68
0.75	11.26	0.40	0.63	1.24	12.50	10.02
1.00	11.25	0.28	0.53	1.04	12.29	10.21
2.00	12.84	0.24	0.49	0.96	13.80	11.90
4.00	13.31	0.21	0.46	0.91	14.21	12.40
8.00	12.98	0.07	0.26	0.52	13.50	12.46
16.00	13.76	0.63	0.80	1.57	15.33	12.19
24.00	13.36	1.41	1.20	2.34	15.70	11.02

Table A9: Average % build-up for ID = 1/2", Q = 0.75 L/s, and α =0°.

Time	Average	Variance	Std.Error	CI=95%	Av+STf	Av-STf
0.25	8.05	0.09	0.30	0.58	8.64	7.47
0.50	9.36	0.06	0.24	0.48	9.84	8.88
0.75	10.51	0.37	0.61	1.20	11.72	9.31
1.00	13.50	0.69	0.83	1.64	15.14	11.86
2.00	13.83	1.27	1.12	2.22	16.04	11.61
4.00	16.33	1.52	1.23	2.43	18.76	13.90
8.00	15.70	0.08	0.28	0.55	16.25	15.14
16.00	16.57	2.60	1.61	3.18	19.75	13.39
24.00	17.10	0.25	0.50	0.98	18.08	16.12

Table A10: Average % build-up for ID = 1/2", Q = 1 L/s, and α = 0°.

Time	Average	Variance	Std.Error	CI=95%	Av+STf	Av-STf
0.25	13.55	0.002	0.041	0.08	13.63	13.47
0.50	14.68	0.05	0.22	0.42	15.11	14.26
0.75	14.86	0.40	0.63	1.24	16.10	13.61
1.00	15.33	0.16	0.40	0.79	16.12	14.54
2.00	17.26	0.08	0.28	0.54	17.81	16.72
4.00	17.50	0.06	0.24	0.48	17.98	17.02
8.00	16.82	0.12	0.34	0.67	17.49	16.15
16.00	17.59	0.17	0.41	0.81	18.40	16.78
24.00	17.72	0.19	0.43	0.85	18.60	16.87

Table A11: Reynolds number vs C/Co for both ID= 1/4" and 1/2" after 24 hours of pumping.

ID = 1/4"		ID = 1/2"	
C/Co	Re	C/Co	Re
1.36	2452.48	1.12	1226.24
1.37	2452.48	1.11	1226.24
1.35	2452.48	1.13	1226.24
1.33	223.90	1.09	264.10
1.30	223.90	1.06	264.10
1.31	223.90	1.12	264.10
1.16	98.10	1.06	136.25
1.17	98.10	1.05	136.25
1.17	98.10	1.08	136.25
1.37	3269.97	1.15	1634.98
1.36	3269.97	1.15	1634.98
1.38	3269.97	1.15	1634.98
1.30	298.53	1.10	352.13
1.33	298.53	1.09	352.13
1.31	298.53	1.10	352.13
1.16	130.80	1.08	181.66
1.17	130.80	1.08	181.66
1.16	130.80	1.09	181.66

Table A12: Pressure distribution for ID=1/4", alpha=0, and Q=0.75 l/s

Time hrs	Port 1	Port 2	Port 3	Port 4	Port 5	Port 6
0.15	0.13	0.37	-1.43	-2.36	-2.96	-3.82
0.15	0.12	0.45	-1.79	-2.35	-2.97	-3.87
0.15	0.11	0.49	-1.71	-2.46	-3.07	-3.97
0.30	0.13	0.37	-1.77	-2.35	-2.94	-3.84
0.30	0.12	0.37	-2.01	-2.31	-2.92	-3.82
0.30	0.11	0.35	-1.97	-2.32	-2.91	-3.81
0.45	0.12	0.36	-1.80	-2.19	-2.85	-3.61
0.45	0.12	0.36	-1.83	-2.19	-2.86	-3.56
0.45	0.12	0.33	-1.86	-2.00	-2.62	-3.47
1.00	0.12	0.36	-2.18	-2.21	-2.84	-3.59
1.00	0.12	0.35	-2.22	-2.30	-2.93	-3.84
1.00	0.12	0.36	-2.25	-2.29	-2.90	-3.72
2.00	0.13	0.37	-1.90	-2.25	-2.87	-3.70
2.00	0.12	0.37	-2.22	-2.23	-2.82	-3.65
2.00	0.12	0.36	-1.90	-2.23	-2.80	-3.64
4.00	0.12	0.38	-1.72	-2.34	-2.94	-3.84
4.00	0.12	0.38	-1.66	-2.35	-2.94	-3.85
4.00	0.12	0.47	-1.62	-2.29	-2.90	-3.78
8.00	0.12	0.37	-2.08	-2.29	-2.90	-3.82
8.00	0.11	0.36	-1.97	-2.36	-2.95	-3.86
8.00	0.11	0.35	-1.97	-2.33	-2.93	-3.83
16.00	0.12	0.37	-1.76	-2.21	-2.93	-3.84
16.00	0.11	0.34	-1.65	-2.22	-2.93	-3.80
16.00	0.12	0.35	-1.67	-2.21	-2.93	-3.84
24.00	0.10	0.33	-2.18	-2.26	-2.90	-3.80
24.00	0.10	0.34	-2.18	-2.26	-2.90	-3.79
24.00	0.10	0.33	-2.18	-2.26	-2.82	-3.83

Table A13: Pressure distribution for ID=1/4", alpha=0, and Q=1 l/s

Time hrs	Port 1	Port 2	Port 3	Port 4	Port 5	Port 6
0.15	0.07	0.47	-2.78	-3.49	-4.71	-6.15
0.15	0.08	0.48	-2.78	-3.44	-4.30	-5.55
0.15	0.07	0.47	-2.86	-3.46	-4.27	-5.89
0.30	0.08	0.52	-2.60	-3.45	-4.51	-5.98
0.30	0.07	0.53	-3.59	-3.84	-4.77	-6.22
0.30	0.10	0.53	-3.70	-3.85	-4.78	-6.13
0.45	0.09	0.52	-3.71	-3.87	-4.78	-6.16
0.45	0.08	0.52	-3.69	-3.86	-4.79	-6.13
0.45	0.08	0.51	-3.14	-3.83	-4.74	-6.13
1.00	0.08	0.49	-3.73	-3.84	-4.76	-6.13
1.00	0.07	0.50	-3.71	-3.86	-4.77	-6.18
1.00	0.07	0.49	-3.70	-3.85	-4.76	-6.17
2.00	0.09	0.50	-3.32	-3.45	-4.40	-5.85
2.00	0.09	0.53	-3.63	-3.80	-4.73	-6.13
2.00	0.07	0.45	-3.68	-3.79	-4.76	-6.06
4.00	0.07	0.50	-2.68	-3.86	-4.77	-6.19
4.00	0.08	0.54	-2.71	-3.81	-4.71	-5.83
4.00	0.07	0.43	-2.43	-3.82	-4.71	-6.11
8.00	0.09	0.51	-2.80	-3.87	-4.80	-6.14
8.00	0.08	0.52	-3.04	-3.84	-4.75	-5.89
8.00	0.08	0.49	-3.49	-3.75	-4.56	-6.10
16.00	0.08	0.52	-3.32	-3.45	-4.74	-6.13
16.00	0.07	0.52	-3.63	-3.80	-4.76	-6.18
16.00	0.07	0.51	-3.68	-3.79	-4.77	-6.17
24.00	0.09	0.49	-2.68	-3.86	-4.76	-6.06
24.00	0.10	0.50	-2.71	-3.81	-4.40	-6.19
24.00	0.08	0.49	-2.43	-3.82	-4.73	-5.83

Table A14: Pressure distribution for ID=1/4", alpha=30, an Q=0.75 l/s

Time hrs	Port 1	Port 2	Port 3	Port 4	Port 5	Port 6
0.15	0.13	0.38	-2.71	-2.05	-2.65	-3.61
0.15	0.12	0.37	-2.63	-2.04	-2.65	-3.59
0.15	0.13	0.37	-2.64	-2.03	-2.64	-3.58
0.30	0.13	0.37	-2.67	-2.04	-2.66	-3.61
0.30	0.12	0.36	-2.71	-2.02	-2.65	-3.62
0.30	0.12	0.36	-2.77	-2.05	-2.68	-3.62
0.45	0.12	0.36	-2.67	-2.05	-2.68	-3.64
0.45	0.12	0.36	-2.78	-2.04	-2.66	-3.62
0.45	0.11	0.36	-2.76	-2.04	-2.66	-3.64
1.00	0.12	0.37	-2.70	-2.06	-2.68	-3.64
1.00	0.11	0.36	-2.81	-2.05	-2.66	-3.64
1.00	0.12	0.36	-2.96	-2.04	-2.67	-3.62
2.00	0.11	0.36	-2.67	-2.04	-2.66	-3.64
2.00	0.11	0.35	-2.86	-2.04	-2.68	-3.65
2.00	0.10	0.36	-2.90	-2.04	-2.68	-3.63
4.00	0.11	0.36	-2.62	-2.04	-2.67	-3.63
4.00	0.10	0.35	-3.00	-2.05	-2.69	-3.64
4.00	0.10	0.35	-2.81	-2.05	-2.69	-3.63
8.00	0.11	0.36	-2.66	-2.02	-2.65	-3.62
8.00	0.09	0.34	-2.75	-1.93	-2.66	-3.49
8.00	0.09	0.34	-2.79	-1.92	-2.64	-3.50
16.00	0.10	0.35	-2.66	-2.00	-2.63	-3.53
16.00	0.09	0.35	-2.74	-2.01	-2.65	-3.52
16.00	0.09	0.34	-2.65	-1.89	-2.63	-3.39
24.00	0.09	0.35	-2.55	-1.84	-2.53	-3.49
24.00	0.09	0.34	-2.66	-1.99	-2.60	-3.40
24.00	0.10	0.35	-2.53	-1.94	-2.55	-3.28

Table A15: Pressure distribution for ID=1/4", alpha=30, an Q=1 l/s.

Time hrs	Port 1	Port 2	Port 3	Port 4	Port 5	Port 6
0.15	0.09	0.52	-4.67	-3.71	-4.81	-6.57
0.15	0.06	0.52	-4.89	-3.70	-4.79	-6.55
0.15	0.06	0.51	-4.90	-3.69	-4.79	-6.53
0.30	0.08	0.52	-4.77	-3.69	-4.79	-6.54
0.30	0.07	0.53	-4.86	-3.68	-4.77	-6.53
0.30	0.06	0.51	-4.87	-3.65	-4.75	-6.50
0.45	0.08	0.53	-4.73	-3.62	-4.71	-6.47
0.45	0.08	0.52	-4.83	-3.61	-4.71	-6.45
0.45	0.07	0.52	-4.82	-3.61	-4.71	-6.41
1.00	0.08	0.52	-4.54	-3.61	-4.71	-6.42
1.00	0.08	0.52	-4.89	-3.60	-4.69	-6.42
1.00	0.07	0.52	-4.91	-3.59	-4.69	-6.46
2.00	0.03	0.50	-4.73	-3.61	-4.71	-6.46
2.00	0.07	0.52	-4.91	-3.60	-4.70	-6.48
2.00	0.07	0.53	-4.84	-3.60	-4.72	-6.46
4.00	0.08	0.53	-4.91	-3.62	-4.73	-6.47
4.00	0.07	0.52	-4.93	-3.62	-4.70	-6.41
4.00	0.07	0.52	-4.90	-3.60	-4.69	-6.31
8.00	0.08	0.52	-4.62	-3.59	-4.69	-6.12
8.00	0.08	0.51	-4.70	-3.60	-4.69	-6.16
8.00	0.08	0.52	-4.78	-3.59	-4.69	-6.05
16.00	0.08	0.52	-4.76	-3.64	-4.73	-6.42
16.00	0.07	0.50	-4.84	-3.64	-4.72	-6.45
16.00	0.06	0.51	-4.80	-3.63	-4.73	-6.27
24.00	0.07	0.50	-4.38	-3.56	-4.62	-6.25
24.00	0.06	0.50	-4.73	-3.56	-4.50	-6.27
24.00	0.08	0.51	-4.55	-3.50	-4.55	-6.27

Table A16: Pressure distribution for ID=1/4", alpha=45, an Q=0.75 l/s.

Time hrs	Port 1	Port 2	Port 3	Port 4	Port 5	Port 6
0.15	0.13	0.37	-2.76	-2.21	-2.87	-3.84
0.10	0.13	0.37	-3.06	-2.21	-2.87	-3.85
0.10	0.12	0.35	-3.05	-2.20	-2.85	-3.81
0.30	0.11	0.37	-3.07	-2.20	-2.84	-3.83
0.30	0.12	0.37	-3.14	-2.20	-2.84	-3.81
0.30	0.11	0.36	-3.10	-2.20	-2.85	-3.80
0.45	0.11	0.36	-3.15	-2.19	-2.83	-3.79
0.45	0.11	0.36	-3.22	-2.19	-2.82	-3.75
0.45	0.12	0.37	-3.22	-2.19	-2.83	-3.74
1.00	0.11	0.36	-3.01	-2.19	-2.82	-3.70
1.00	0.11	0.36	-3.07	-2.18	-2.82	-3.65
1.00	0.11	0.35	-3.23	-2.19	-2.82	-3.70
2.00	0.11	0.35	-2.96	-2.18	-2.81	-3.68
2.00	0.10	0.35	-3.25	-2.18	-2.83	-3.69
2.00	0.10	0.35	-3.09	-2.18	-2.83	-3.70
4.00	0.10	0.35	-2.96	-2.17	-2.82	-3.67
4.00	0.10	0.35	-2.92	-2.16	-2.83	-3.62
4.00	0.11	0.36	-2.90	-2.16	-2.84	-3.76
8.00	0.12	0.37	-2.50	-2.18	-2.85	-3.79
8.00	0.09	0.06	-2.78	-2.20	-2.89	-3.86
8.00	0.10	0.07	-2.71	-2.22	-2.89	-3.87
16.00	0.10	0.06	-2.34	-2.14	-2.78	-3.70
16.00	0.10	0.06	-2.29	-2.13	-2.77	-3.71
16.00	0.10	0.06	-2.69	-2.13	-2.78	-3.76
24.00	0.10	0.08	-2.64	-2.08	-2.73	-3.43
24.00	0.11	0.07	-2.70	-2.07	-2.73	-3.42
24.00	0.10	0.06	-2.59	-2.09	-2.73	-3.42

Table A17: Pressure distribution for ID=1/4", alpha=45, an Q=1 l/s.

Time hrs	Port 1	Port 2	Port 3	Port 4	Port 5	Port 6
0.15	0.09	0.40	-4.52	-3.76	-4.87	-6.46
0.15	0.10	0.33	-4.67	-3.74	-4.82	-6.43
0.15	0.10	0.40	-5.06	-3.74	-4.80	-6.37
0.30	0.09	0.37	-4.85	-3.82	-4.91	-6.53
0.30	0.08	0.38	-4.87	-3.82	-4.89	-6.47
0.30	0.09	0.37	-5.27	-3.78	-4.87	-6.46
0.45	0.05	0.39	-4.78	-3.73	-4.81	-6.38
0.45	0.09	0.38	-5.35	-3.73	-4.80	-6.44
0.45	0.10	0.39	-5.46	-3.73	-4.79	-6.43
1.00	0.11	0.42	-4.91	-3.76	-4.84	-6.47
1.00	0.11	0.43	-5.40	-3.73	-4.82	-6.46
1.00	0.10	0.41	-5.61	-3.75	-4.86	-6.48
2.00	0.11	0.41	-5.02	-3.74	-4.83	-6.46
2.00	0.09	0.41	-5.24	-3.77	-4.87	-6.49
2.00	0.08	0.40	-5.34	-3.76	-4.86	-6.51
4.00	0.19	0.43	-4.86	-3.78	-4.89	-6.51
4.00	0.11	0.42	-5.89	-3.74	-4.83	-6.51
4.00	0.11	0.43	-5.62	-3.76	-4.86	-6.48
8.00	0.10	0.43	-5.63	-3.76	-4.85	-6.47
8.00	0.11	0.44	-5.43	-3.73	-4.82	-6.46
8.00	0.10	0.43	-5.46	-3.75	-4.86	-6.48
16.00	0.09	0.40	-5.03	-3.72	-4.81	-6.30
16.00	0.08	0.40	-5.42	-3.70	-4.80	-6.27
16.00	0.10	0.43	-5.43	-3.69	-4.80	-6.33
24.00	0.11	0.43	-5.19	-3.73	-4.83	-6.46
24.00	0.12	0.43	-5.24	-3.75	-4.87	-6.49
24.00	0.09	0.45	-5.34	-3.74	-4.86	-6.51

Table A18: Statistical analysis for the correlation for the 1/4" case.

X-value	Y-value	Y-Predict	-95% Prediction	+95% Prediction	Residual	Resid%
89.10	1.17	1.15	1.07	1.23	0.027	2.3231
89.10	1.16	1.15	1.07	1.23	0.018	1.557
89.10	1.17	1.15	1.07	1.23	0.022	1.882
130.80	1.16	1.22	1.14	1.29	-0.061	-5.320
130.80	1.17	1.22	1.14	1.29	-0.046	-3.957
130.80	1.16	1.22	1.14	1.29	-0.060	-5.103
223.90	1.33	1.28	1.21	1.36	0.0445	3.356
223.90	1.31	1.28	1.21	1.36	0.0313	2.389
223.90	1.30	1.28	1.21	1.36	0.0226	1.735
298.53	1.30	1.30	1.23	1.38	-0.0017	-0.133
298.53	1.33	1.30	1.23	1.38	0.0253	1.909
298.53	1.31	1.30	1.23	1.38	0.00337	0.2578
2452.47	1.35	1.37	1.29	1.44	-0.01618	-1.198
2452.47	1.36	1.37	1.29	1.44	-0.01212	-0.894
2452.47	1.37	1.37	1.29	1.44	0.00571	0.416
3269.97	1.38	1.37	1.30	1.45	0.01280	0.926
3269.97	1.36	1.37	1.30	1.45	-0.0128	-0.947
3269.97	1.37	1.37	1.30	1.45	-0.0033	-0.242

Table A19: Statistical analysis for the correlation for the 1/2" case.

X- value	Y-value	Y-predict	-95% Prediction	+95% Prediction	Residual	Resid%
136.25	1.06	1.067	1.035	1.099	-0.0050	-0.48
136.25	1.05	1.067	1.035	1.099	-0.0170	-1.62
136.25	1.08	1.067	1.035	1.099	0.0108	1.007
181.66	1.09	1.076	1.046	1.106	0.0095	0.874
181.66	1.08	1.076	1.046	1.106	0.0042	0.393
181.66	1.08	1.076	1.046	1.106	0.0003	0.025
264.10	1.06	1.087	1.057	1.118	-0.027	-2.56
264.10	1.09	1.087	1.057	1.118	-0.0001	-0.010
264.10	1.12	1.087	1.057	1.118	0.0295	2.642
352.13	1.10	1.095	1.064	1.126	0.0050	0.460
352.13	1.10	1.095	1.064	1.126	0.0019	0.172
352.13	1.09	1.095	1.064	1.126	-0.007	-0.66
1226.24	1.11	1.12	1.094	1.155	-0.017	-1.53
1226.24	1.12	1.12	1.094	1.155	-0.0077	-0.68
1226.24	1.13	1.12	1.094	1.155	0.00163	0.145
1634.98	1.14	1.13	1.098	1.162	0.00941	0.826
1634.98	1.30	1.13	1.098	1.162	0.00050	0.044
1634.98	1.14	1.13	1.098	1.162	0.00840	0.738

APPENDIX B: Figures

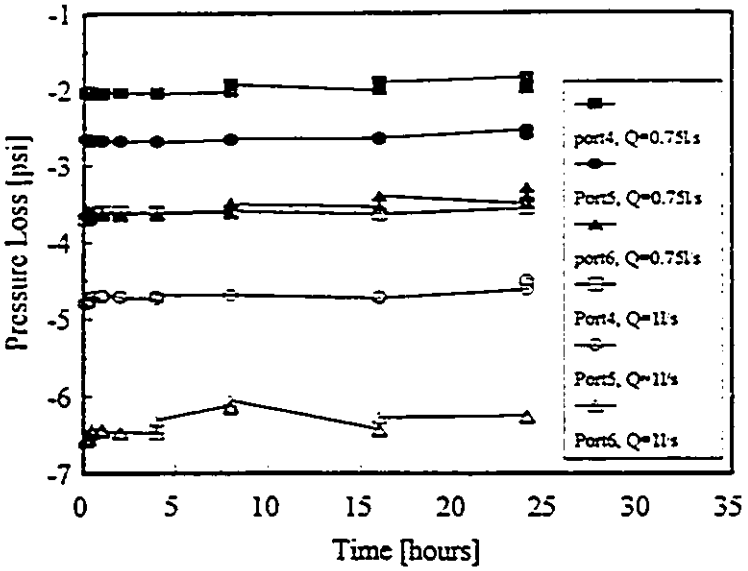

Fig.B1: Pres. loss in the tube vs time
For ID=1/4", Alpha=30, at different Q.

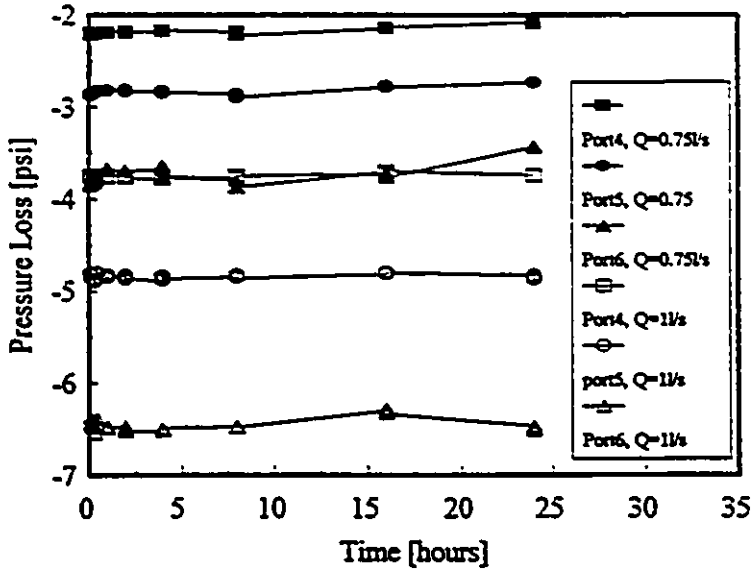

Fig.B2: Pres. loss in the tube vs time
For ID=1/4", alpha=45, at different Q.

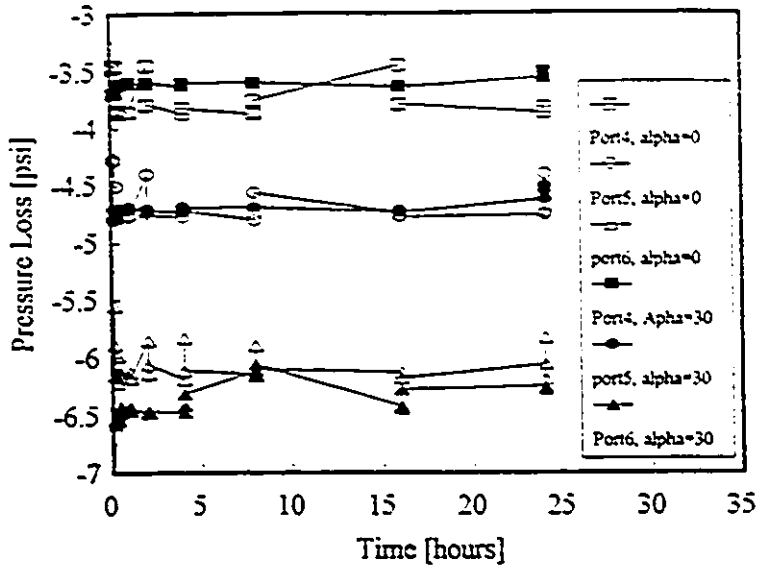

FigB3a: Pres. loss in the tube vs time
For ID=1/4", Q=1l/s, at dif. alpha.

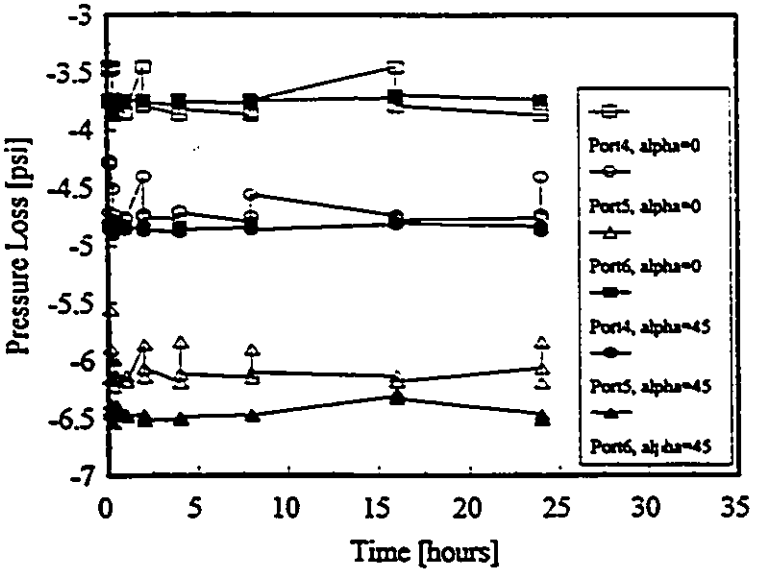

FigB3b: Pres. loss in the tube vs time
For ID=1/4", Q=1l/s, at dif. alpha

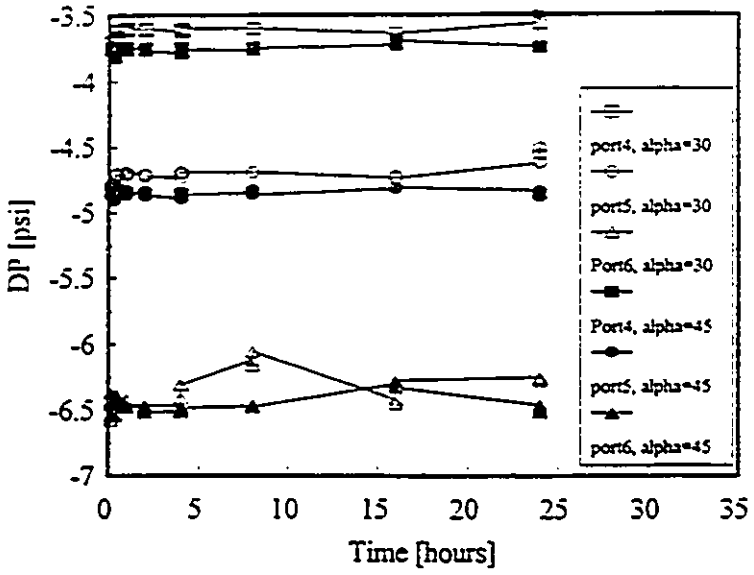

FigB3c: Pres. loss in the tube vs time
For ID=1/4", Q=1l/s, at dif. alpha

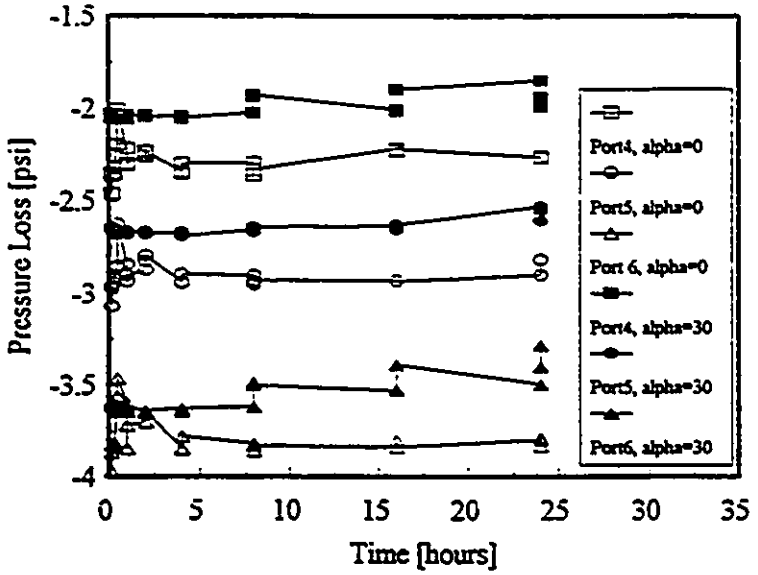

FigB4a: Pres. loss in the tube vs time
For ID=1/4", Q=0.75l/s, at dif. alpha.

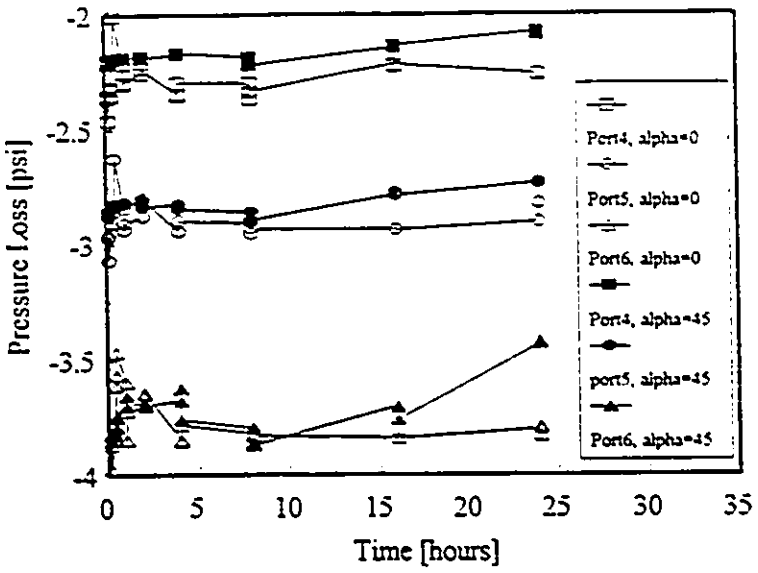

FigB4b: Pres. loss in the tube vs time
For ID=1/4", Q=0.75l/s, at dif. alpha.

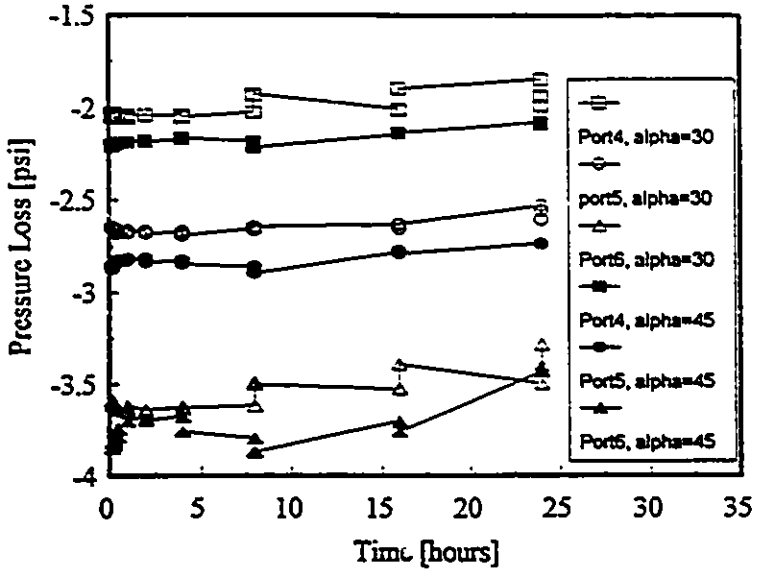

FigB4c: Pres. loss in the tube vs time
For ID=1/4", Q=0.75l/s, at dif. alpha

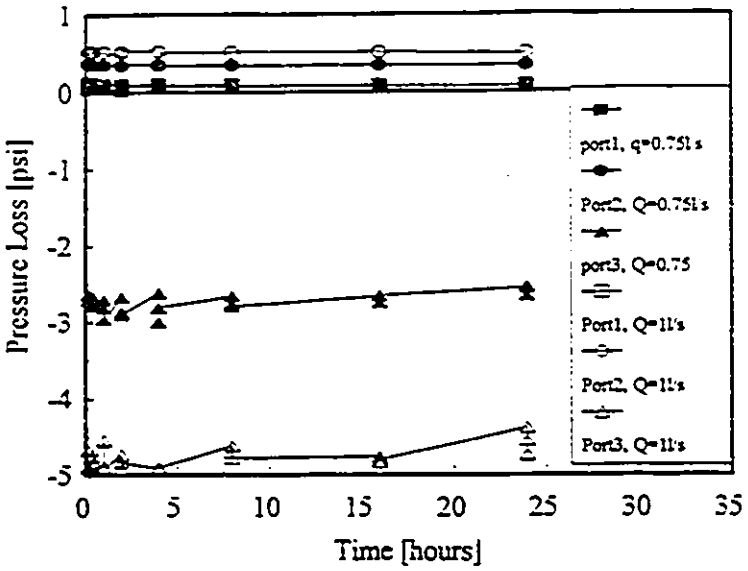

Fig.B5: Pres. loss in the cell vs time
For ID=1/4", alpha=30, at different Q.

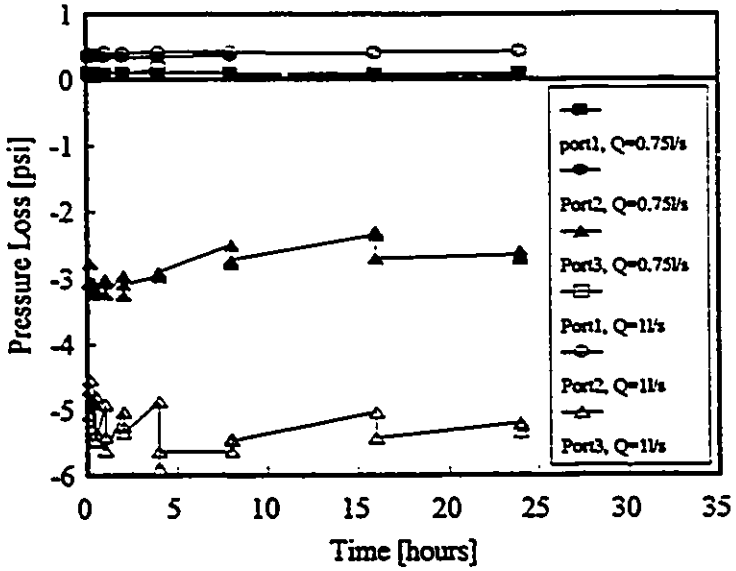

Fig.B6: Pres. loss in the cell vs time
For ID=1/4", alpha=45, at different Q.

APPENDIX C: Sample calculation for the dimensions needed to design the prototype module

As discussed earlier, it was necessary to design a series of header with different inner diameters and different entry shape, to do so this following calculation were made.

R: radius of the disk $R = 3"$

δ: thickness of the disk $\delta = 0.5"$

β: angle dividing the hole disk by 5 $\beta = 72^{o}$

d_1: distance between the center of the disk and that of the holes $d_1 = 1.625"$

d_2: distance between centers of the holes = 2*(sin36*1.625) $d_2 = 1.9013"$

α: deviation angle $\alpha = 0, 30, 45^{o}$

l: distance between the wall of the holes (see attached figure)

l': distance between the wall of the hole and that of the disk (see figure C1)

D: hole diameter as function of α.

Using some geometric formulas:

$$D = tg\alpha + ID. \tag{33}$$

$$l'(in) = 3(in) - 1.625(in) - \frac{D(in)}{2}. \tag{34}$$

$$l(in) = [2*(\sin 36*1.625)] - D(in). \tag{35}$$

Therefore D, l, and l' were calculated as function of α, where α vary from 0, 30, to 45°. All result are provided in Table C1. Figure C1 present a schematic diagram of the top and cross-sectional view of the header plate.

Table C1: Calculation of all designed header parameter.

ID (inches)	OD (inches)	α (degrees)	D (inches)	l (inches)	l' (inches)
1/2	3/4	0	0.5000	1.4103	1.1250
1/2	3/4	30	1.0774	0.8329	0.8363
1/2	3/4	45	1.5000	0.4103	0.6250
1/4	1/2	0	0.2500	1.6603	1.2500
1/4	1/2	30	0.8274	1.0830	0.9613
1/4	1/2	45	1.2500	0.6603	0.7500
1/4	1/2	55	1.6780	0.2323	0.5360
1/8	3/8	0	0.1250	1.7853	1.3125
1/8	3/8	30	0.7024	1.2080	1.0238
1/8	3/8	45	1.1250	0.7853	0.8125

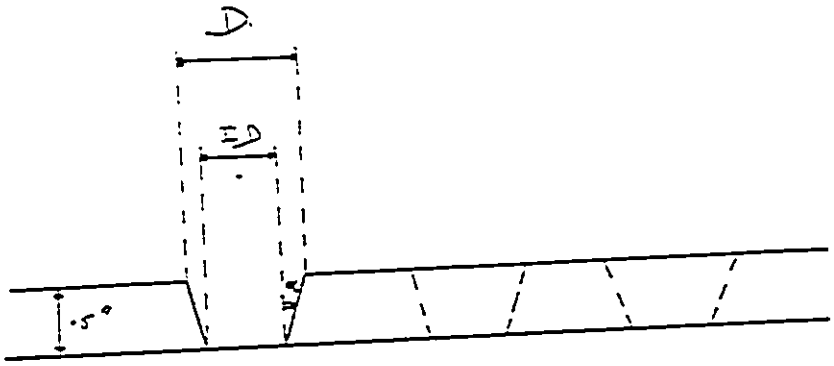

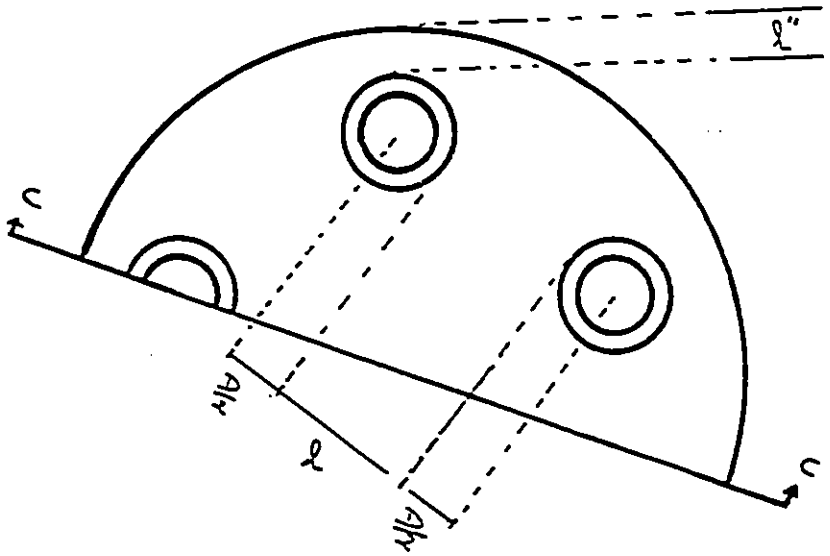

Figure C1: Schematic diagram of the top and cross sectional view of the header plate.

APPENDIX D: Computer Programs

APPENDIX D1: Data Acquisition Program

This Program was written by Dr. A. Tremblay in QBasic Language. It was used as a data acquisition and registration program.

```
      DIM pressures(6)


      TIMES = "00:00:00"
      GOSUB initialscreen: GOSUB openall: CLOSE

5     GOSUB openandappend

      CLS : LOCATE 5, 10
      PRINT TAB(5); "Press any key to record 6 pressures"
      PRINT TAB(5); "Once a key is pressed, you have 15 seconds before the first
reading."
      PRINT " "
      PRINT TAB(5); "Readings are performed at 30 second intervals"
      PRINT TAB(5); " - First 10 seconds is allowed for switching"
      PRINT TAB(5); " - Pressure will be averaged over the remaining 20 seconds"

      GOSUB keytocontinue
      CLS : LOCATE 10, 40: PRINT "15 second delay"

      interval = 15!: GOSUB delay

      GOSUB disp1
      interval = 10!: GOSUB delay
      avginterval = 20!: GOSUB avgpress
      pressures(1) = averagepress
      GOSUB disp2
      interval = 10!: GOSUB delay
      avginterval = 20!: GOSUB avgpress
      pressures(2) = averagepress
      GOSUB disp3
      interval = 10!: GOSUB delay
      avginterval = 20!: GOSUB avgpress
```

```
        pressures(3) = averagepress
        GOSUB disp4
        interval = 10!: GOSUB delay
        avginterval = 20!: GOSUB avgpress
        pressures(4) = averagepress
        GOSUB disp5
        interval = 10!: GOSUB delay
        avginterval = 20!: GOSUB avgpress
        pressures(5) = averagepress
        GOSUB disp6
        interval = 10!: GOSUB delay
        avginterval = 20!: GOSUB avgpress
        pressures(6) = averagepress
        FOR j = 1 TO 6: PRINT #2, pressures(j); "  "; : NEXT j: PRINT #2, CHR$(10)
        CLOSE

        GOSUB initialscreen

        GOTO 5
        STOP

keytocontinue:

        LOCATE 15, 25
        PRINT "Press space to continue, S to stop"

10      a$ = INKEY$
        IF a$ = "S" OR a$ = "s" THEN STOP
        IF a$ = CHR$(32) THEN RETURN
        GOTO 10

avgpress:
        iniavgpresstime = TIMER
        sum = 0!: jjj = 0!

100     jjj = jjj + 1!
        GOSUB readpress
        sum = sum + psi
        LOCATE 10, 50: PRINT "                    "
        LOCATE 10, 50: PRINT "Pressure (psi): "; psi
        interval = .5: GOSUB delay
        IF avginterval >= TIMER - iniavgpresstime THEN 100
        averagepress = sum / jjj
        RETURN
```

```
readpress:

20
     PRINT #4, "SVRD"; CHRS(13);
30    INPUT #4, voltS
     IF LEN(voltS) < 10 GOTO 30
     rlvolt = VAL(MIDS(voltS, 2, 9))

     psi = 12.5 * rlvolt / 5000!
     RETURN

delay:
     oldtime = TIMER
40     IF interval >= TIMER - oldtime THEN 40
     RETURN

openall:

     CLS : OPEN "A:TEST.DAT" FOR RANDOM AS #2: CLOSE : FILES "A:*.dat"

     PRINT "              ENTER FILE NAME WITHOUT FILE EXTENSION"
     PRINT "          ( Duplicate file names will be overwritten ) "
     PRINT "                              "; : INPUT FILES
     OPEN "A:" + FILES + ".dat" FOR RANDOM AS #2
     OPEN "COM1:9600,N,8,1,RS,ASC" FOR RANDOM AS #4
     RETURN

openandappend:


     OPEN "A:" + FILES + ".dat" FOR APPEND AS #2
     OPEN "COM1:9600,N,8,1,RS,ASC" FOR RANDOM AS #4
     RETURN

initialscreen:

     CLS : LOCATE 10, 10
     PRINT "Power to instruments must be ON before running this program."
     GOSUB keytocontinue


disp1:
     CLS : BEEP
     LOCATE 5, 20
```

```
        PRINT "  ______  "
        PRINT TAB(19); "  __  __  "
        PRINT TAB(19); "  __  "
        PRINT TAB(19); "  __  "
        PRINT TAB(19); "  __  "
        PRINT TAB(19); "  __  "
        PRINT TAB(19); "  __  "
        PRINT TAB(19); "  __  "
        PRINT TAB(19); "  __  "
        PRINT TAB(19); "  __  "
        PRINT TAB(19); "  __  "
        PRINT TAB(19); "  ________  "
        RETURN
disp2:
        CLS : BEEP
        LOCATE 5, 20
        PRINT "  _______  "
        PRINT TAB(19); "  __  __  "
        PRINT TAB(19); "  __  "
        PRINT TAB(19); "  __  "
        PRINT TAB(19); "  __  "
        PRINT TAB(19); "  __  "
        PRINT TAB(19); "  ________  "
        PRINT TAB(19); "  __  "
        PRINT TAB(19); "  __  "
        PRINT TAB(19); "  __  "
        PRINT TAB(19); "  __  "
        PRINT TAB(19); "  ________  "
        RETURN
disp3:
        CLS : BEEP
        LOCATE 5, 20
        PRINT "  _______  "
        PRINT TAB(19); "  __  "
        PRINT TAB(19); "  __  "
        PRINT TAB(19); "  __  "
        PRINT TAB(19); "  __  "
        PRINT TAB(19); "  ________  "
        PRINT TAB(19); "  __  "
        PRINT TAB(19); "  __  "
        PRINT TAB(19); "  __  "
        PRINT TAB(19); "  __  "
        PRINT TAB(19); "  __  "
        PRINT TAB(19); "  ________  "
```

```
    RETURN
disp4:
    CLS : BEEP
    LOCATE 5, 20
    PRINT "  __      __  "
    PRINT TAB(19); "    __      __  "
    PRINT TAB(19); "    __      __  "
    PRINT TAB(19); "    __      __  "
    PRINT TAB(19); "    __      __  "
    PRINT TAB(19); "    ____________"
    PRINT TAB(19); "          __    "
    PRINT TAB(19); "          __    "
    PRINT TAB(19); "          __    "
    PRINT TAB(19); "          __    "
    PRINT TAB(19); "          __    "
    RETURN
disp5:
    CLS : BEEP
    LOCATE 5, 20
    PRINT "  __________      "
    PRINT TAB(19); "    __          "
    PRINT TAB(19); "    __          "
    PRINT TAB(19); "    __          "
    PRINT TAB(19); "    __          "
    PRINT TAB(19); "    __          "
    PRINT TAB(19); "    ____________"
    PRINT TAB(19); "          __    "
    PRINT TAB(19); "          __    "
    PRINT TAB(19); "          __    "
    PRINT TAB(19); "          __    "
    PRINT TAB(19); "    __________  "
    RETURN
disp6:
    CLS : BEEP
    LOCATE 5, 20
    PRINT "  __________      "
    PRINT TAB(19); "    __          "
    PRINT TAB(19); "    __          "
    PRINT TAB(19); "    __          "
    PRINT TAB(19); "    __          "
    PRINT TAB(19); "    __          "
    PRINT TAB(19); "    ____________"
    PRINT TAB(19); "    __      __  "
    PRINT TAB(19); "    __      __  "
```

```
PRINT TAB(19); "      __      __ "
PRINT TAB(19); "     __      __ "
PRINT TAB(19); "     ____________  "
RETURN
END
```

APPENDIX D2: Re-f Relationship

> This program is written by Edgard Chehab in Maple V, and that to calculate the Reynolds number for any value of friction factor, and that using a correlation that relate both functions in all regimes. The purpose was to replace the standard graphic method provided in the literature.

```
> R := proc (f)
> local Reynolds;
> if f>35 then
> Reynolds :=24/f;
> elif f>1.49 then
> Reynolds := (18.5/f)^1.6667;
> elif f>0.48 then
> Reynolds :=
> 13172.622*f^4-(52444.2627*f^3)+(76353.3137*f^2)-(48900.6253*f)+11918.95832;
> fi;
> end:
>
```

APPENDIX D3: Evaluation of n'

> This spreadsheet was written by Edgard Chehab in Maple V. It was used to evaluate the value of n' in a complexe equation as the following.

```
> a :=(0.0127^n')*(4.736^(2-n'))*975*(2983^n')/(25.43*8^(n'-1));
> b:=((n'^1.95/(4*n'^1.2*log10(0.0127^n'*975^(n'/2)*25.43^(1-(n'/2))*2983^n'/(2^(3.5*n'-4)
> *25.43))-0.4*n'^0.75))^2)^(1-(n'/2));
> c:=(2*(0.0127^n'*975^(n'/2)*25.43^(1-(n'/2))*2983^n'/(2^(3.5*n'-4)*25.43)));

> plot(a*b-c,n'=0..1);
> Solve(a*b-c=0);
```